1-1-2011

Supercritical carbon dioxide-processed resorbable polymer nanocomposites for bone graft substitute applications

Kevin Baker
Wayne State University,

SUPERCRITICAL CARBON DIOXIDE-PROCESSED RESORBABLE POLYMER NANOCOMPOSITES FOR BONE GRAFT SUBSTITUTE APPLICATIONS

by

KEVIN C. BAKER

DISSERTATION

Submitted to the Graduate School

of Wayne State University,

Detroit, Michigan

in partial fulfillment of the requirements

for the degree of

DOCTOR OF PHILOSOPHY

2011

MAJOR: BIOMEDICAL ENGINEERING

Approved by:

_____

Advisor Date

_____

_____

_____

DEDICATION

"All endeavor calls for the ability to tramp the last mile, shape the last plan, endure the last hours toil. The fight to the finish spirit is the one characteristic we must possess if we are to face the future as finishers."

Henry David Thoreau

ACKNOWLEDGMENTS

First and foremost, I would like to thank my committee members (Drs. Sandro da Rocha, Howard Matthew and Pamela VandeVord) for their time, consideration and support. I would also like to thank my advisor, Dr. Rangaramanujam M. Kannan, for always being understanding and willing to work with a sometimes challenging work and family schedule. His mentorship and direction over the years have certainly shaped who I am today and sharpened my focus on performing research of exceptional quality and significant societal impact. I would also like to thank my former lab-mates (Drs. Robert Bellair, Emre Kurtoglu and Mihai Manitiu) for guiding me through the maze that is graduate school. Their technical assistance with research was surpassed only by their constant encouragement. I would also like to acknowledge my current lab-mate in the Nanocomposite Group, Fengyuan Yang, for his technical assistance with rheology. A big thanks also goes out to Wayne State University's Graduate School for the Graduate-Professional Scholarship that allowed me to remain a student in the program. From Beaumont Health System, I would like to thank my employees for being understanding of my hectic schedule over the last few months and for always offering to assist. I would also like to thank my Chair, Dr. Harry Herkowitz, who has become not only a vehement supporter and caring mentor, but someone who I consider to be a close friend. Of course, none of this would be possible without family. I would like to thank my Mother and Father, as well as my Mother-in-Law and Father-in-Law. The sacrifices that you all have made in terms of watching the boys, helping with projects around the house have helped to make this possible. Finally, I would like to thank my wife Erin and my two sons, Everett and Miles. We have been through so much together. Without your constant support, words of encouragement and tremendous sacrifice, none of this would be possible. I am forever indebted to you and cannot wait to return the favor as you begin your Ph.D. I know we can get through anything life throws our way!

TABLE OF CONTENTS

LIST OF TABLES

LIST OF FIGURES

CHAPTER 1: THE STRUCTURE, FUNCTION AND REGENERATION OF BONE

Background

Orthopaedic surgery is a field of healthcare concerned with the diagnosis and treatment of disorders of the musculoskeletal system resulting from trauma, congenital abnormalities, tissue degeneration, or other pathology. These disorders may effect any structural component of the musculoskeletal system, including cartilage, tendon, ligaments, muscle and bone. Frequently, injury or pathology affecting these structural components result in extreme dysfunction, pain and an overall reduction in the patient's quality of life. The societal impact of musculoskeletal disorders is significant both from a financial and social perspective. It is estimated that more than one in four Americans have musculoskeletal pathology or injury requiring direct medical attention, which is associated with the expenditure of $849 Billion in indirect costs annually (www.boneandjointburden.org). Musculoskeletal injuries and disorders account for nearly one third of work days missed by employees.

Owing to the significant impact of musculoskeletal disorders, continuous research and development work is being performed by scientists and physicians to enhance patient outcomes associated with orthopaedic surgical procedures. One of the main methods of improving patient outcomes of surgical procedures is to enhance the rate of healing of the tissue being repaired. As the primary structural support of the body, bone has received a significant amount of attention in terms of research aimed at improving healing and regeneration of this important tissue. Most modern research in the area of bone healing centers on the use of tissue engineering techniques, including the use of growth factors, multi-potent cells and scaffolds. Research into novel scaffold constructs for structural bone tissue engineering has lagged behind the considerable advancements made in growth factor and stem cells research.

While numerous materials have been developed to support new bone growth, the vast majority of these constructs lack the static mechanical properties to support *in vivo* biomechanical loading. Non-resorbable materials, such as porous metals, possess adequate compressive strength, but their permanence in vivo represents a challenge to surgeons performing revision surgeries. Device permanence also increases the patients risk for late-onset infection. Ceramic materials, such as sintered calcium phosphates, are attractive from the standpoint of biocompatibility, favorable surface chemistry and porosity. The brittle behavior of these materials is concerning in the setting of structural bone grafting, especially if there is a bending or torsional component to biomechanical loading in the desired anatomic location. Resorbable polymers, especially those based on lactic and glycolic acid are attractive candidate materials. The predictable and labile degradation profile and nearly four decades of in vivo use are desirable characteristics. However, concerns persist regarding both the initial mechanical properties and loss of mechanical strength as a function of construct degradation. This concern is especially warranted considering the relatively poor mechanical behavior of resorbable polymer constructs with a porous morphology.

A considerable amount of new research is now focused on reinforcing resorbable polymer matrices with nanostructured filler materials, such as hydroxyapatite, β-tricalcium phosphate and phosphate glasses. The addition of these filler materials has been associated with improvements in in vitro osteoblast response, due to their biologic activity. However, only modest gains in mechanical strength have been reported with these filler particles in lactic and glycolic acid-based polymer matrices. The lack of significant improvements in reinforcement have been attribute to the inability to adequately disperse the ceramic particulate in the polymer matrix. Additionally, it is hypothesized that the poor interaction between polymer chains and the

ceramic materials does not allow for the effective restriction of polymer chain mobility, which is necessary for significant improvements in mechanical strength.

A promising new method for synthesizing porous, resorbable polymer nanocomposite materials has been developed (Baker et al., 2008; Baker et al., 2011). This method shows promise in terms of the rapid synthesis of nanocomposites suitable for in vivo load-bearing bone graft substitute applications. The method consists of dispersing organically-modified Montmorillonite clays (nanoclay) in a matrix of poly(D-lactide) (PDLA) using supercritical carbon dioxide ($scCO_2$) processing. In addition to effectively dispersing the nanoclay throughout the PDLA matrix, $scCO_2$ processing simultaneously imparts an interconnected porous morphology to the material. The porous morphology is of the resulting nanocomposite construct is similar that of human cancellous bone. Resulting compressive mechanical properties are similar to normal human cortico-cancellous bone. In vitro and in vivo analyses illustrate the ability of the $scCO_2$-processed resorbable polymer nanocomposites to support bone formation, thus making it an ideal candidate for bone graft substitute applications.

Structure of Human Bone

In order to effectively develop a material to replace a tissue, a knowledge about the structure and biology of the tissue is required. Bone is a true composite material comprised of a predominantly organic matrix, reinforced by inorganic consituents. The organic matrix of bone consists primarily of Type I collagen (90%), with additional collagens, non-collagenous extracellular matrix proteins, lipids, growth factors and cytokines. This organic matrix is reinforced by inorganic substances, principally hydroxyapatite. Hydroxyapatite is a calcium phosphate-based mineral ($Ca_{10}(PO_4)_6(OH)_2$), which is present within the collagenous organic matrix as plate-like crystals approximately 20-80 nm in length and 2-5 nm in thickness.

Numerous elemental substitutions are possible within hydroxyapatite crystals, including Mg^{2+}, Sr^{2+}, Na^{+} and K^{+} substituting for calcium. Phosphate groups can be replaced by carbonate groups, or hydrogenated phosphates, while the hydroxyl group can also become carbonated, or fluorinated. These substitutions depend on age, anatomic location and the presence of disease states and tend to have a large effect on solubility, rather than structural properties (Bolstrom et al., 2000)

On a macroscopic scale, human long bones (i.e. femur, humerus, tibia, etc.) are comprised of a dense outer shell called cortical bone. The dense cortical bone transitions abruptly to a porous morphology referred to as cancellous bone. Cortical bone is comprised of individual functional units called osteons, which are oriented longitudinally in most long bones, as shown in Figure 1. Osteons are composed of rings of cortical bone, referred to as lamellae, which surround the Haversian canal. Bone's neurovascular supply runs through these canals after being fed from the outer sheath of tissue known as the periosteum. Osteons are bonded to one another at the periphery by the cement line, which is a region rich in glycosaminoglycans. Volkmann's canals run in a pseudo-tangential path and act as the connection between individual osteons and also serve as connections between the osteon and periosteum.

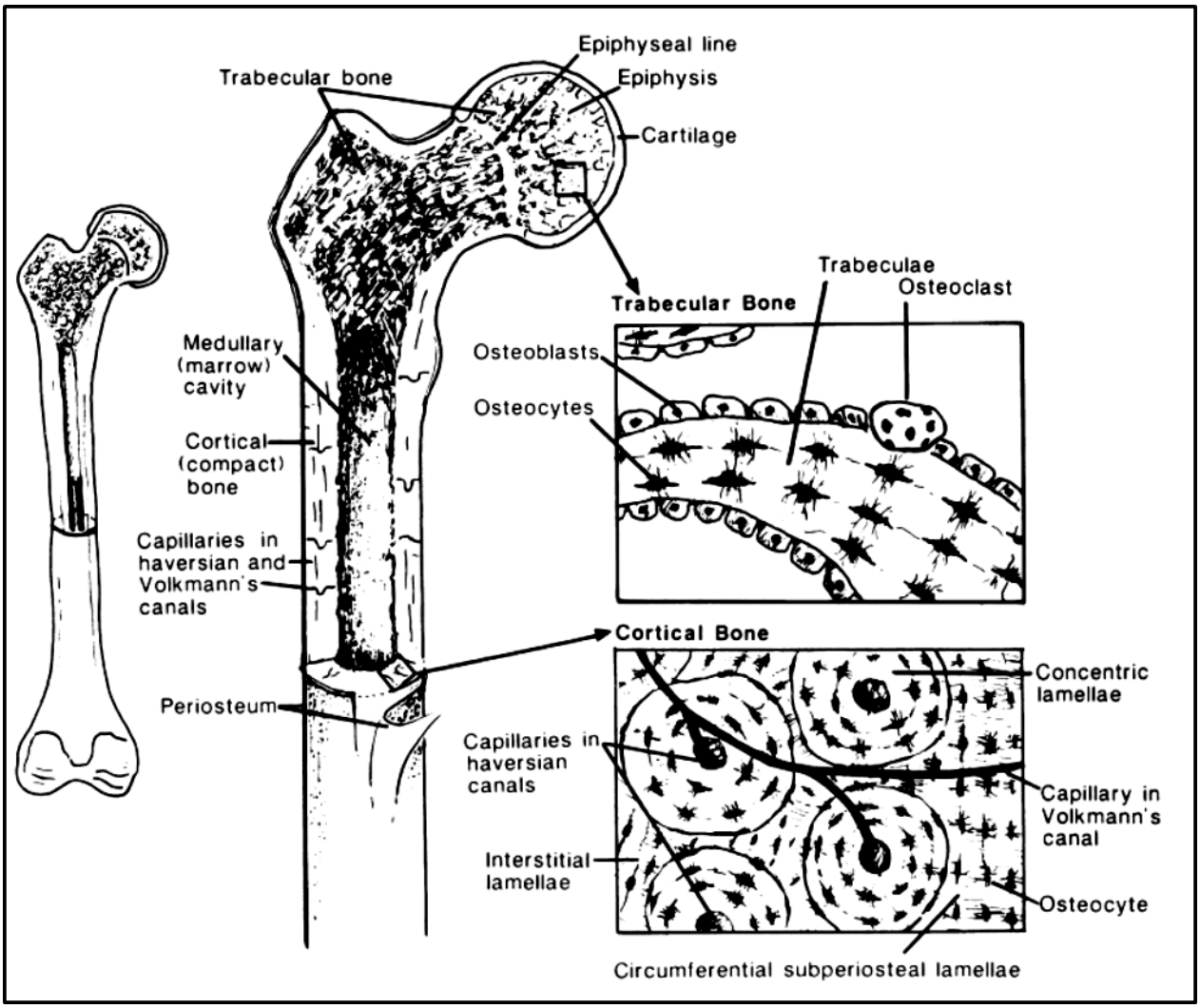

Figure 1. *Illustration of the hierarchical structure of cortical and cancellous bone. (Image taken from Haeys WC: Biomechanics of cortical and trabecular bone: Implications for assessment of fracture risk, in Basic Orthopaedic Biomechanics. New York, NY, Raven Press, 1991, pp 93-142.)*

The porous core of the long bone is comprised of cancellous bone, which is extremely porous in morphology, but rigid enough to withstand biomechanical loading. On an ultrastructural and compositional level, cancellous bone is identical to that of cortical bone. The main difference is the density of the tissue. As previously mentioned, cortical bone is comprised

of densely packed osteons running in a longitudinal direction, parallel to the primary direction of biomechanical loading. Cancellous bone is comprised of a network of interconnected trabecular struts, as shown in Figure 2, and does not contain the same Haversian system that cortical bone does. Depending on the anatomic location and even the location within the long bone, the morphology of the functional units (trabeculae) of cancellous bone vary from being rod-like to plate-like. Similar to cortical bone, trabeculae are composed of lamellae, which are oriented in a longitudinal fashion, rather than concentrically.

Figure 2. *Interconnected porous morphology of human cancellous bone. Image taken from www.sciencephoto.com.*

Cell Biology of Bone

Functionally, bone hosts three distinct cell types, which include osteoblasts, osteocytes and osteoclasts. Bone is the only tissue that contains two specific cell types that are responsible

for tissue formation and tissue destruction. Tissue formation and destruction is a normal process within human bone and relies on the coupling between osteoblast and osteoclast function. Osteoclasts are the cell type responsible for resorption of bone and are descended from marrow-derived hematopoietic progenitor cells that additionally give rise to a monocytic lineage. Mature osteoclasts reside within the structure of bone in small cavities called Howships lacunae and express tartrate-resistant acid phosphatase (TRAP). In order to resorb bone, osteoclasts attach to the proposed site of resorption through integrin binding. Once attached, osteoclasts utilize a carbonic anhydrase system to produce pH-lowering hydrogen ions. The significant reduction in local pH solubilizes the inorganic constituent of bone and hydrolytically digests the organic matrix.

The anabolic counterpart to an osteoclasts is the osteoblast. Osteoblasts line surfaces of bone and express Type I collagen and other phenotypic markers, including osteocalcin, bone sialoprotein and several other extracellular matrix proteins. The extracellular matrix produced by osteoblasts is referred to as osteoid and acts as an interface between the osteoblast and host bone. Osteoblasts are responsible for regulating the process of mineralization, which occurs in two specific phases: nucleation and growth (Bolstrom et al., 2000). The nucleation phase of mineralization consists of a local supersaturation of precipitating species, including Ca^{2+} which is accomplished by extracellular secretion by osteoblasts. Following the build-up of precipitating species, nucleation sites are exposed on the osteoid extracellular matrix. The nucleation of Ca^{2+} and PO_4^- groups is followed by a rapid accumulation and growth phase. The addition of more hydroxyapatite crystals during this phase improves the rigidity of the substrate and provides the structural basis of new bone formation.

Osteocytes are another integral cell component of bone. Osteocytes are actually osteoblasts that have been completely surrounded by mineralized osteoid and are considered to be the terminal phase of the osteoblastic lineage. Within a section of cortical bone, osteocytes are distributed in concentric rings of the osteon. The immobile osteocytes communicate with each other by extended cell processes that travel through the canaliculi of bone (Keaveny and Hall, 1993). Osteocyte communication, which is both autocrine and paracrine (communicating directly with osteoblasts on the bone surface) in nature can help to regulate the homeostasis of bone and is implicated in one of the main driving forces of new bone remodeling (Bolstrom et al., 2000).

Bone Remodeling

The function of osteoblasts and osteoclasts are coupled during the process of bone remodeling by a distinct set of pathways. Bone remodeling is necessary for two distinct reasons: 1. maintenance of systemic (circulating) calcium concentrations and 2. optimization of bone geometry and structure for adequate load bearing capacity. For the purposes of this discussion, we will focus on the second reason. It is known that new bone forms and existing bone remodels according to the mechanical loading that it experiences; a property known as Wolff's Law. This mechanism optimizes the geometric and material properties of bone based on predominant loading amplitudes, frequencies and directions. Even in skeletally mature humans, bone continuously remodels as a function of body mass index, level of activity, diet and pathology.

While the exact mechanisms of how mechanical forces are converted to cell-level communication are unknown, it is understood that the process is dependent on the coupling of anabolic and catabolic activity by osteoblasts and osteoclasts, respectively. The functional

coupling of these cells is accomplished through a variety of physicochemical and biochemical signals. In terms of physical signaling, osteoclast-mediated bone resorption can be mediated by osteoblast signaling. Upon exposure to elevated levels of 1,25-dihydroxyvitamin D_3, osteoblastic lining cells are stimulated to contract, which exposes mineralized osteoid. Activation of osteoclastic resorption requires exposure of mineralized matrix, as well as exposure to matrix-bound proteins. Osteoblast surfaces express receptor activator for nuclear factor-κB ligand (RANKL) (Bolstrom et al., 2000). RANKL is a cell surface protein that is necessary for receptor activator for nuclear factor-κB- (RANK) induced activation of nuclear factor-κβ (NF-κB), as well as nuclear factor of activated T cells (NFATc1). Activation of NF-κB and NFATc1 stimulates active resoprtion, as well as the recruitment and differentiation of osteoclast precursors. To inhibit resorption, other local osteoblasts begin to express osteoprotegerin (OPG). OPG binds to RANKL on osteoblast surfaces, which eliminates NF-κB and NFATc1 activation and brings the process of resorption to a halt. Active degradation of the bone results in the release of growth factors with osteogenic activity, including bone morphogetic proteins (BMPs), which are members of the transforming growth factor-beta (TGF-β) superfamily of proteins. Release of these growth factors from the matrix results in increased matrix production by osteoblasts. As shown, the process of osteoclastic bone resorption and osteoblastic bone formation is a continuous feedback loop relying with each cell relying on the function of the other to maintain homeostasis.

Fracture Healing and Bone Regeneration

Despite the hierchical structure of human cortical and cancellous bone and the complex cellular basis for homeostatic balance between anabolism and catabolism, bone is still prone to

mechanical failure. Fractures accounted for over 20% of all reported musculoskeletal injuries in 2008 (www.boneandjointburden.org). Long bones of the upper and lower extremities are the most common anatomic locations of these fractures, followed closely by fractures of the vertebral column. Severe fractures are associated with significant physical limitations and the greatest number of missed days of work compared to any other type of musculoskeletal injury (www.aaos.org).

Bone is a tissue that does have a relatively potent intrinsic healing mechanism in the event of fracture (Day et al., 2000). Depending on the magnitude, direction and mode of loading, immediately upon fracture, there is a disruption in the structural aspect of the tissue, its blood supply and surrounding soft tissues. Attending physicians attempt to reduce the fracture, which involves the direct application of force to restore the normal anatomy of the fractured bone. Depending on the type of injury, stability of the reduced fracture and anatomic location, the extremity affected by the fracture may be placed in a cast to reduce mobility. In other situations, open reduction and internal fixation (ORIF) is necessary. In the case of ORIF, metallic implants, such as intramedullary nails or screw and plate constructs will be used to create rigid fixation at the site of fracture. Both the quality of the fracture reduction and the degree of fixation used dictate the healing response of the bone. Primary cortical healing is one such healing response, which entails the attempt by the bone to re-establish osteon-osteon contact between the fracture fragments. Gaps that persist between fracture fragments after reduction become vascularized and a callus forms. The callus consists of a milieu of cytokines which direct neoangiogenesis, facilitate cellular infiltration to the fracture site and provide the biochemical impetus for healing. MSCs differentiate towards an osteoblastic lineage and begin to express osteoid, which later becomes mineralized. These initial phases of osteogenesis occur

in the absence of osteoclastic bone resorption, as the direct need is for tissue anabolism. Days after this period of pure anabolic response at the fracture site, osteoclastogenesis occurs. Osteoclasts activate and begin to chemically debride any non-viable bone at the fracture site. The fracture callus is then resorbed and osteoblast-osteoclast coupling occurs to initiate the process of remodeling. With an appropriately rigid reduction and fracture fixation, stresses and strains will still be effectively transmitted to the tissue, as the patient is encouraged to begin using the affected limb. Osteoclasts form cutting cones to remodel the newly formed bone to be optimized for bearing of biomechanical loads (Bolstrom et al., 2000; Day et al., 2000).

Secondary healing is another mechanism by which fractures can heal. Unlike primary healing, secondary healing does not involve the re-establishment of osteonal contact between the fracture fragments. Instead, a potent reaction by the bone's outer sheath-like covering (periosteum) immediate initiates the formation of a callus that covers the entire fracture site (Day et al., 2000). The biochemical and biologic microenvironment of the callus contains a high concentration of endogenous promoters of neoangiogenesis and osteogenesis. Host osteoblasts in each of the fracture fragments are encouraged to excrete a collagenous extracellular matrix. Secondary healing often involves bone formation by endochondral ossification. This method of bone formation mimics embryonic bone formation and involves the formation of a collagenous template by MSCs. The collagenous template is subsequently mineralized to form highly functional bone tissue in a relatively short period of time. Similar to primary healing, osteoclasts begin to remodel the newly formed bone to ensure a return to normal weight bearing status with minimal dysfunction.

The Need for Bone Grafting

Despite the ability of bone to heal through a variety of intrinsic processes and pathways, several clinical situations arise where the patient's healing and regeneration response is insufficient to provide a return of the bone to a normal structure. Measures are taken by surgeons to restore the load bearing capacity of the bone by augmenting the site of bone injury or dysfunction with biologic, or synthetic constructs. These constructs are meant to serve not only as load bearing structures, but also scaffolds onto which the patient's new bone will form. Sometimes these constructs contain endogenous, or exogenous factors that promote the recruitment of stem cells to the site to speed the rate and amount of new bone formation. Regardless of the configuration, these constructs are referred to as bone grafts and are used quite frequently in orthopaedic surgery. In 2003, over 1 million bone grafting procedures were performed in the United States alone (www.aaos.org). While use of bone grafting in musculoskeletal trauma situations is obvious, there are two other scenarios that account for a significant portion of the number of bone grafting procedures performed each year. As both of these scenarios have become increasingly more common, even over the last decade, it is pertinent to discuss the application of bone grafting in these situations.

Bone Grafts for Osseous Neoplasms

The presence of malignant or benign neoplasms, or tumors, within osseous tissue is a relatively common occurrence (Clohisy 2000). Several types of benign tumors exist, including aneurysmal bone cysts, osteoid osteomas and osteochondromas. Aneurysmal bone cysts frequently occur as a result of a pre-existing bone tumor, which can lead to increases in local blood flow. This increase in local blood flow, as well as local blood pressure cause the formation of a cyst in a location previously occupied by the bone tumor. These types of tumors can arise on the surface of a bone, or remain confined within the marrow cavity. Osteoid

osteomas are small focal lesions that tend to occur in the vertebrae and are characterized by a dense area of random oriented (woven) bone, fibrovascular tissue with a focal area of osteolysis (bone resorption) and a dense ring of sclerotic (non-viable) bone (Clohisy 2000). Osteochondromas are tumors that present as osseous outgrowths on a bone. The outgrowth often has a cap of cartilage at the most distal end and tend to affect the long bones of the extremities. Malignant tumors of bone include osteosarcomas, Ewing's sarcomas and secondary tumors arising from metastatic cancer. Malignant tumors tend to be quite aggressive and destructive in nature. Osteosarcoma is the most common primary osseous tumor and occurs frequently in the pediatric population. Ewing's sarcoma is another malignancy that tends to affect the adolescent population and is characterized by an expansile lesion, usually found in the femur, humerus or tibia.

Aside from presenting with constitutional symptoms (fever, chills, night sweats) and the insidious onset of pain, another common clinical presentation of a bone tumor is fracture of a bone from a seemingly low energy event. Frequently, a patient will describe falling from a standing height and present with a fracture. Upon analysis of X-rays, the presence of a lesion is in the region of the fracture is observed. The so-called "pathologic fracture" is a function of the structural compromise of a bone affected by either a benign or malignant tumor (Day et al., 2000). All of the above-described benign and malignant tumors are associated with focal disruption of cortical bone in load bearing anatomic locations, including the vertebrae, femur, tibia and humerus. Disruption of the cortices creates a stress riser in the bone, which can lead to compression fractures in the spine, or transverse and oblique fractures in long bones.

In a setting where an osseous tumor is discovered prior to pathologic fracture by X-ray, computed tomography (CT) or bone scintigraphy, treatment often involves surgical excision of

the lesion. Debridement of a wide margin of bone accompanies excision of the lesion, in an attempt to remove the full extent of malignant or non-normal tissue. Because of both the excision and debridement, the bone still remains susceptible to fracture through the original site of the tumor. Extremely aggressive tumors can also compromise the integrity of a an entire region of bone, necessitating radical resection of entire sections of bone to prevent spread of malignancy.

In addition to surgical excision of the bone tumor, radiation and/or chemotherapy is frequently employed to reduce the size and viability of a tumor. Post-operative radiation is often used to ensure that the, even when wide margin excision or resections are performed, the tumorous tissue will not return. Radiation and certain types of chemotherapy have been shown to alter the biology within bone. Further evidence exists which details the effect of radiation on local MSC populations in terms of their ability to differentiate towards an osteoblastic lineage and, ultimately, to repair bone. Chemotherapeutic agents, such as methotrexate and Adriamycin have been shown to alter systemic bone formation dynamics, leading to an uncoupling between osteoclastic bone resorption and osteoblastic bone formation. Georgiou, et al. demonstrated the effect of methotrexate on the differentiation capacity of marrow-derived MSCs in a rate model. In animals treated with methotrexate, MSCs were more likely to differentiate towards an adipogenic lineage, rather than an osteoblastic lineage.

As described, the presence, as well as the treatment of osseous neoplasms results in a challenging clinical situation in terms of affecting bone healing. The excision of a bone tumor, or resection of an entire section of bone creates a critical defect that necessitates the use of a bone graft construct to support biomechanical loading. Pre- and post-operative radiotherapy and/or chemotherapy can have a negative effect on the potential of the patient to rapidly

regenerate bone at the site of excision. As such, the bone graft employed must present a surface and morphology conducive to bone formation. Additional agents, endogenous or exogenous, locally or systemically administered may be necessary to induce the rapid formation of bone at the grafting site.

Hariri, et al recently described the use of a free vascularized fibular graft for reconstruction of metadiaphyseal bone of the femur and tibia following resection for expansile neoplasms, such as Ewing's sarcomas (Hariri et al., 2010). The graft was harvested from the fibula on the same side as the femur affected by the tumor. This type of graft provides excellent load bearing support, due to the high ratio of cortical to cancellous bone. In addition to load bearing support, this graft also contains fresh vascular tissue, which aids in the formation of a callus. Callus formation precedes new bone formation due to the high concentrations of osteoinductive proteins and chemotactic agents for MSCs (Day, 2000)

Bone Grafts for Spine Fusion

Spinal arthrodesis, also known as spinal fusion, is a procedure which relies on the creation of a bony bridge between adjacent vertebrae, as shown in Figure 3. Spine fusion is indicated for the treatment of both acute and chronic conditions of the spine, such as intervertebral disc herniation, degenerative disc disease, spondylolisthesis and spondyloarthropathy (DePalma et al., 1972; Hu and Bohlman, 1994; Malloy and Hilibrand, 2002). These conditions most often involve impingement of neurovascular structures by herniated intervertebral disc tissue, or vertebrae which have translated too far in relation to adjacent vertebrae. Patients experiencing this impingement may present clinically with radiating pain (radiculopathy) throughout an extremity, numbness, tingling, loss of motor function and

even cognitive deficits (DePalma et al., 1972). Other patients will present with debilitating axial back pain, which is confined to the midline of the spine without any radicular symptoms.

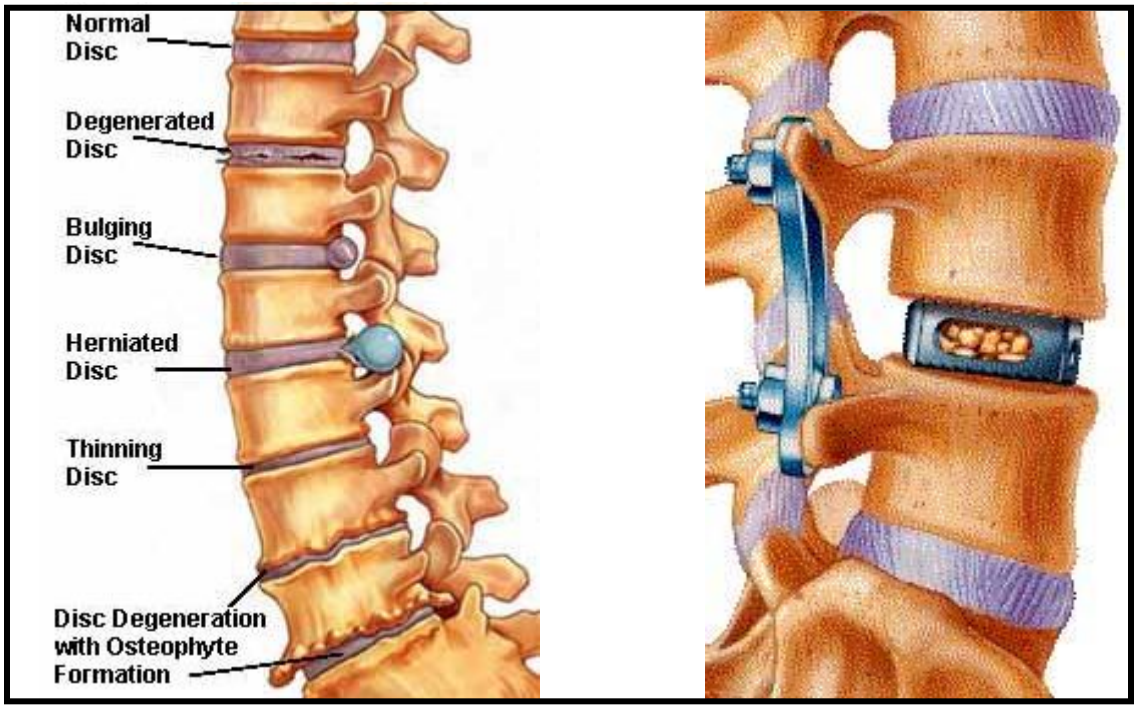

Figure 3. *Illustration of common intervertebral disc pathology leading to pain and dysfunction (right) and the technique of interbody fusion (right). Image taken from www.orthogate.com/spine.*

Treatment of the symptomatic spine level involves the formation of a bony bridge between adjacent vertebrae. The spine level is fused to restore the normal lordotic or kyphotic curvature of the spine, while increasing stability of the segment, thus reducing the incidence of future compromise of neurovascular structures, pain and dysfunction. In the case of interbody fusion, arthrodesis is created between the vertebral bodies of adjacent vertebrae (DePalma et al.,

1972). This procedure involves making an incision to the outer annulus fibrosus of the intervertebral disc. Once access is gained through the annulus fibrosus, the nucleus pulposus and inner annulus fibrosus tissue is removed by rongeurs and suction. The endplates of the vertebral bodies within the intervertebral disc space are decorticated to yield bleeding bone, which theoretically aids in the migration of mesenchymal stem cells from the marrow cavities in the vertebral body. Bone graft material is then placed between the vertebral bodies to maintain distance between vertebrae (disc height) and to induce and/or facilitate the growth of new bone, thus stabilizing the spine segment, as shown in Figure 4. Depending on the technique used, a metallic plate may be placed in the anterior portion of the spine to prevent extrusion of the bone graft material, which, in the case of interbody fusion of the cervical spine, could cause damage to vital structures such as the trachea.

Figure 4. *X-ray of a patient who underwent cervical interbody fusion.*

In applications, such as interbody fusion, the bone graft material must be capable of withstanding substantial static compressive loads, as well as cyclic compression, bending and torsion (DePalma et al., 1972; Lippman et al., 2004; Shikinami and Okuno, 2003). While the biomechanical loading within the long bones of the extremities and in the spine are significant, the mechanical properties of the bone graft should not exceed that of native bone. Specifically, if the elastic modulus of a bone graft material greatly exceeds the elastic modulus of the bone that it is replacing, a phenomenon known as stress shielding may occur. Stress shielding is the result of ineffective load transmission to growing bone, due to the mismatch in static mechanical properties. Stress shielding renders bone growth slow and random according to Wolff's Law and

frequently results in the formation of fibrous tissue, which is not conducive to load bearing (Shikinami and Okuno, 2003).

In addition to the mechanical requirements of a bone graft material, numerous basic and translational science studies have described the importance of bone graft porosity. Interconnected pores with an average diameter of 250 μm have been shown to facilitate cellular infiltration and neovascularization, which are critical components to bone growth (Georgiou et al., 2007; Kruyt et al., 2004; Mathieu et al., 2005). Appositional bone growth, such as that which occurs on the outside edges of a dense construct, is not capable of bearing the high compressive loads in long bones of the extremities or in the spine. A final requirement of a bone graft material is the ability to induce bone formation; a property referred to as osteoinductivity (Buck et al., 1989; Fini et al., 2004; Malloy and Hilibrand, 2002; Wigfield and Nelson, 2001; Wimmer et al., 2001). In biologic materials, this property is mediated by endogenous biomolecules (i.e. growth factors) and pluripotent cells. The process of osteoinduction begins with chemotactic recruitment of progenitor cells and the subsequent differentiation of these cells to an osteoblastic lineage. The differentiated cells then form a collagenous matrix, which is subsequently mineralized resulting in the formation of bone.

References

Baker KC, Bellair R, Manitiu, Herkowitz HN, Kannan RM. 2009. Structure and mechanical properties of supercritical carbon dioxide processed porous resorbable polymer constructs. Journal of the Mechanical Behavior of Biomedical Materials 2(6), 620-626.

Baker KC, Manitiu M, Bellair R, Gratopp CA, Herkowitz HN, Kannan RM. 2011. Supercritical carbon dioxide processed resorbable polymer nanocomposite bone graft substitutes. Acta Biomaterialia. May 14 [Epub Ahead of Print].

Bostrom MPG., Boskey A., Kaufman JK., Einhorn TA. 2000. Form and function of bone. In: Einhorn TA, Buckwalter JA, Simon SR (Eds.). Orthopaedic Basic Science – 2nd Edition. American Academy of Orthopaedic Surgeons, Rosemont, IL. pp. 319 – 369.

Buck B., Malinin T. and Brown M. 1989. Bone transplantation and human immunodeficiency virus: An estimate of risk of acquired immunodeficiency syndrome (AIDS). Clinical Orthopaedics and Related Research. 240, 129-136.

Clohisy DR. 2000. Growth and metastasis of musculoskeletal tumors. In: Einhorn TA, Buckwalter JA, Simon SR (Eds.). Orthopaedic Basic Science – 2nd Edition. American Academy of Orthopaedic Surgeons, Rosemont, IL. pp. 319 – 369.

Day SM., Ostrum RF, Chao EYS., Rubin CT., Aro HT., Einhorn TA. 2000. Bone injury regeneration and repair. In: Einhorn TA, Buckwalter JA, Simon SR (Eds.). Orthopaedic Basic Science – 2nd Edition. American Academy of Orthopaedic Surgeons, Rosemont, IL. pp. 371 – 399.

DePalma A.F., Rothman R.H., Lewinnek G.E. and Canale S.T. 1972. Anterior interbody fusion for severe cervical disk degeneration. Surgical Gynecology and Obstetrics 134, 755-758.

Fini, M., Giavaresi, G., Torricelli, P., Borsari, V., Giardino, R., Nicolini, A. and Carpi, A. 2004. Osteoporosis and biomaterial osteointegration. Biomedicine & Pharmacotherapy 58, 487-493.

Georgiou, G., Mathieu, L., Pioletti, D.P., Bourban P.-E., Manson, J.-A.E., Knowles, J.C., and Nazhat, S.N. 2007. Polylactic acid-phosphate glass composite foams as scaffolds for bone

tissue engineering. Journal of Biomedical Materials Research: Part B Applied Biomaterials 80B, 322-331.

Georgiu KR., Scherer MA, Fan CM, Cool JC, King TJ, Foster BK, Xian CJ. 2011. Methotrexate chemotherapy reduces osteogenesis but increases adipogenesis potential in the bone marrow. Journal of Cellular Physiology. [Epub ahead of print]

Hariri A, Mascard E, Atlan F, Germain MA, Heming N, Dubousset JF, Wicart P. 2010. Free vascularized fibular graft for reconstruction of defects of the lower limb after resection of tumor. Journal of Bone and Joint Surgery (American) 92(11), 1574-1579.

Hu R.W. and Bohlman H.H. 1994. Fracture at the iliac bone graft harvest site after fusion of the spine. Clinical Orthopaedics and Related Research 309, 208-213.

Keaveny TM., Hayes WS. Mechanical properties of cortical and trabecular bone. In: Hall BD. (Ed.) Bone. CRC Press, Boca Raton, FL. pp: 285-344.

Kruyt M.C., van Gaalen S.M., Oner F.C., Verbout A.J., de Bruijn J.D., Dhert W.J.A. 2004. Bone tissue engineering and spinal fusion: the potential of hybrid constructs by combining osteoprogenitor cells and scaffolds. Biomaterials 25, 1463-1473.

Lippman, C.R., Hajjar, M., Abshire, B., Martin, G., Engelman, R.W. and Cahill, D.W. 2004. Cervical spine fusion with bioabsorbable cages. Neurosurgery Focus 16(3), Article 4.

Malloy K.M. and Hilibrand, A.S. 2002. Autograft versus allograft in degenerative cervical disease. Clinical Orthopaedics and Related Research 394, 27-38.

Mathieu, L.M., Montjovent, M.-O., Bourban, P-E., Pioletti, D.P. and Manson, J.-A.E. 2005. Bioresorbable composites prepared by supercritical fluid foaming. Journal of Biomedical Materials Research: Part A 75A, 89-97.

Shikinami, Y. and Okuno, M. 2003. Mechanical evaluation of novel spinal interbody fusion cages made of bioactive, resorbable composites. Biomaterials 24, 3161-3170.

Wigfield C.C., Nelson R.J. 2001. Non-autologousinterbody fusion materials in cervical spine surgery: How strong is the evidence to justify their use? Spine 26(6), 687-694.

Wimmer C., Krismer M., Gluch H., Ogon M., and Stockl B. 1999. Autogenic versus allogenic bone grafts in anterior lumbar interbody fusion. Clinical Orthopaedics and Related Research 360, 122-126.

CHAPTER 2:BONE GRAFT MATERIALS - FROM AUTOLOGOUS TO SYNTHETIC

Background

Bone grafting was first attempted and reported in 1668 in the Netherlands by Dr. van Meekeren. This surgeon described the repair of a soldier's traumatic cranial defect with bone harvested from a canine skull. Nearly 250 years later, Dr. Albee described the use of autologous bone harvested from the lower extremity in achieving successful spine fusion. Later that century as autologous bone grafting gained popularity, surgeons began attempting to isolate the growth factors from harvested bone to enhance fracture healing. Dr. Urist, in 1965, was the first to isolate bone morphogenetic proteins from bone and later described the process by which these proteins led to bone formation by a process he termed "autoinduction."

The technique of bone grafting is now an extremely common adjunctive procedure performed in a variety of surgical scenarios to ensure rapid, complete healing of injured, or pathologically compromised bone. Today, more than 1 million procedures are performed annually in the United States which involve the use of bone graft materials. A sizeable market now surrounds bone graft and bone graft substitute materials, which generates in excess of $2.5 billion in sales per year. These numbers are continuing to climb as the average life expectancy of humans increase while simultaneously, the average age of orthopaedic patients decreases creating an ever-increasing demand.

Despite significant progress in the techniques and materials used for bone grafting, as well as the increasing frequency with which these procedures are performed, there is still a substantial amount of room available for improvement. Regardless of the use of cutting-edge recombinant human proteins and novel material processing methods, non-union (failure of bone formation) still persists as a common complication associated with bone grafting. A comparison

of currently used materials, from biologic to synthetic, is presented with the intention of identifying the multi-factorial requirements of bone graft materials, advantages with specific clinically-used constructs and disadvantages which lead to clinical failure. Since the focus is on bone graft materials used strictly for structural or load bearing applications, the discussion of various types of bone graft materials is focused nearly exclusively on graft materials used in spine fusion procedures.

Requirements of Bone Graft Materials

The mechanical strength of bone graft materials, is of primary importance as these constructs are meant to replace sections of bone damaged by trauma or biochemically altered by pathology. Initial mechanical properties of the construct must be sufficient to support both static and dynamic loading in a variety of configurations, including compression, bending and torsion. Depending on the anatomic location, compressive loading in a long bone of the lower extremity can exceed several times body weight for common activities of daily living, such as jumping, walking down a flight of stairs and running (Day et al., 2000; Keaveny 1993). While it is important for the bone graft constructs to support biomechanical loading by possessing adequate mechanical properties, it is equally important that the stiffness, or modulus of the material does not greatly exceed that of the bone that the construct is attempting to replace. When a material with an elastic modulus that greatly exceeds that of the host bone is implanted, a process known as stress shielding is likely to occur. Stress shielding is a phenomenon that results in new bone formation being slowed and random, in terms of its structure. Both new bone formation, as well as bone remodeling require the adequate transmission of load to the cells responsible for forming the tissue. If a bone graft construct has an elastic modulus that greatly exceeds that of the bone it is replacing, the construct itself absorbs the vast majority of the biomechanical loading without

effective transmission to the newly forming bone. According to Wolff's Law, bone growth happens in a manner proportional to the stresses and strains that the bone experiences (Day et al., 2000). Without effective load sharing between the bone graft material and host bone, newly formed bone will be incapable of supporting biomechanical loads and will most often take on a fibrous appearance. Stress shielding often requires a revision procedure to correct the problem (Day et al., 2000; Keaveny 1993).

Constructs used as bone graft substitute materials should also possess characteristics conducive to their controlled resorption *in vivo*. A goal of bone grafting is to use a construct as a temporary load bearing structure and scaffold for new bone formation. The bone graft material is intended to be eventually replaced by host bone. The temporary nature of a bone graft construct obviates the problems associated with permanent devices, which include an omnipresent risk of infection. Additionally, permanent constructs, depending on their composition and properties, may complicate future surgeries that the patient may need. For instance, the presence of a large synthetic scaffold used to heal a femur fracture, may create a difficult obstruction to the proper placement of a total hip replacement component that the patient may need several years later. Non-resorbable materials used for bone graft application may also interfere with radiographic imaging, which is used to assess healing post-operatively.

An obvious goal of bone grafting is to encourage new bone formation. Autograft has the capability of inducing new bone formation, a process known as osteoinduction, due to endogenous growth factors and mesenchymal stem cells (MSCs). This process was first described by Urist, et al. who examined bone formation due to "autoinduction" following implantation of demineralized bone matrix (Urist, 1965). This group identified endogenous growth factors, such as bone morphogenetic protein-2 (BMP-2), transforming growth factor-beta

(TGF-β) and platelet-derived growth factor (PDGF) as some of the main proteins involved in the process. These proteins are chemotactic for mesenchymal stem cells. Once recruited to the site, the MSCs begin to differentiate towards an osteoblastic lineage. A collagenous extracellular matrix is deposited and subsequently mineralized by host osteoblasts, as well as recently differentiated MSCs. Currently, recombinant technology is used to synthesize human BMP-2 and BMP-7 for the purposes of enhancing bone formation following fracture or in the setting of spine fusion. These growth factors can be used to confer the attribute of osteoinductivity to bone graft materials of all types, including synthetic constructs. Another method used to encourage bone formation is the use of bone marrow aspirate. Bone marrow is known to contain MSCs, as well as a complex milieu of biochemical factors that are capable of inducing bone formation. The use of bone marrow aspirate is accomplished via a needle biopsy of an anatomic location known to contain a significant volume of bone marrow and marrow-derived MSCs. The iliac crest, vertebral bodies and proximal humerus are common locations for harvesting bone marrow aspirate. The aspirate is then applied to the site of intended bone formation.Numerous clinical and pre-clinical trials exist outlining the success of these osteoindutive techniques.

The property of *osteoconductivity* is another important requirement of bone graft materials. This attribute refers to the ability of a construct to facilitate, rather than induce, new bone formation. Numerous factors contribute to the development of osteoconduction of a material. Scaffold materials should be porous to facilitate cellular infiltration within the three dimensional structure of the graft. If cells are unable to penetrate a construct, appositional bone growth may occur. Appositional bone growth is the generation of a ring of bone that forms along the outside of the graft constructs, rather than throughout the entire load bearing structure. Appositional bone growth is insufficient to support biomechanical loads, especially when the

graft material is designed to resorb over time *in vivo*. If bone is to grow throughout the three dimensional structure of a graft construct, there must be a method to facilitate nutrient transport to the center of the graft to keep cells healthy and to continue the process of bone formation and maturation. Nutrient transports is accomplished by the generation of microvasculature at the site of bone healing. An average pore size of 100-300 μm has been shown to be adequate to support the development of neovascularization and efficient microvascular infiltration of three dimensional constructs. In addition to a porous microstructure, surface chemistry and topography of the scaffold has also been shown to be an important contributor to osteoblast attachment and proliferation. surfaces promote osteoblas

Autologous Bone Graft

Autogenous iliac crest bone graft, shown in Figure 1, has been used extensively in cervical, thoracic and lumbar interbody spine fusion procedures with a high degree of clinical success. Despite the success rate of the spine fusion procedures, harvest of autograft bone is associated with numerous harvest site complications (Buck et al., 1989; Hu and Bohlman, 1994; Malloy and Hilibrand, 2002; Samartzis et al., 2005; Wigfield and Nelson, 2001; Wimmer et al., 1999; Zdeblick and Ducker 1991). Donor site complication rates as high as 20-30% have been reported after performing iliac crest graft harvest procedures (Hu and Bohlman, 1994; Malloy and Hilibrand, 2002; Wigfield and Nelson, 2001). An iliac wing fracture rate of 7% was reported by Hu and Bohlman when harvesting for spinal fusion procedures (Hu and Bohlman, 1994). Even if the patient does not present postoperatively with symptoms of donor site morbidity, fracture initiating from the harvest site, or infection, DePalma and others found that the incidence of pain after iliac crest graft harvest was as high as 36% (DePalma et al., 1972).

Exposure of the patient to this additional procedure of graft harvest also increases the likelihood of infection.

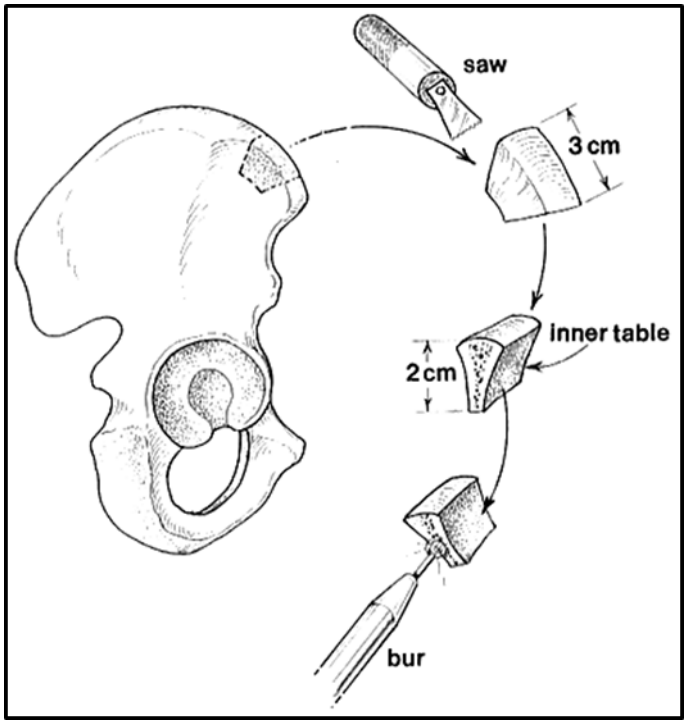

Figure 1. *Anterosuperior harvest location for iliac crest bone graft. American Journal of Sports Medicine.*

Allogenic Bone Graft

Due to the high rates of post-operative complications associated with the harvest of autograft bone, allogenic bone (allograft) has been proposed as an alternative (Malloy and Hilibrand, 2002; Samartzis et al., 2005; Wimmer et al., 1999). Allograft is bone harvested from a donor, usually at the time of death. The bone is aseptically harvested from the donor, sterilized and stored in a freeze-dried state in a tissue bank. A number of reports in the literature have shown an increase in the use of allograft in spinal fusion applications. In 1991, Zdeblick and Ducker experienced only a 78% rate of cervical arthrodesis when using allograft, as compared to 92% who received autograft (Zdeblick and Ducker, 1991). Similarly, Nugent and Dawson

reported a lumbar fusion rate of only 70% with allograft, compared to 92% with iliac crest autograft (Nugent and Dawson, 1993). Recently, fusion procedures implementing allograft have achieved rates of fusion comparable to those using autograft. In 2005, Samartzis and others achieved a 100% rate of cervical arthrodesis with allograft. They found no statistically significant difference in the fusion rates between allograft and autograft (Samartzis et al., 2005). Functional outcomes are also slightly higher for allograft groups due to the elimination of harvest site complications associated with autograft harvest.

However, numerous disadvantages of allograft usage exist. While careful donor screening and sterilization procedures have reduced the incidence of disease transmission, reports still surface. Specifically, the transmission of Hepatitis and HIV associated with allograft bone have been reported in the literature (Buck et al., 1989). Additionally, the same sterilization procedure that reduces the risk of disease transmission has also been shown to reduce the osteoinductivity of the graft (Malloy and Hilibrand, 2002; Samartzis et al., 2005; Wigfield and Nelson, 2001). Sterilization methods, such as gas plasma, ethylene oxide and gamma irradiation have been shown to have an effect on the concentration and efficacy of osteoinductive proteins endogenous to allograft. Denaturation of these proteins compromises the ability of allograft bone to induce desired bone formation. In addition to reduced osteoinductivity, allograft bone is subject to the finite supply of donor tissue. Tissue banks in the European Union, as well as the United States have reported shortages of allograft tissue (Wigfield and Nelson, 2001; Wuisman and Smit, 2006; Zdeblick and Ducker, 1991). Further, allograft is much less available in rural and geographically isolated hospitals.

Clinically-Used Bone Graft Substitutes

Among the first substitutes explored were the calcium phosphates, particularly hydroxyapatite. Hydroxyapatite (HA) is a ceramic material that is compositionally similar to native bone mineral, with a calcium to phosphorus ratio of 1.67. HA that is currently in use is derived from sea coral, which is composed of calcium carbonate (Suetsuna et al., 2001; Zdeblick et al., 1994). The calcium carbonate undergoes a hydrothermal conversion to HA. The end result is a highly interconnected porous structure that compositionally and morphologically mimics cancellous bone. Coralline HA has been used clinically in interbody spinal fusion procedures. While corraline HA is an effective osteoconductive scaffold, it lacks the osteoinductive potential of autograft and allograft, which has resulted in inferior performance. Further, complications associated with fracture of the brittle ceramic have been reported. These brittle failures result in reduced intervertebral disc height and subsequent compromise of neurovascular structures, necessitating immediate revision surgical procedures (Suetsuna et al., 2001; Zdeblick et al., 1994).

Calcium phosphates have also been used in particulate form for spinal fusion procedures. Several phases of particulate calcium phosphates are in current clinical use, including beta-tricalcium phosphate (β-TCP), HA and dicalcium phosphate dihydrate (DCPD). The porosity, surface chemistry and composition have been shown to facilitate bone growth. However, the particulate materials lack load-bearing capacity and therefore must be used with additional instrumentation, such as fusion cages. These cages act as the load bearing component and also facilitate containment of the calcium phosphate material. The mechanical properties of these cages, specifically the modulus of elasticity, exceeds that of native bone. This results in the previously mentioned phenomenon of stress shielding, which renders bone growth slow and random.

To address the brittle nature of coralline HA and the non-load bearing capacity of particulate calcium phosphates, porous metal constructs have recently been introduced (Wigfield and Nelson, 2001). The metallic constructs are fabricated using a number of different techniques, all resulting in the formation of highly porous structures resembling the architecture of cancellous bone. The metals used, including tantalum, pure titanium and titanium alloys, have mechanical properties that make them capable of withstanding physiologic loading. The open porous morphology of the construct decreases the bulk elastic modulus, reducing the incidence of stress shielding with these metals. However, these porous metal constructs have not found great clinical acceptance in spine fusion procedures. The non-resorbable nature of metals presents an omnipresent risk of infection to the patient. Non-resorption also limits the options of a surgeon who is performing a revision procedure on the patient. Metallic constructs also present a challenge to imaging modalities, such as computed tomography (CT) and magnetic resonance imaging (MRI). The radiopacity of metals, can also reduce the accuracy of radiographic assessment of bone growth and fusion.

Collagen-based sponges have shown a great deal of promise recently as bone graft substitute materials (Wigfield and Nelson, 2001). These sponges are composed primarily of bovine type I collagen and may (HEALOS, Depuy Spine; CRM, Medtronic Inc.) or may not (INFUSE, Medtronic Inc.) be reinforced with calcium phosphates. Collagen sponges have a fibrous structure with a high degree of interconnected porosity and are completely resorbable*in vivo*. These constructs have been used in spine fusion, primarily for the delivery of osteoinductive growth factors, such as recombinant human bone morphogenetic protein-2 and -7 (rhBMP-2, rhBMP-7 or OP-1). While the growth factor-collagen sponges constructs have enjoyed widespread success, they still lack the ability to support biomechanical loading as a

standalone implant. As such, they must be used in conjunction with permanent hardware, such as titanium or poly ether ether ketone (PEEK) fusion cages.

Resorbable Polymers as Emerging Candidates for Bone Graft Substitute Applications

Resorbable polymers, such as poly-L-lactic acid (PLLA) and poly-L-glycolic acid (PLGA), have been investigated for use as bone graft substitute materials (Georgiou et al., 2007; Kruyt et al., 2004; Mathieu et al., 2005; Tsuji et al., 2003; van Dijk et al., 2003). While not currently used for this application clinically, these materials have shown excellent biocompatibility and resorb predictably *in vivo*. Degradation is dominated by hydrolytic cleavage of ester linkages in the polymer backbone. The byproducts of degradation are lactic and/or glycolic acid, which are easily metabolized *in vivo* to pyruvate, water and carbon dioxide. Controlled degradation of the polymer has been shown to facilitate slow release of therapeutic substances, such as growth factors used to induce bone formation.

As previously stated, an interconnected porous morphology is a requirement of bone graft substitute materials. The porous morphology supports cellular infiltration and nutrient transport affected by neovascularization. Numerous methods have also been shown to be effective in synthesizing porous constructs from PLLA and PLGA polymers, including thermal-induced phase separation, particulate leeching and three dimensional free-form fabrication techniques. These techniques require the use of volatile organic solvents, such as chloroform or dichloromethane, to dissolve the polymer. Even after several hours under vacuum, residual levels of organic solvent persist within the material. These solvents leech from the construct when it is placed in an aqueous environment and can induce an inflammatory response.

Evidence also exists supporting the claim that organic solvent content can also induce a cytotoxic response, both *in vitro* and *in vivo*.

Despite all of the potential benefits of resorbable polymer constructs, limited mechanical strength, especially of porous constructs, has kept PLLA and PLGA from clinical use in structural bone graft substitute applications. Numerous filler materials have been investigated as agents to mechanically reinforce porous resorbable polymer matrices. Calcium phosphates including HA and β-TCP have shown efficacy in increasing the mechanical strength of porous PLLA and PLGA constructs. Calcium phosphates also increase bioactivity of the constructs, by enhancing osteoblastic adhesion and differentiation. Single and multi-walled carbon nanotubes have also been used to reinforce porous PLLA and PLGA constructs. Despite the numerous filler materials investigated to reinforce the mechanical properties of porous resorbable polymer matrices, compressive strengths of these constructs are still below the threshold required for spine fusion applications. This lack of reinforcement efficacy has been attributed to poor filler-polymer matrix interaction. It has also been observed that current techniques employed to disperse fillers in resorbable polymers are not able to overcome the agglomeration of small particles. Agglomerated particles within a polymer matrix lead to reduced mechanical properties. Additionally, a lack of positive interaction between the polymer chains and the filler particles results in poor restriction of polymer chain mobility, which is a necessary component of reinforcement in polymer matrix composites.

Resorbable polymer nanocomposites demonstrate a significant amount of promise as bone graft substitute materials. To overcome current challenges associated with nanocomposite technology, a novel material formulation and synthesis route is needed. The proposed method must ultimately result in a resorbable construct with an interconnected porous morphology,

which is capable of supporting new bone formation, as well as withstanding biomechanical loading.

References

Buck B., Malinin T. and Brown M. 1989. Bone transplantation and human immunodeficiency virus: An estimate of risk of acquired immunodeficiency syndrome (AIDS). Clinical Orthopaedics and Related Research. 240, 129-136.

Day SM., Ostrum RF, Chao EYS., Rubin CT., Aro HT., Einhorn TA. 2000. Bone injury regeneration and repair. In: Einhorn TA, Buckwalter JA, Simon SR (Eds.). Orthopaedic Basic Science – 2nd Edition. American Academy of Orthopaedic Surgeons, Rosemont, IL. pp. 371 – 399.

DePalma A.F., Rothman R.H., Lewinnek G.E. and Canale S.T. 1972. Anterior interbody fusion for severe cervical disk degeneration. Surgical Gynecology and Obstetrics 134, 755-758.

Fini, M., Giavaresi, G., Torricelli, P., Borsari, V., Giardino, R., Nicolini, A. and Carpi, A. 2004. Osteoporosis and biomaterial osteointegration. Biomedicine & Pharmacotherapy 58, 487-493.

Georgiou, G., Mathieu, L., Pioletti, D.P., Bourban P.-E., Manson, J.-A.E., Knowles, J.C., and Nazhat, S.N. 2007. Polylactic acid-phosphate glass composite foams as scaffolds for bone tissue engineering. Journal of Biomedical Materials Research: Part B Applied Biomaterials 80B, 322-331.

Hu R.W. and Bohlman H.H. 1994. Fracture at the iliac bone graft harvest site after fusion of the spine. Clinical Orthopaedics and Related Research 309, 208-213.

Keaveny TM., Hayes WS. Mechanical properties of cortical and trabecular bone. In: Hall BD. (Ed.) Bone. CRC Press, Boca Raton, FL. pp: 285-344.

Kruyt M.C., van Gaalen S.M., Oner F.C., Verbout A.J., de Bruijn J.D., Dhert W.J.A. 2004. Bone tissue engineering and spinal fusion: the potential of hybrid constructs by combining osteoprogenitor cells and scaffolds. Biomaterials 25, 1463-1473.

Malloy K.M. and Hilibrand, A.S. 2002. Autograft versus allograft in degenerative cervical disease. Clinical Orthopaedics and Related Research 394, 27-38.

Mathieu, L.M., Montjovent, M.-O., Bourban, P-E., Pioletti, D.P. and Manson, J.-A.E. 2005. Bioresorbable composites prepared by supercritical fluid foaming. Journal of Biomedical Materials Research: Part A 75A, 89-97.

Nugent P.J. and Dawson, E.G. 1993. Intratransverse process lumbar arthrodesis with allogenic fresh-frozen bone graft. Clinical Orthopaedics and Related Research 287, 107-111.

Samartzis D., Shen F.H., Goldberg E.J. and An, H.S. 2005. Is autograft the gold standard in achieving radiographic fusion in one-level anterior cervical discectomy and fusion with rigid anterior plate fixation? Spine 30(15), 1756-1761.

Suetsuna, F., Yokoyama, T., Kenuka E. and Harata, S. 2001. Anterior cervical fusion using porous hydroxyapatite ceramics for cervical disc herniation: A two year follow-up. The Spine Journal 1(5), 348-357.

Tsuji, H. and Yamada, T. 2003. Blends of aliphatic polyesters. VIII. Effects of poly (L-lactide-co-ε-caprolactone) on enzymatic hydrolysis of poly(L-lactide), poly(ε-caprolactone), and their blend films. Journal of Applied Polymer Science 87, 412-419.

Urist MR. 1965. Bone: formation by autoinduction. Science 150(698), 893-899.

van Dijk, M., Smit, T.H., Arnoe, M.F., Burger, E.H. and Wuisman, P.I. 2003. The use of poly-L-lactic acid in lumbar interbody cages: design and biomechanical evaluation in vitro. European Spine Journal 12, 34-40

Wigfield C.C., Nelson R.J. 2001. Non-autologousinterbody fusion materials in cervical spine surgery: How strong is the evidence to justify their use? Spine 26(6), 687-694.

Wimmer C., Krismer M., Gluch H., Ogon M., and Stockl B. 1999. Autogenic versus allogenic bone grafts in anterior lumbar interbody fusion. Clinical Orthopaedics and Related Research 360, 122-126.

Wuisman P.I.J. and Smit, T.H. 2006. Bioresorbable polymers: heading for a new generation of spinal cages. European Spine Journal 15, 133-148.

Zdeblick T.A. and Ducker T.B. 1991. The use of freeze-dried allograft bone for anterior cervical fusions. Spine 16(7), 726-729.

Zdeblick T.A., CookeM.E., Kunz D.N., Wilson D. and McCabe, R.P. 1994. Anterior cervical discectomy and fusion using a porous hydroxyapatite bone graft substitute. Spine 19(20), 2348-2357.

CHAPTER 3: POLYMER-MONTMORILLONITE CLAY NANOCOMPOSITES

Background

Resorbable polymers show promise as potential materials for use as synthetic bone graft substitute materials. Their predictable degradation *in vivo* and track record of biocompatibility in multiple forms speak to this promise. Unfortunately, the mechanical properties of resorbable polymers with a porous morphology are not sufficient for load bearing applications in the human spine or long bones of the extremities. Due to this poor mechanical behavior, there is significant interest in developing a composite material. Successful creation of a composite material would still allow physicians to take advantage of the desirable physical and chemical properties of the polymer, while reinforcing the matrix with a functional filler material. Further, since bone is essentially a composite material (collagen matrix reinforced by hydroxyapatite) it is logical to replace that tissue with a synthetic composite material. Nanocomposites consisting of a polymeric matrix reinforced by layered silicate fillers are a strong candidate for bone graft substitutes. Specifically, lactic or glycolic acid-based polymers reinforced with organically modified Montmorillonite clays (nanoclay) are promising options for this biomedical application. The exceptional improvements in mechanical properties associated with loading polymer matrices with nanoclays have stimulated a significant amount of research for non-biomedical applications, as well.

Structure of Montmorillonite Clay

Montmorillonite clays are naturally-occurring layered aluminosilicate minerals that are the main constituent of Bentonite, which is found in volcanic ash. The structure of the clay is characterized by an octahedral sheet sandwiched by two tetrahedral sheets. The octahedral sheet

is composed primarily of aluminum oxide, while the tetrahedral sheets are primarily silicon oxide (Pavlidou and Papaspyrides, 2008). Aluminum atoms within the octahedral sheet can be substituted with other cations, which require a positive charge to balance the structure. This positive charge often comes in the form of an alkaline earth cation (most often Na^+, in Montmorillonite), which reside on top of the tetrahedral sheet (Ray and Okamoto, 2002). The thickness of a single layer of Montmorillonite is approximately 1 nm, while the width can vary from 30 nm to several microns, giving the clays an extremely high aspect ratio and thus a very high reinforcement capacity in polymer matrices. As is the case with many aluminosilicates, the tetrahedral-octahedral-tetrahedral structure repeats to form a layered structure with a regular van der Waals gap between layers, referred to as the gallery spacing (Pavlidou and Papaspyrides, 2008). Clays can be organically modified to increase the spacing between layers via ion exchange with cationic surfactants, such as alkyl ammonium salts. The increase in intergallery spacing improves the dispersion of nanoclay within polymeric matrices and reduces the likelihood of particle agglomeration, which can negatively impact mechanical behavior (Horsch et al., 2006).

Polymer-Clay Nanocomposites

Polymer-nanoclay nanocomposites were first introduced by Toyota in the 1990's and were based on Nylon-6 reinforced with unmodified Montmorillonite clay (Pavlidou and Papaspyrides, 2008; Ray and Okamoto, 2002). Numerous processing methods exist to disperse natural and organically modified Montmorillonite clays within polymer matrices. Regardless of the method, the overall goal remains the same: maximize polymer nanoclay interaction to reduce polymer chain mobility, thus enhancing static and dynamic mechanical properties. In order to maximize polymer-clay interaction, processing methods are aimed at delaminating the layered

silicate structure into individual clay platelets (1 nm x 30 nm), which are subsequently dispersed in a random orientation throughout a polymer matrix. Delamination and dispersion of the layered structure of clay is accomplished by infiltration of the intergallery space by polymer chains. Infiltration of polymer chains may be significant enough to cause delamination of the layered structure resulting in individual clay platelets dispersed throughout the matrix. Increased motion of the polymer chains within the intergallery space during high-shear mixing may also encourage delamination and dispersion of clay platelets.

There exists three different classes of polymer-layered silicate nanocomposites, which are based on the extent of dispersion of clay platelets in the polymer. The first type is known as an intercalated nanocomposite and is characterized morphologically by infiltration of polymer chains within the intergallery space of the clay. The infiltration of the polymer increases the intergallery spacing of the clay, but does not result in delamination of the layered structure. Intercalated morphologies lend themselves to both strong polymer-clay interaction, as well as considerable nanoclay-nanoclay interaction since the layered structure has not become completely delaminated. Intercalated nanocomposites typically exhibit a high elastic modulus (tensile), significantly reduced ultimate strength and improved fracture toughness. The improvement in fracture toughness is thought to be related to the increased surface area, associated with intercalated morphologies. A second class of nanocomposites, which is closely related to the intercalated morphology, is termed flocculated. Similar to intercalated nanocomposites, polymer chains have infiltrated the intergallery space, but have not resulted in platelet delamination and subsequent dispersion. The main difference between intercalated and flocculated nanocomposites is the interaction between whole clay particles within the polymer matrix. In flocculated nanocomposites, clay particles, each consisting of a layered structure,

interact with each other leading to flocculation or agglomeration of the particles within the matrix. Interaction between clay particles is mediated by the hydroxylated silicate layers. Flocculated nanocomposites have mechanical property changes similar to that of intercalated nanocomposites, but tend to have lower ultimate strength and stiffness. These similarities arise from the fact that there is still significant infiltration of polymer chains within the layered structure of the nanoclay. However, flocculation of the particulate within the polymer matrix often leads to significant variation in properties due to non-uniform dispersion of the clay within the matrix. Non-unifiorm dispersion is attributed to nanoclay-nanoclay interaction, which leads to the development of clay-rich and clay-poor regions of a nanocomposites construct. The final class of nanocomposites is the exfoliated structure. This morphology is characterized by clay particles with layered structures that have been completely delaminated and dispersed at random throughout the polymer matrix, as shown in Figure 1. In exfoliated nanocomposites, polymer chain infiltration and subsequent interaction overcome platelet-platelet attraction resulting in complete delamination and dispersion of individual clay platelets throughout the matrix. Exfoliated nanocomposites typically exhibit significant increases in both static and dynamic mechanical properties, even at low clay loading levels. Exfoliated nanocomposites do not exhibit as significant of improvements in fracture toughness when compared with intercalated nanocomposites. However, the random orientation of individual clay platelets within the polymer matrix does result in toughening compared to native polymer structures.

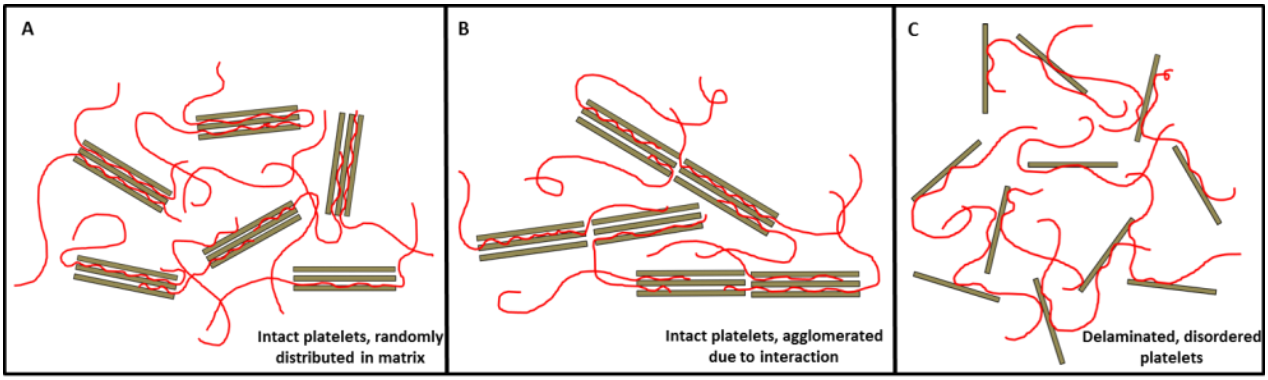

Figure 1. *Illustration of clay platelet morphology in intercalated (A), intercalated-flocculated (B) and exfoliated (C) polymer-clay nanocomposites.*

Supercritical CO_2 Processing of Polymer-Clay Nanocomposites

To achieve the various morphologies of polymer-clay nanocomposites, a number of processing methods have been employed including in situ polymerization, melt intercalation, extruding and solvent processing (Pavlidou and Papaspyrides, 2008; Ray and Okamoto, 2002). Another method of processing exists, which utilizes supercritical carbon dioxide as the solvent for processing (Horsch et al., 2006; Manitiu et al., 2008). Supercritical carbon dioxide ($scCO_2$) processing is technique that is growing in popularity in terms of its use in the creation of polymer-clay composites. $scCO_2$processing involves mechanical mixing of nanoclays with polymers. The subsequent mixture is poured into a mold and placed inside of a sealed, high-pressure reactor vessel. The vessel is then filled with CO_2 from a high pressure source. The internal temperature and pressure of the vessel is then elevated to bring the CO_2 to the supercritical region of the temperature-pressure phase diagram. In this region, CO_2 has the excellent mass transfer characteristics, as simultaneously possesses the density of the liquid state and diffusivity of the gas state. Elevation of the CO_2 to the supercritical region also increases the solubility of many polymer systems. During saturation and subsequent temperature-pressure

elevation, the polymer becomes solvated within the reactor vessel. CO_2 also diffuses into the intergallery region of the clay particles, as solvated polymer chains also infiltrate the layered structure. After a specified duration of exposure to the supercritical fluid, the reactor vessel is rapidly depressurized, inducing a thermodynamic instability within the polymer-clay mixture. Rapid CO_2 bubble nucleation and growth, as well as polymer chain infiltration, delaminate the layered structure of the nanoclay and uniformly disperse the filler throughout the matrix (Horsch et al., 2006; Manitiu et al., 2008).

Proposed Use of $scCO_2$ Processing to Create Synthetic Bone Graft Substitute Materials

While $scCO_2$ processing has been used primarily in the synthesis of polymer nanocomposites for automotive and textile applications, it may be useful in the development of synthetic bone graft substitute constructs (Baker et al., 2009; Baker et al., 2011). The proposed material would be composed organically modified nanoclay dispersed in a poly-D-lactide (PDLA) matrix, with an interconnected porous morphology. The hypothesized method of synthesis includes mechanical mixing of as-received, organically-modified Montmorillonite clay with particles of PDLA in a mold. The mixture would be placed in a high pressure reactor vessel, and subjected to CO_2 at elevated temperatures and pressures. Following a specific duration of saturation, the system would be depressurized. Catastrophic depressurization delaminates the layered platelet structure of the clay, as previously described. In addition to delamination of clay platelets, CO_2 bubble nucleation and growth will take place during depressurization. As the structure solidifies, the coalescence of CO_2 bubbles yields an interconnected porosity throughout the construct. Both pressure of the composite material

expanding against the mold, as well as heat transfer characteristics of the mold will contribute to the formation of a dense shell, resembling the structure of cortical bone. This shell will transition abruptly to a porous core, which resembles the interconnected porous morphology of cancellous bone. The resulting construct will mimic the dense-porous morphology of cortico-cancellous grafts used in structural bone grafting applications. *In vivo*, it is proposed that the porous core will facilitate three-dimensional cellular infiltration by osteoprogenitor cells. The average pore diameter will also be sufficient to support neovascularization that is necessary for nutrient transport throughout the construct. The dense "cortical" shell of the construct will support biomechanical loading in a manner similar to cortico-cancellous bone graft.

Supercritical CO_2 processing has been used by other researchers to create porous polymeric scaffolds and even composite materials (Georgiou et al., 2005; Mathieu et al., 2008). Mathieu et al. synthesized poly(L-lactic acid) foams reinforced with calcium phosphate particulate. From the same group, Georgeiou, et al. used $scCO_2$ processing to create phosphate glass-reinforced porous PLLA constructs. In both instances, considerable improvements in *in vitro* biologic response was observed. However, both studies demonstrated only modest gains in static mechanical properties. The authors attributed this to poor dispersion of the filler materials within the resorbable polymer matrix. It is hypothesized that increased positive interaction between the polymer chains and filler material will result in improved dispersion, which should lead to uniform structural properties.

A key aspect of the $scCO_2$ process that makes it especially attractive for the application of creating bone graft substitutes is the ability to impart a porous morphology to the constructs. Pores in the construct arise from the nucleation of CO_2 bubbles within the solvated polymer upon depressurization of the vessel. In a pure polymer construct, the formation of pores follows a

classical homogenous nucleation model. However, when processing nanocomposites, heterogeneous nucleation of CO_2 bubbles dominates. As described by Tomasko, the rate of heterogeneous nucleation can be described by classical heterogeneous nucleation theory, as described below:

$$N = f_1 C_1 \exp[-\Delta G^*_{het}/kT] \quad [1]$$

where f_1 is the gas frequency factor and C_1 is the concentration of nucleation sites. For the purposes of a polymer-clay nanocomposite processed by $scCO_2$, C_1 is proportional to the concentration of clay platelets within the polymer. In this Ahrennius eqution, *k* is also the Boltzmann constant and T is absolute temperature. The Gibb's free energy of heterogenous nucleation (ΔG^*_{het}) is a function of the interfacial tension between the supercritical fluid and polymer-clay mixture (σ), supersaturation of the mixture with CO_2 ($\Delta P = P_{saturation} - P_{actual}$) and the three component contact angle (θ) at the polymer-clay-fluid interface. ΔG^*_{het} can be expressed as:

$$\Delta G^*_{het} = 16\pi\sigma^3 f(\theta)/(3\Delta P^2) \quad [2]$$

where,

$$f(\theta) = \tfrac{1}{4}(2+\cos\theta)(1-\cos\theta)^2 \quad [3]$$

From these equations (Eq. 1, Eq. 2 and Eq. 3), it can be seen that $scCO_2$ processing parameters can play an important role in determining the porous morphology of bone graft substitute materials. Specifically, the alteration of saturation pressure, processing temperature and effective clay concentration should have a significant effect on the rate of bubble nucleation.

The C_1 term in Equation 1 actually shows a dependence of the nucleation rate on the dispersion of clay within the polymer matrix. Fully exfoliated nanocomposites would have a higher concentration of nucleation sites, compared to intercalated, or intercalated-flocculated nanocomposite morphologies. As Zeng, et al. found, an increased number of nucleation sites in well-dispersed PMMA-clay nanocomposites results in the formation of a material with a high degree of total porosity and pores with a small average diameter (Zeng et al., 2003).

Supercritical CO2 processing is a promising method for the rapid synthesis of resorbable polymer-clay nanocomposites for bone graft substitute applications. The process itself lends itself to a substantial amount of control over the resulting morphology and properties of the synthesized construct. An additional benefit to utilizing scCO2 processing is the lack of harmful organic solvents during processing. Since lactic acid polymers are very soluble in CO2, the use of chloroform and dichloromethane is no longer a concern.

References

Baker KC, Bellair R, Manitiu, Herkowitz HN, Kannan RM. 2009. Structure and mechanical properties of supercritical carbon dioxide processed porous resorbable polymer constructs. Journal of the Mechanical Behavior of Biomedical Materials 2(6), 620-626.

Baker KC, Manitiu M, Bellair R, Gratopp CA, Herkowitz HN, Kannan RM. 2011. Supercritical carbon dioxide processed resorbable polymer nanocomposite bone graft substitutes. Acta Biomaterialia. May 14 [Epub Ahead of Print].

Horsch S, Serhatkulu G, Gulari E, Kannan RM. Supercritical CO_2 dispersion of nano-clays and clay/polymer nanocomposites. Polymer 47, 7485-7496.

Manitiu M, Bellair RJ, Horsch S, Gulari E, Kannan RM. 2008. Supercritical carbon dioxide-processed dispersed polystyrene-clay nanocomposites. Macromolecules 41, 8038-8046.

Pavlidou S, Papaspyrides CD. 2008. A review on polymer-layered silicate nanocomposites. Progress in Polymer Science 33, 1119-1198.

Ray SS, Maiti P, Okamoto M, Yamada K, Ueda K. 2002. New polylactide/layered silicate nanocomposites. 1. Preparation, characterization and properties. Macromolecules 35(8), 3104-3110.

Tsimpliaraki A, Tsivintzelis I, Marras SI, Zuburtikudis I, Panayiotou C. 2011. The effect of surface chemistry and nanoclay loading on the microcellular structure of porous poly(D,L lactic acid) nanocomposites. The Journal of Supercritical Fluids 57(3), 278-287.

Zeng C, Han X, Lee LJ, Koelling KW, Tomasko DL. 2003. Polymer-clay nanocomposite foams prepared using carbon dioxide. Advanced Materials 15(20), 1743-1747.

CHAPTER 4: STRUCTURE AND MECHANICAL PROPERTIES OF SUPERCRITICAL CARBON DIOXIDE PROCESSED POROUS RESORBABLE POLYMER CONSTRUCTS: INFLUENCE OF POLYMER COMPOSITION AND PROCESSING PARAMETERS

Introduction

Currently, there are over 1 million surgical procedures performed annually in the United States that require the use of bone graft materials. Spinal fusion, which is a surgical intervention used to alleviate nerve root impingement and restore spinal segmental stability, accounts for greater than 60% of bone graft material usage (www.aaos.org). In interbody (or intervertebral) spinal fusion procedures, the gel-like nucleus pulposus is removed, the vertebral endplates are decorticated and a bone graft material is placed in the disk space between adjacent vertebrae. The role of the bone graft material is to facilitate bone growth and subsequent fusion between the adjacent vertebrae, while withstanding biomechanical loading. For this reason, the highly porous, yet structurally stable bone harvested from the antero-superior portion of the patients' iliac crest is considered to be the gold standard in achieving successful fusion (Samartzis et al., 2005; Wimmer et al., 1999; Zdeblick et al., 1994).

Despite the high clinical success surrounding the use of autologous iliac crest bone in spinal fusion procedures, the graft harvest procedure is not without risk. Donor site complication rates as high as 33% have been reported in the literature and include an increased probability of iliac wing fracture, tissue necrosis and infection (DePalma et al., 1972; Hu and Bohlman, 1994; Samartzis et al., 2005; Wimmer et al., 1999). Allogenic iliac crest has been used in place of autograft to reduce these complications, but has yet to attain comparable rates of fusion (Samartzis et al, 2005; Wimmer et al., 1999).

Synthetic bone graft substitutes consisting of porous metals, or calcium phosphate-based ceramics have been introduced (Sidhu et al., 2001; Zdeblick et al., 1994). While the architecture

of these substitute materials does accurately simulate the trabecular morphology of iliac crest, the fracture toughness of ceramic-based constructs is a concern with reports in the literature of subsidence and loss of disk space height (Sidhu et al., 2001; Zdeblick et al., 1994). Porous metals are also not without disadvantage as they obstruct medical imaging studies and are a source of increased patient risk, due to device permanence (Lippman et al, 2004; Sidhu et al., 2001; Wuisman and Smit, 2006).

Resorbable polymers, which are currently in use in orthopaedic surgery, avoid the problems associated with permanent metallic constructs since the polymers degrade at a predictable rate in vivo (Lippman et al., 2004; Vacaaro et al., 2004; Wuisman and Smit, 2006). The radiolucency of the polymers also facilitates *in vivo* imaging without construct artifact (Lippman et al., 2004; Vacaaro et al., 2004; Wuisman and Smit, 2006). Gradual dissolution of the polymers *in vivo* also guarantees that a significant percentage of the biomechanical loading will be transferred to de novo bone. This load transmission is essential to bone growth and remodeling according to Wolff's Law (Lippman et al., 2004; Samartzis et al., 2005; Sidhu et al., 2001; Vacaaro et al., 2004; Wuisman and Smit, 2006).

Resorbable polymer devices currently in use are not suited for bone graft applications due to the non-porous nature of their structure. Numerous techniques have been explored in tissue engineering literature, which seek to synthesize resorbable polymer constructs with porous structures (Georgiou et al, 2007; Hu Y et al., 2001; Kim et al., 2007; Mathieu et al., 2005; Nam and Park, 1999; Teng et al., 2007; Wang Y et al., 2008; Zeng et al., 2003). Phase separation processes, which involve the dissolution of a polymer in a volatile organic solvent and subsequent induction of a thermodynamic instability (i.e. rapid changes in temperature and/or pressure), have been used with success (Hu Y et al., 2001; Nam and Park, 1999; Wang Y et al.,

2008). Wang et al. recently reported success in using a collagen/PLA/hydroxyapatite composite fabricated by a freeze-drying method in the healing of a 15 mm segmental defect in the rabbit radius.

Despite reported pre-clinical successes, there is a biological concern regarding the residual solvent content within the porous polymer structures. Recently, supercritical carbon dioxide ($scCO_2$) processing has been investigated as a biologically and environmentally friendly alternative to creating porous, resorbable polymer structures (Georgiou et al, 2007; Kim et al., 2007; Mathieu et al., 2005; Teng et al., 2007; Zeng et al., 2003). Several of the studies have examined the effects of process parameters and nanoparticle incorporation on the resulting structures. To date, no literature exists which compares the architectural, mechanical and surface chemical properties of porous resorbable poly (lactic-co-glycolic acid) (PLGA) polymer constructs prepared by $scCO_2$ processing.

Synthesis of porous, resorbable polymer constructs with differing lactide-to-glycolide ratios may aid in the development of bone grafts with tailored degradation kinetics and mechanical properties. An understanding of the interplay between processing parameters and polymer chemistry will lead to reproducible synthesis of polymer constructs with porous architecture approximating that of trabecular bone. Therefore, this study seeks to evaluate the effect of $scCO_2$ processing parameters on the resulting architecture of porous, resorbable PLGA constructs with different glycolic acid contents. Additionally, the effect of lactide-to-glycolide ratio on the resulting architecture, static mechanical properties and hydrophilic surface character will be characterized.

Materials and Methods

Pure poly-D-lactide (100PDLA) and poly-D-lactide-co-glycolide with molar ratios of D-lactide to glycolide of 85:15 (85:15PDLGA) and 65:35 (65:35PDLGA) were purchased from Lakeshore Biomaterials. All polymers had intrinsic viscosities in the range of 0.40-0.60 dL/g and were terminated by ester groups.

Polymers were ground to an average particle size of 250-500 μm and placed in 20 mL borosilicate glass vials (28 mm O.D. x 61 mm H). The vials restrict radial expansion of the polymer, but allow for expansion in the vertical direction. The polymer-filled vials, each with 2.0 g of ground polymer, were placed into a supercritical fluid reactor and saturated with CO_2. The internal pressure was elevated to 10.3, 13.8, or 27.6 MPa at an internal temperature of 35^{o}C, or 100^{o}C to induce a supercritical phase transformation in the CO_2. After 20 minutes of soaking, the reactor was rapidly depressurized at a rate of 0.3-0.4 Mpa/s. To examine the effect of confining the samples after processing, the glass vials were either broken immediately, or kept intact for 48 hours.

Constructs were freeze-fractured with liquid nitrogen in the vertical (direction of CO_2 escape) and transverse (direction perpendicular to CO_2 escape) directions. Fracture surfaces were coated with a thin film of AuPd and subjected to scanning electron microscopy (SEM, JEOL JSM 6400, JEOL Ltd.). SEM was performed at a working distance of 15 mm and an accelerating voltage of 20 kV. Measurements of pore size and pore wall thickness and assessments of pore interconnectivity were performed using digital image analysis software (Revolution, 4Pi Analysis). Measurements were conducted on a minimum of three vertical and three transverse fracture surfaces. At least eight images were taken from each fracture surface. Pore dimensions were measured for 20 pores per fracture surface image.

Mechanical testing was performed on samples with interconnected pores ranging in diameter from 150-250 μm, which is similar to the architecture of iliac crest bone (Mosekilde and Mosekilde, 1982; Samartzis et al., 2005). Cylindrical cores were removed from the specimens using a 10 mm diameter osteochondralautograft transplant system (OATS, Arthrex Inc.). The sample areas cored were chosen to not include the dense cortical shell that was formed at the periphery of the foams during processing. The cores were sectioned with a scalpel to a height of 10 mm. Six samples from each co-polymer formulation were then subjected to axial compression in a servo-hydraulic material testing machine (850 Mini-Bionix Bi-axial, MTS Corporation). Loading took place between lubricated, stainless steel platens at a rate of 0.5 mm/min, as previously described (Georgiou et al, 2007; Mathieu et al., 2005). The samples were compressed to a displacement equal to 50% of their original height. This displacement was chosen because a loss of disk space height of this magnitude would represent a compromise of neurovascular structures (Zdeblick et al., 1994). Compressive strength of the constructs was determined by dividing the peak load by the original cross-sectional area. The compressive modulus was quantified by calculating the slope of the elastic region of the stress-strain curve. Elastic recovery of the samples was determined by measuring the height of the samples five minutes after mechanical testing. The recovered height was divided by the original height and reported as a percentage of the original height.

Water uptake experiments were performed on 10 mm x 10 mm cylinders sectioned from the same cores used for mechanical testing. Five cylinders from each of the polymer formulations were initially weighed and subsequently immersed in deionized water. The cylinders were removed from the water and weighed at 1, 2, 4, 8, 12 and 24 hours. Prior to weighing, the samples were placed on absorbent towels for 5 minutes and subjected to

compressed air (145 psi, or 1.0 Mpa). The overall change in mass was determined by dividing the difference between the new weight and the original weight by the original weight and multiplying by 100%. Water uptake experiements are used frequently to assess the ability to load exogenous growth factors or autologous bone marrow aspirate into porous constructs. Additionally, water uptake experiments provide information about the ability of cells to penetrate a matrix. Finally, water uptake experiments are a very bulk method to determing surface character of a materials. The surface character and hydrophilicity of implant materials have been shown to influence osteoblast response (Baker et al., 2006; Bren et al., 2004).

Results

Effects of Processing Conditions and Polymer Composition

Processing temperature was found to influence the pore size of $scCO_2$ processed constructs (Figure 1, Table 1) with unconstrained radial expansion. Samples processed at 35^{o}C exhibited mean pore sizes of 238.0 μm (+/- 4.83 μm), with a few pores as large as 400 μm in diameter. Pore walls were 32.23 μm (+/- 2.47 μm) thick on average. In contrast, the samples processed at 100^{o}C had pore sizes that averaged 21.5 μm (+/- 1.53 μm), 17.03 μm (+/- 2.33 μm) thick pore walls and a very low extent of pore interconnectivity.

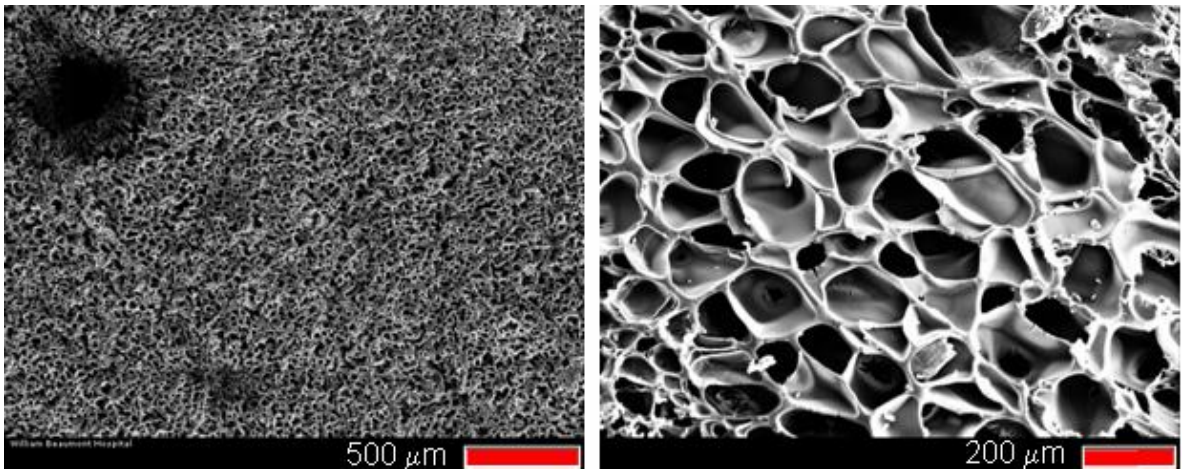

FIGURE 1. *SEM images of longitudinal fracture surfaces of 65:35PDLGA samples processed at 100°C (left) and 35°C (right) with a pressure of 13.8 Mpa and unconstrained radial expansion.*

TABLE 1. *Pore diameters and pore wall thicknesses of polymeric constructs as a function of temperature (unconstrained radial expansion).*

Polymer	Average Pore Wall Diameter (mm)		Average Pore Wall Thickness (mm)	
100 PDLA				
35°C – 2000 psi	236.2	±4.8	32.1	±1.1
100°C – 2000 psi	22.3	±1.3	17.4	±3.5
85:15 PDLGA				
35°C – 2000 psi	238.6	±6.5	33.0	±4.2
100°C – 2000 psi	22.1	±2.1	16.8	±1.2
65:35 PDLGA				
35°C – 2000 psi	239.3	±3.2	31.6	±2.1
100°C – 2000 psi	20.1	±1.2	16.9	±2.3

Construct architecture was found to be nearly identical for samples processed at 10.3, 13.8, 26.7 Mpa. Processing samples at a higher pressure did not increase the pore diameters. Samples processed at a temperature of 100^{o}C again showed an order of magnitude decrease in pore size, in comparison to samples processed at 35^{o}C, regardless of pressure.

Removal of the samples was accomplished by shattering the glass vials that contained the sample. When samples were processed at a temperature of 35^{o}C and were immediately removed from the vials, a rapid increase in sample volume occurred. This volume change was not observed upon removal after 48 hours of confinement in the glass vials. Confining the samples for 48 hours after $scCO_2$ processing had an effect on both average pore size and pore interconnectivity (Figure 2). Average pore diameters decreased to 183.9 μm, 216.3 μm and 203.7 μm for 100PDLA, 85:15PDLGA and 65:35PDLGA constructs processed at 35^{o}C, respectively. Confinement also increased the degree of interconnectivity of the constructs processed at 35^{o}C, as observed by SEM. Despite the fact that no method was employed to directly quantify interconnectivity, qualitative characterization of construct architecture from SEM images revealed that constrained samples showed more open pores and pore-pore connections. No changes in construct architecture due to confinement were observed for samples processed at 100^{o}C, again demonstrating the importance of processing temperature.

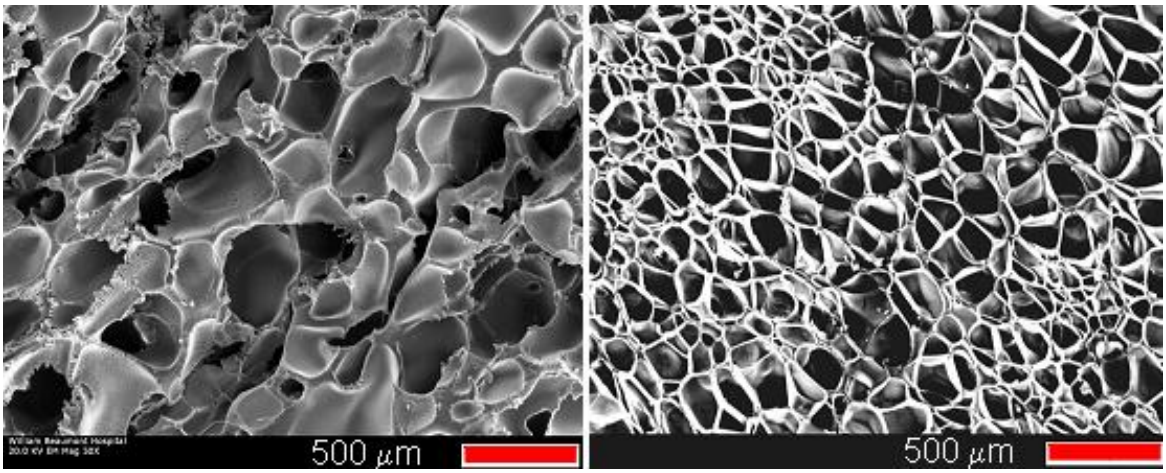

FIGURE 2. *SEM images of longitudinal cross-sections of 85:15 PDLGA constructs unconstrained (left) and constrained (right) after processing.*

Supercritical CO_2 processing of the resorbable polymers in glass vials results in the formation of a dense outer layer on the constructs, which is rigidly attached to the porous core (Figure 3). It should be noted that the samples used in this study underwent mechanical testing *without* the dense outer layer intact.

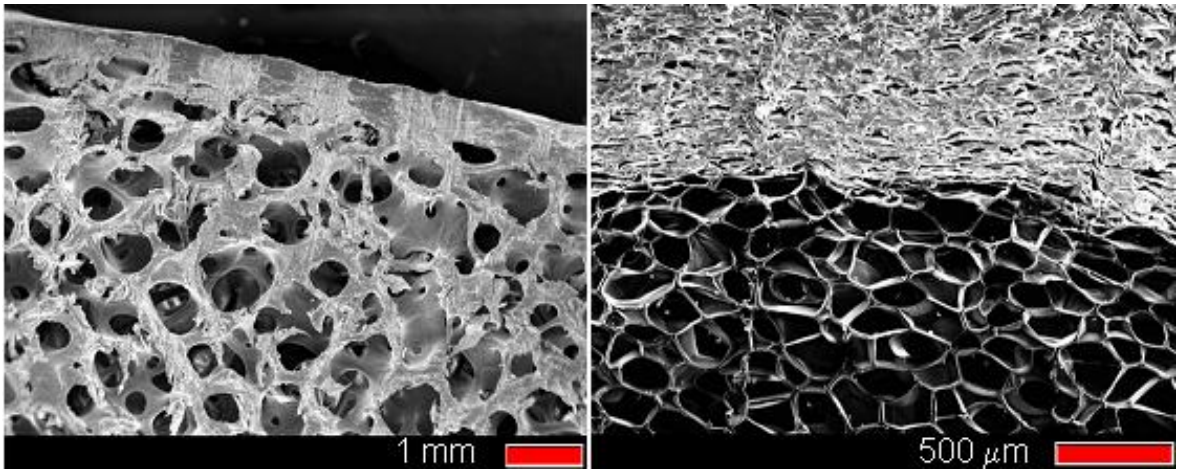

FIGURE 3. *SEM images of an iliac crest bone graft (left) and a 100PDLA construct showing similar porous morphology and "cortical" shell.*

Mechanical Properties of Constructs

Mechanical testing of the porous polymer constructs yielded information about the resulting static mechanical properties of the constructs. Overall, 85:15 PDLGA had the highest compressive strength (4.35 +/- 1.78 Mpa) and compressive modulus (36.41 +/- 12.13), as shown in Table 2. The compressive strength of 100 PDLA (3.40 +/- 0.54 Mpa) and compressive modulus (33.79 +/- 9.3 Mpa) were lower than that of the 85:15 PDLGA, but significantly higher than the compressive strength and modulus of 65:35 PDLGA (1.11 +/- 0.34 Mpa and 6.56 +/- 4.04 Mpa, respectively). Elastic recovery was greatest for the 65:35 PDLGA constructs (70.92%), followed by the 100 PDLA (63.84%) and 85:15 PDLGA constructs (61.89%).

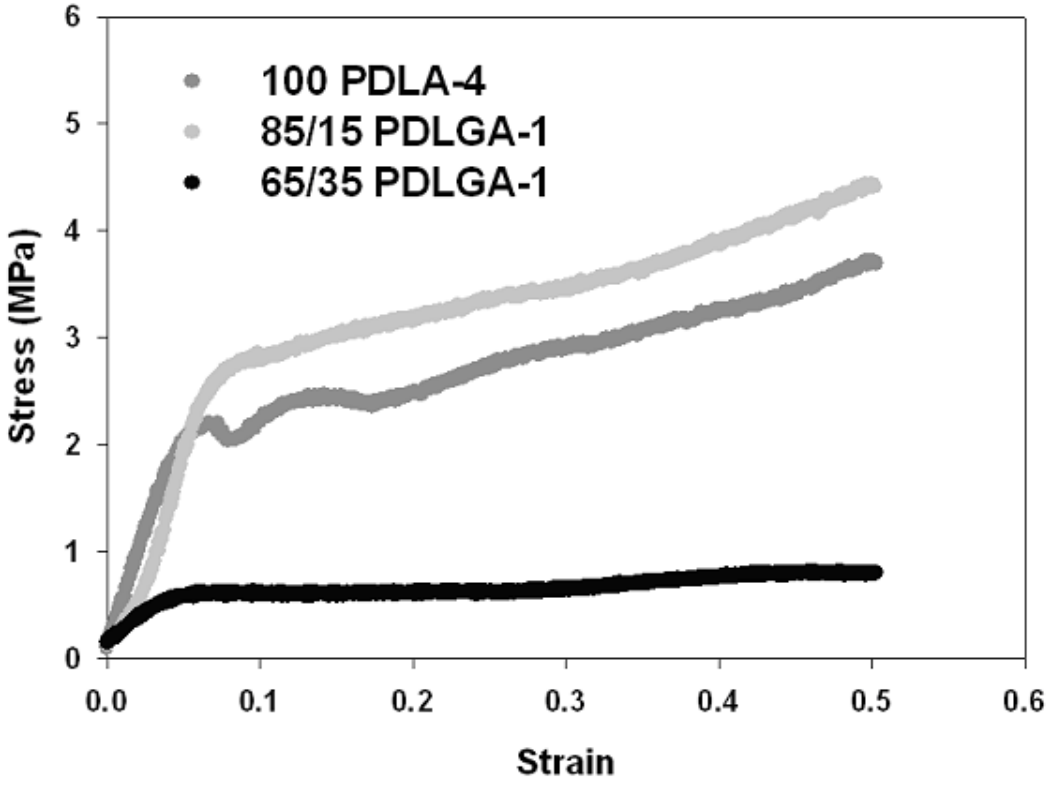

FIGURE 4. *Representative compressive stress-strain curves from each of the co-polymer constructs, with varying PGA compositions. Samples were processed at 35°C at a pressure of 13.8 Mpa and constrained radial expansion.*

TABLE 2. *Static mechanical properties of porous resorbable polymer constructs synthesized by supercritical carbon dioxide processing. Samples were processed at 35°C with a pressure of 13.8 Mpa and constrained radial expansion.*

Polymer	**Elastic Recovery** *(% of original height)*		**Compressive Strength** (Mpa)		**Compressive Modulus** (Mpa)	
100PDLA	63.84%	±4.02%	3.40	±0.54	202.72	±55.8
85:15PDLGA	61.89%	±3.22%	4.35	±1.78	218.43	±72.76
65:35PDLGA	70.92%	±10.42%	1.11	±0.34	39.38	±24.26

Water Uptake Capacity of Constructs

All constructs demonstrated a significant weight gain within the first two hours of immersion in deionized water (Figure 5). The weight gains tapered off significantly after the first two hours as the polymer swelling began to approach equilibrium with the solution. The 100PDLA and 85:15PDLGA samples showed similar weight gains throughout the duration of immersion, while the 65:35PDLGA samples exhibited a much greater weight increase at all time points. The 65:35PDLGA samples began to show a marked decrease in mass after 12 hours of immersion. Hydrophilicity of the polymers increases with increasing glycolic acid content, which would enhance water uptake. As such, it was expected that the 85:15PDLGA and 65:35PDLGA samples would show larger changes in weight upon immersion. The 100PDLA

sample does show a slightly higher weight gain than the 85:15PDLGA, but there is a significant standard deviation in both of these sample populations.

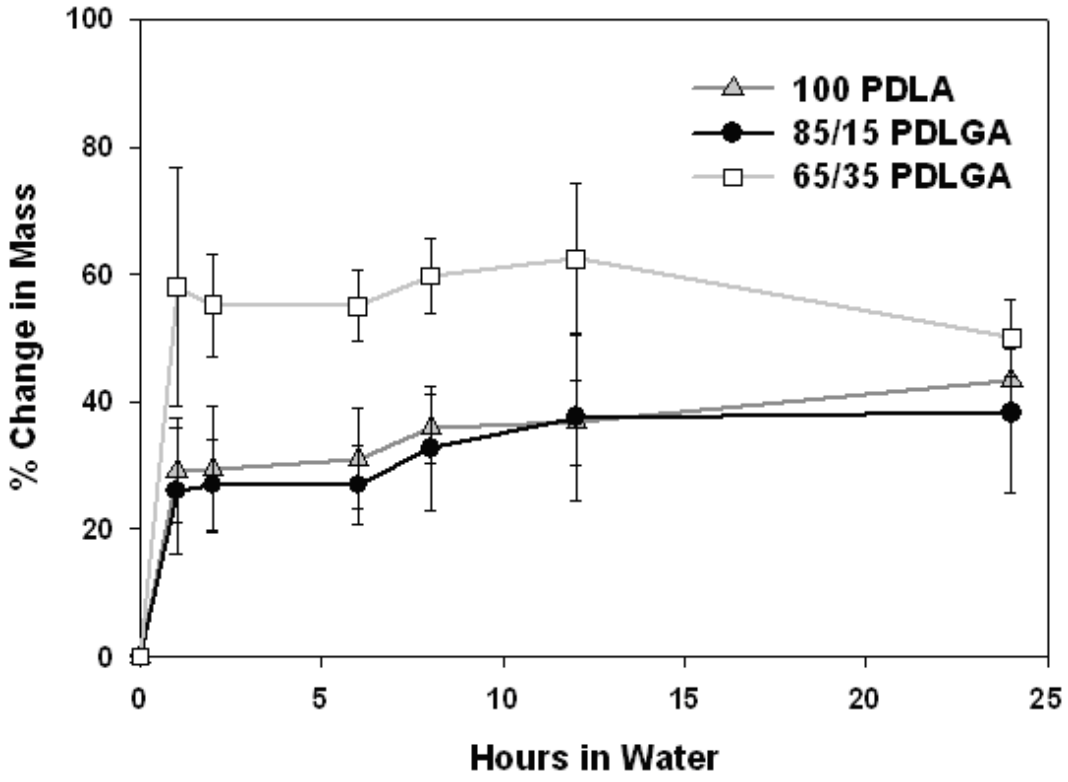

FIGURE 5.*Graph showing the change in mass of the constructs as a function of duration immersed in deionized water.*

Discussion

This study focused on the copolymer composition, mechanical behavior and hydrophilicity of porous, resorbable polymer constructs synthesized by supercritical CO_2 processing. The influence of $scCO_2$ processing parameters on construct microstructure (i.e. pore diameter, pore wall thickness and interconnectivity) was characterized by SEM, while mechanical compression testing elucidated the static mechanical properties. Hydrophilicity and

potential for growth factor loading of the porous constructs was determined by water uptake assays.

Pore structures of the constructs were significantly influenced by the processing temperature. This influence may be explained by the physical events that occur during $scCO_2$ processing. When the polymer is soaked in $scCO_2$ at elevated temperatures, significant swelling occurs. During depressurization of the system, primary pore formation arises from the CO_2 bubble nucleation and growth. The pore structure continues to evolve as a function of CO_2 escaping from the sample, which creates expansile, bi-axial flow in the polymer structure. The combination of the low processing temperature (35˚C) and the cooling due to CO_2 expansion may reduce the sample temperature to below its glass transition during depressurization, even with the solvation effect of any residual CO_2. As the solidified sample warms up again, the residual trapped CO_2 continues to try to expand resulting in larger pores for the unconfined construct. At 100˚C, the polymer is less viscous and the Joule-Thompson cooling due to rapid CO_2 expansion is not sufficient to reduce the temperature below the glass transition temperature of the polymer. Therefore, all of the CO_2 has escaped upon depressurization, resulting in negligible expansion after releasing confinement. The significant difference in pore size between constructs processed at 35˚C and 100˚C may be attributable to a nearly fourfold decrease in CO_2 density at the higher temperature. Alternatively, process pressure was not found to play a significant role in altering the pore structure of the resorbable polymer constructs, possibly due to the relatively insignificant difference in the density of the CO_2 at the three chosen pressures.

Constructs synthesized by the $scCO_2$ process exhibited a porous core and a dense outer layer. This morphology is similar to the structure of an iliac crest bone graft, which has a thin

cortical shell that surrounds the trabecular core (Mosekilde and Mosekilde, 1982; Samartzis et al, 2005; Sidhu et al., 2001; Zdeblick et al., 1994). The cortical shell of the iliac crest bone graft provides structural support during biomechanical loading. It is hypothesized that the dense outer layer of the porous, PLGA polymer constructs would provide similar structural support. The outlayer observed on the constructs is a function of the rapid diffusion of CO_2 from the surface of the polymer construct. In the center of the construct, CO_2 escape is much slower allowing for the evolution of a porous structure. Siripurapu et al. examined methods to encourage pore formation at the periphery of the constructs in an effort to reduce skin formation in PMMA porous-thin film applications. Constraining the polymer limited the rapid diffusion of CO_2 from the construct surface, which encouraged the nucleation and growth of pores at the construct surface, rather than a dense skin. Increasing depressurization rate also increased cell density in this system. In the present study, polymers were constrained in the radial direction and unconstrained in the vertical direction. Lack of constraint in this direction likely facilitated rapid CO_2 escape from the surface and subsequent formation of a dense shell on the constructs. Again, for this specific application, a dense "cortical shell" is desired to enhance load bearing capacity.

Pore interconnectivity is essential to the process of bone formation, which consists of cellular infiltration, neovascularization and nutrient transport (DePalma et al, 1972; Samartzis et al, 2005; Wimmer et al., 1999; Zdeblick et al., 1994). Confining the samples for 48 hours after processing at 35^{o}C decreased the average pore size and increased the pore interconnectivity of all constructs, regardless of glycolic acid content. Radial expansion of the construct is limited by the diameter of the glass vial, which results in significant internal stresses. These internal stresses limit pore diameter and lead to pore wall collapse, which results in interconnected pores. Immediate removal of the samples from the glass vials after processing leads to unconstrained

expansion in the radial direction. Since there is no physical boundary to expansion, pores can grow with less risk of wall collapse.

While the constructs showed similar architectures with the varying processing parameters, the different polymer blends exhibited variations in static mechanical properties. The mechanical compression testing of the constructs suggests that 85:15PDLGA and 100PDLA samples exhibit the significantly higher compressive strength and compressive moduli (Figure 4, Table 2) compared to the 65:35PDLGA. These have compressive strengths of 4.35 Mpa (+/- 1.78 Mpa) and 3.40 Mpa (+/-0.54 Mpa), respectively, which are comparable to cancellous bone found in veretebral bodies (Jensen et al., 1990; Mosekilde and Mosekilde, 1982). The elastic moduli of the 85:15PDLGA and 100PDLA samples, 36.41 Mpa (+/- 12.13 Mpa) and 33.79 Mpa (+/- 9.30 Mpa) respectively, are significantly lower than the reported values of cancellous bone. The 65:35PDLGA samples had significantly lower compressive strength and compressive modulus of elasticity as compared to the 85:15PDLGA and 100PDLA samples. A compressive strength of 1.11 Mpa (+/- 0.34 Mpa) and an elastic modulus of 6.56 Mpa (+/- 4.04 Mpa) suggest that the 65:35PDLGA porous constructs may be unsuitable for orthopaedic, load-bearing applications, such as that encountered by bone graft materials, unless a different type of construct is considered However, these results indicate that 85:15PDLGA and 100PDLA constructs may withstand biomechanical loads found in the cervical spine (Patwardhan et al., 2000). The standard deviations of the compressive strength and elastic moduli values were significant, due to regional variations in pore architecture between samples.

The recovery of sample height after the removal of the compressive load was similar for all samples, as shown in Table 2. The 65:35PDLGA constructs showed a 70.92% (+/-10.42%) recovery of their initial height, five minutes after the removal of the load. This value is

somewhat higher than the values reported for 100PDLA (63.84% +/-4.02%) and 85:15PDLGA (61.89% +/-3.22%). This small difference may be attributed to the retention of some residual CO_2 by the 65:35PDLGA constructs. Recovery of construct height upon removal of the simulated biomechanical load is important in terms of maintaining disk space height (distance between vertebrae) in the spine (Zdeblick et al., 1994).

The compressive strengths of resorbable polymer devices (dense) currently used in spine surgery far exceed that of the porous constructs presented in this study. However, the porous morphology of the constructs achieved by $scCO_2$ processing offers a distinct advantage over dense constructs, in terms of bone in-growth. Pore sizes in the range of 200-250 μm are essential for neovascularization of the graft and subsequent nutrient transport (DePalma et al., 1972; Samartzis et al., 2005; Wimmer et al., 1999; Zdeblick et al., 1994). The dense morphology of current resorbable polymer devices does not support the process of bone in-growth and thus must be used in conjunction with an osteoconductive scaffold material. It is thus desireable to use the $scCO_2$ process to develop constructs that can simultaneously support the biomechanical loads and provide a scaffold for bone growth.

The hydrophilic character of the polymers plays a role in the biocompatibility of the constructs. Water uptake experiments are a bulk method for comparing surface character of materials. Specifically, osteoblasts have been shown to differentiate faster on hydrophilic surfaces, rather than hydrophobic ones (Baker et al, 2006; Bren et al., 2004). Generally, polymers that are lactic acid-based are very hydrophobic. Addition of glycolic acid to these polymers increases the hydrophilic character of the constructs, as was evidenced by the increased water uptake (Figure 5). Small variations in polymer chemistry, which impart a hydrophilic character to the constructs, may be possible without sacrificing the mechanical properties of the

construct. These water uptake experiments are also frequently used clinically to assess the ability to load porous constructs with exogenous growth factors or autologous bone marrow aspirate. Polymers (non-porous) currently in use in orthopaedic surgery are predominantly comprised of lactic acid, with small amounts of glycolic acid. Further research should focus on examining the mechanical properties of resorbable polymer constructs with molar glycolic acid contents of less than 15%, as mechanical testing of 65:35PDLGA constructs demonstrated that polymer blends with higher glycolic acid contents have poor structural properties. The $scCO_2$ processing method allows for a safe, versatile solvent that enables a wide range of pore architecture and the resultant properties.

Potential limitations of this study include the use of SEM to measure pore interconnecitivty and pore structure. Also, the overall level of porosity was not reported for the various constructs synthesized with different processing conditions. Intrusion porisometric, or pyncnometric techniques are commonly employed in the quantification of pore structure, interconnectivty and degree of porosity. While these properties were not reported, SEM was used to ensure that the pore structure and degree of porosity were similar between all samples that underwent mechanical testing and water uptake studies.

The fact that the compression testing was performed in a non-physiological environment may be limitation. Hydrolytic breakdown of the biodegradable polymer has been shown to reduce static mechanical properties, as a function of time spent in an aqueous environment. The objective of the current study was to quantify and compare the compressive mechanical properties at time zero, to engineer superior constructs based on pore size and processing parameters. Experimentation is ongoing, which will seek to quantify the changes in both pore

structure and mechanical properties as a function of duration of exposure to a simulated physiologic environment.

Conclusions

Supercritical CO_2 processing has been demonstrated to be a viable method to synthesize porous resorbable PDLGA constructs with varying glycolic acid compositions. Further, the pore size range (236-239 μm) and degree of pore interconnectivity of the constructs synthesized by $scCO_2$ processing is similar to that found in iliac crest bone graft, which is considered to be the gold standard in spinal fusion procedures.

The mechanical properties of 85:15PDLGA and 100PDLA samples indicate that these constructs may be suitable as bone graft substitutes for use in spinal fusion procedures. Our study indicates that, through the use of $scCO_2$ processing, it is possible to create resorbable constructs that possess the mechanical properties necessary to support biomechanical loads and architectures to facilitate bone in-growth.

Incorporation of 35wt% glycolic acid improves the water uptake capacity of the constructs by altering the hydrophilic character of the polymer. This increase in hydrophilicity may also enhance the bone in-growth capacity of the constructs by enhancing osteoblast response.

In summary, $scCO_2$ processing was found to be a promising method to develop porous, resorbable polymer constructs. The mechanical properties, porous morphology and hydrophilic character of the resulting PDLGA constructs make them a potential candidate for bone grafting procedures in orthopaedic surgical procedures.

References

Baker, K.C., et al., 2006. Growth, characterization and biocompatibility of bone-like calcium phosphate layers biomimetically deposited on metallic substrata. Materials Science and Engineerin: Part C 26(8), 1351-1360.

Bren, L., et al., 2004. Hydrophilic/electron-acceptor surface properties of metallic biomaterials and their effect on osteoblast cell activity. Journal of Adhesion Science and Technology 18, 1711-1722.

DePalma, A.F., et al., 1972. Anterior interbody fusion for severe cervical disk degeneration. Surgical Gynecology and Obstetrics 134, 755-758.

Georgiou, G., et al., 2007. Polylactic acid-phosphate glass composite foams as scaffolds for bone tissue engineering. Journal of Biomedical Materials Research Part B: Applied Biomaterials 80B, 322-331.

Hu, R.W., Bohlman, H.H., 1994. Fracture at the iliac bone graft harvest site after fusion of the spine. Clinical Orthopaedics and Related Research 309, 208-213.

Hu, Y., et al., 2001. Fabrication of poly(alpha-hydroxy acid) foam scaffolds using multiple solvent systems. Journal of Biomedical Materials Research 59, 563-572.

Jensen KS., et al., 1990. A model of vertebral trabecular bone architecture and its mechanical properties. Bone 11(6), 417-423.

Kim, S.S., et al., 2007. A poly(lactide-co-glycolide)/hydroxyapatite composite scaffold with enhanced osteoconductivity. Journal of Biomedical Materials Research: Part A 80A, 206-215.

Lippman, C.R., et al., 2004. Cervical spine fusion with bioabsorbable cages. Neurosurgery Focus. 16(3), Article 4.

Mathieu, L.M., et al., 2005. Bioresorbable composites prepared by supercritical fluid foaming. Journal of Biomedical Materials Research: Part A 75A, 89-97.

Mosekilde L., Mosekilde L., 1982. Normal vertebral body size and compressive strength: relation to age and to vertebral and iliac trabecular bone compressive strength. Bone 7(3), 207-212.

Nam, Y.S., Park, T.G., 1999. Porous biodegradable polymeric scaffolds prepared by thermally induced phase separation. Journal of Biomedical Materials Research 47, 8-17.

Patwardhan, A.G., et al., 2000. Load-carrying capacity of the human cervical spine in compression is increased under a follower load. Spine 25(12), 1548-1554.

Samartzis, D., et al., 2005. Is autograft the gold standard in achieving radiographic fusion in one-level anterior cervical discectomy and fusion with rigid anterior plate fixation? Spine. 30(15), 1756-1761.

Sidhu, K.S., et al., 2001. Anterior cervical interbody fusion with rhBMP-2 and tantalum in a goat model. The Spine Journal 1(5), 331-340.

Teng, X., et al. 2007. Preparation and characterization of porous PDLLA/HA composite foams by cupercritical carbon dioxide technology. Journal of Biomedical Materials Research B: Applied Biomaterials 81B, 185-193.

Vaccaaro, A.R., et al., 2004. Early findings in a pilot study of anterior cervical fusion in which bioabsorbableinterbody spacers were used in the treatment of cervical degenerative disease. Neurosurgery Focus 16(3), E7.

Wang, Y., et al., 2008. Synthesis and characterization of collagen-chitosan-hydroxyapatite artificial bone matrix. Journal of Biomedical Materials Research: Part A. 86A(1), 244-252.

Wimmer, C., et al., 1999. Autogenic versus allogenic bone grafts in anterior lumbar interbody fusion. Clinical Orthopaedics and Related Research 360, 22-126.

Wuisman PIJ, Smit TH. 2006. Bioresorbable polymers: heading for a new generation of spinal cages. European Spine Journal 15, 133-148.

Zdeblick, T.A., et al., 1994. Anterior cervical discectomy and fusion using a porous hydroxyapatite bone graft substitute. Spine 19(20) 2348-2357.

Zeng, C., et al. 2003. Polymer-clay nanocomposite foams prepared using carbon dioxide. Advanced Materials. 15(20), 1743-1747.

CHAPTER 5: SUPERCRITICAL CARBON DIOXIDE PROCESSED RESORBABLE POLYMER NANOCOMPOSITES AS BONE GRAFT SUBSTITUTES

Introduction

Autogenous bone (autograft) remains a gold standard in numerous surgeries requiring bone grafting to achieve arthrodesis and fracture union. The inherent osteoinductivity of autograft, coupled with its biomechanical strength make it a clear choice for the reconstruction or replacement of load bearing structures in the body. Despite the success of surgical procedures utilizing autograft, complication rates as high as 30% have been associated with the harvest procedure (Malloy and Hillibrand, 2003; Samartzis et al., 2003; Wigfield and Nelson, 2001). These complications include harvest site necrosis, significant post-operative pain and fracture at the harvest site (Arribas-Garcia et al., 2009; Hu and Bohlman, 1994). Allogenic bone (allograft) has been used in place of autograft with a high degree of success (Samartzis et al., 2003; Wigfield and Nelson, 2001). Modern donor screening and sterilization methods have significantly reduced the rates of disease transmission, which until recently, was a significant risk in allogenic bone graft procedures (Mally and Hilibrand, 2002; Samartzis et al., 2003). The mechanical properties as well as the osteoinductive capacity of allograft have been shown to be dependent on the type of sterilization employed (Malloy and Hilibrand, 2002; Chau and Mobbs, 2009). Additionally, allograft bone is in limited supply in some regions, which can limit its applicability in major surgical procedures, such as scoliosis correction (Chau and Mobbs, 2009; Moroni et al., 2009).

Given the limitations of autograft and allograft bone, much attention has been given to the development of structural bone graft substitute materials. Ceramic materials, such as calcium phosphates, have been investigated as bone graft substitutes for load bearing applications (Wigfield and Nelson, 2001). While porous calcium phosphates such as corraline hydroxyapatite

have high compressive strengths, the brittle nature of the material can lead to progressive collapse of the graft resulting in poor bone healing (Chau and Mobbs, 2009). Porous metallic constructs, such as Trabecular Metal™ (Tantalum, Zimmer Inc., WarsawIN) and Tritanium™ (commercially pure Titanium, Stryker Orthopaedics, MawahNJ) have also been introduced as structural bone graft substitutes. The load bearing capacities of porous metal constructs are well documented in both static and dynamic conditions. Unfortunately, long-term implantation of non-resorbing implants is associated with an omni-present risk of infection. Further, the presence of a porous metallic construct may severely limit surgical options if a revision procedure is necessary.

Due to such limitations there has been significant interest in developing resorbable polymers, such as poly-L-lactide (PLLA) and poly-L-glycolide (PLGA), for structural bone graft substitute applications (Chau and Mobbs, 2009; Moroni et al., 2009). To impart a porous structure to PLLA and PLGA to enable bone growth, methods such as thermal/pressure induced phase separation, particulate leaching and gas foaming (Baker et al., 2009; Georgiou et al., 2007; Hu et al., 2002; Mathieu et al., 2005; Nam and Park, 1999). Phase separation techniques often involve the use of volatile organic solvents which can be detrimental to cell growth (Nam and Park, 1999; Teng et al., 2007). Particulate leaching must be used in combination with other methods, such as phase separation to yield a construct with connected porosity. Gas foaming techniques, such as supercritical carbon dioxide ($scCO_2$), avoid the use of harmful solvents and may not require additional methods to impart an interconnected porous structure (Baker et al., 2009; Georgiou et al., 2007; Mathieu et al., 2005; Gualandi et al., 2010; Kanczler et al., 2010).

The mechanical properties of porous resorbable constructs synthesized by the aforementioned means are not suitable for load bearing applications as the compressive modulus

and compressive strengths are much lower than that of native bone. Failure of the constructs to withstand physiologic loading conditions may result in a reduced rate of healing and in some conditions may necessitate a revision surgical procedure. Researchers have examined reinforcing the polymer constructs with calcium phosphates (hydroxyapatite, β-TCP), phosphate glass and carbon nanotubes (Georgiou et al., 2007; Mathieu et al., 2005; Kim et al., 2007; Khan et al., 2008; Rezwan et al., 2006; Wang et al., 2008). The addition of these materials to polymer matrices has resulted in modest gains in compressive strength and modulus. Calcium phosphates and phosphate glass particles have a tendency to agglomerate within polymer mixtures, which results in local heterogeneity that is detrimental to mechanical strength (Georgiou et al., 2007). There is therefore a need to develop a resorbable polymer nanocomposite system and a synthesis route which results in porous constructs with a relatively uniform dispersion of reinforcing particles.

Recently, organically modified montmorillonite clays have been investigated as potential reinforcing agents in polymeric matrices (Horsch et al., 2006; Manitiu et al., 2008; Pavlidou and Papspyrides, 2008; Ray and Okamoto, 2003; Zeng et al., 2003). The clay particles are composed of high aspect ratio silicate platelets which are approximately 100 – 500 nm in length and 1 nm thick. These platelets are held together in stacks by *van der Waals* forces and the equilibrium platelet spacing of 1 nm is generally modified by chemical techniques. One common method of increasing platelet spacing is modification of the clay surface with alkylammonium salts. Increasing the spacing or the dispersion of the clay platelets increases the potential for intimate contact between polymer chains and numerous clay platelets, thus reducing polymer chain mobility and improving mechanical properties (Horsch et al. 2006; Manitiu et al., 2008; Pavlidou and Papspyrides, 2008; Ray and Okamoto, 2003). The processing method used to create clay-

polymer nanocomposites also plays a role in the resulting mechanical behavior. Melt processing, high shear mixing and post-processing heat treatments have been employed to enhance polymer chain-clay platelet contact, with moderate property improvements (Pavlidou and Papspyrides, 2008; Ray and Okamoto, 2003). On the other hand, $scCO_2$ processing appears to be a very effective way to improve mechanical properties of polymer-clay nanocomposites (Horsch et al., 2006; Manitiu et al., 2008; Zeng et al., 2003) for film and molded part applications. Diffusion of CO_2 within the clay particles and rapid depressurization leads to an increase in platelet spacing, as well as polymer chain contact (Horsch et al., 2006; Manitiu et al., 2008). The use of $scCO_2$ processing for dispersed biodegradable poly-d-lactide (PDLA) nanocomposites is a new concept explored in this study.

Supercritical CO_2 processing has been previously used to disperse nanoclays in resorbable polymer matrices and to synthesize porous resorbable polymer scaffolds (Baker et al., 2009; Zeng et al., 2003). Using $scCO_2$ processing to synthesize nanoclay-resorbable polymer nanocomposites may result in the production of porous scaffolds, which are suitable for structural bone graft substitute applications. The purpose of this study is to examine the structure, mechanical properties and biocompatibility of porous resorbable PDLA polymer nanocomposites synthesized by supercritical carbon-dioxide processing.

Materials and methods

Materials-

Constructs were prepared from 100% poly(D-lactic acid) (100PDLA, Lakeshore Biomaterials, Birmingham, AL). Nanocomposites were formed by adding nano-structured Montmorillonite clay platelets (nano-clays). Organic modifiers based on ammonium salts are

used to increase the intergallery spacing between silicate platelets, thus facilitating dispersion. The nano-clay used in this study was organically modified with a methyl dehydrogenated tallow (Cloisite 93A, Southern Clay Products, Austin, TX), as shown in Figure 1, and was used "as-received" from the manufacturer. The size distribution of the dry particles of Cloisite 93A, according to the manufacturer are as follows: 90% of particles are less than 13 μm, 50% less than 6 μm and 10% less than 2 μm.

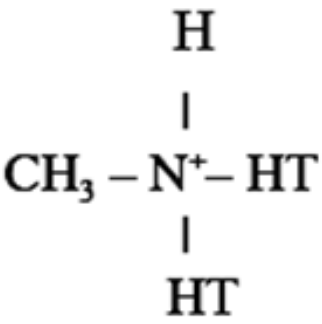

Figure 1. *Illustration of the chemical structure of the organic modifier used to increase basal platelet spacing in Cloisite 93A nanoclay.*

Construct Synthesis

Pure polymer constructs were prepared according the previously described methods (Baker et al., 2009). Briefly, polymers were ground to an average particle size of 250-500 μm and placed in a steel tube (28 mm O.D. x 61 mm H). The tube restricts radial expansion of the polymer, but allows for expansion in the vertical direction. The polymer-filled tube, each with 2.0 g of ground polymer, were placed into a supercritical fluid reactor and saturated with CO_2. The internal pressure was elevated to 13.8 Mpa at an internal temperature of 35^{o}C to induce a supercritical phase transformation in the CO_2. After 60 minutes of soaking, the reactor was rapidly depressurized at a rate of 0.3-0.4 Mpa/s.

Synthesis of clay-polymer nanocomposite constructs was performed similarly. Nanoclay particles were mechanically mixed with 2.0 g of ground polymer with total clay loading of 1wt%, or 2.5wt%. The steel tubes were placed into the supercritical fluid reactor and saturated with CO_2. Processing nanocomposite constructs at 35^{o}C (similar to pure constructs), resulted in pore sizes much smaller than those found in the pure constructs. As such, a higher temperature was utilized for nanocomposite processing, so that both constructs would have similar pore sizes. The internal pressure of the reactor was elevated to 13.8 Mpa and the temperature was raised to 100^{o}C. After 60 minutes of soaking in the supercritical CO_2, the reactor was rapidly depressurized at a rate of 0.3-0.4 Mpa/s. The process was repeated to yield samples of 100PDLA with 1wt% Cloisite 93A (100PDLA-93A-1) and 2.5 wt% 93A (100PDLA-93A-2.5).

Constructs were freeze-fractured with liquid nitrogen in the vertical (direction of CO_2 escape) and transverse (direction perpendicular to CO_2 escape) directions. Fracture surfaces were coated with a thin film of AuPd and subjected to scanning electron microscopy (SEM, JEOL JSM 6400, JEOL Ltd.). SEM was performed at a working distance of 15 mm and an accelerating voltage of 20 kV. Measurements of pore size, pore wall thickness and qualitative assessments of pore interconnectivity were performed using digital image analysis software (Revolution, 4Pi Analysis). Measurements were conducted on a minimum of three vertical and three transverse fracture surfaces. At least eight images were analyzed from each fracture surface. Pore dimensions were measured for 20 pores per fracture surface image.

Characterization of Nanoclay Dispersion

A RigakuSmartLabDiffractometer with a Cu Kα X-ray source (λ = 1.54 Å) and an accelerating voltage of 40 kV at a current of 40 mA was used to determine the intergallery

spacing of the clay/polymer nanocomposites. Samples were placed in a custom made, zero-background quartz sample holder that is 0.9 mm in depth and diffraction scans were collected from 0.1 to 10º 2θ at a scan rate of 3.0 degrees/min at a step size of 0.3 degrees. Several scans were obtained from different locations in the sample and verified to be reproducible when diffraction patterns were superimposed on one another. The 2θ angle was determined using the JADE software that accompanies the diffractometer and the d_{001} spacing for the clays was calculated using Braggs' Law of diffraction. The intergallery spacing was then found by subtracting 1 nm (platelet thickness) from the d_{001} spacing.

Rheology

A Rheometric Scientific RSA II rheometer (shear sandwich geometry 15.98 mm x 12.7 mm x 0.55 mm) was used to perform *melt* rheological measurements under oscillatory shear. Rectangular slabs of samples were prepared by melt pressing the foam constructs into a mold at 80ºC between Teflon plates followed by annealing under vacuum at 80ºC to remove any residual carbon dioxide, and also to remove the porous structure. The materials were loaded and allowed to equilibrate for 1 hour at the desired temperature. Rheological measurements were performed at 80ºC and 120ºC for all samples, and time-temperature superposed Data at both these temperatures are shown with a reference temperature of 80ºC. Strain sweeps were performed to ensure that the dynamic moduli were linear in the strain range used and the linear viscoelastic measurements were made at low strains ($\gamma_o < 0.05$) to minimize microstructure destruction. The frequency range used was $0.01 = \omega = 100$ rad/s and the property of time-temperature superposition was used to create master curves with a reference temperature of 80ºC.

Mechanical Testing

Cylindrical cores (n = 6 per testing group) with a diameter of 10 mm were obtained from the porous PDLA constructs by using an osteochondral biopsy system. Coring the constructs was necessary to ensure that the dense outer skin was not present during mechanical testing. The cores were sectioned to a height of 10 mm and trimmed with a scalpel to ensure that the ends were parallel. The samples were placed between smooth stainless steel platens in a servohydraulic materials testing machine (850 Mini-Bionix, MTS Inc., Eden Prairie, MN). Constructs were loaded in compression under displacement control at a rate of 0.5 mm/min until a strain of 50% was reached.

The compressive strength of the constructs was defined as the maximum load divided by the initial cross sectional area. Compressive modulus was determined by calculating the slope of the linear region of the load-displacement curve. A one-way analysis of variance with a Bonferroni correction and an α of 95% was used to determine the statistical significance of mechanical data as a function of construct composition.

Osteoblast Response to Porous Nanocomposite Constructs

Human osteoblast cells (HOB, PromoCell, Heidelberg, Germany) were cultured in α-modified minimum essential medium (α-MEM, Gibco, USA; containing 2.0 mM L-glutamine and 1 mM sodium pyruvate, without phenol red) supplemented with Osteoblast Growth Medium SupplementMix (PromoCell; containing 10% FBS) and 1% penicillin/streptomycin (Gibco). Cell cultures were maintained in 5% CO_2 with 95% air at 37ºC until 85% confluence. Cells were lifted using 0.05% trypsin/0.5 mM EDTA solution (PromoCell), concentrated, resuspended in growth medium, and counted using a hemocytometer.

Cells were seeded directly onto 10 mm diameter porous cores of 100PDLA, 100PDLA-1 and 100PDLA-2.5 nanocomposite constructs at a density of $4x10^4$ cells per construct,with a sample size of six per treatment group. Controls were performed using the same cell density on polystyrene culture plates (n=6). Cultures were maintained for seven days and medium collected and replaced every 24 hours.

Alkaline phosphatase activity was determined from cell culture supernates every 48 hours by immunoenzymatic assay (QuantiChrom ALP Assay Kit, BioAssay Systems, Hayward, CA). The expression of osteoprotegerin was also quantified in cell culture supernates using a bead-based immunoassay (Human Bone Panel 1B, Millipore, Billerica, MA) at the same time points. All samples were analyzed in duplicate for a total sample size of 12 per treatment group per time point. A one way analysis of variance (ANOVA) with Bonferroni correction was used to compare the expression of alkaline phosphatase and osteoprotegerin by cells cultured on polystyrene culture plates, 100PDLA, 100PDLA-1wt% and 100PDLA-2.5wt% constructs at each time point.

Seeded nanocomposite constructs were also subjected to SEM to examine cell morphology and mineralization. Constructs were fixed in gluteraldehyde for 24 hours and then subjected to critical point drying. After drying, the samples were sputter-coated with AuPd and visualized with SEM at a working distance of 8 mm and an accelerating voltage of 20 kV. Energy dispersive X-ray spectroscopy (EDX, Link Analytical) was used to characterize the composition of regions of suspected mineralization.

In Vitro Osteoclast Response to Nanoclay

To investigate the degree to which bare nanoclay would stimulate an osteolytic response in vivo, rat monocytes from bone marrow (Rat Osteoclast Precursor Cells, Kamiya Biomedical) were cultured on disks of human dentine. Culture media consisted of alpha-minimum essential media (α-MEM) supplemented with macrophage-colony stimulating factor (M-CSF, 50 ng/mL) and receptor activator of nuclear kappa-β ligand (RANKL, 50 ng/mL). M-CSF and RANKL are potent differentiators of macrophages and monocytes to a committed osteoclastic lineage.Cloisite 93A and Cloisite 30B nanoclays were suspended in 95% ethanol and sonicated for 15 minutes. Cloisite 30B is another organically-modified nanoclay, and possesses a similar particle size distribution as Cloisite 93A. Cloisite 30B is modified with methyl tallow bis-2-hydroxyethyl quaternary ammonium, rather than methyl dehydrogenated tallow ammonium like Cloisite 93A. Nanoclays were then dried, lyophilized and suspended in phosphate buffered saline (PBS) at a concentration of 5.0 mg/mL. 100μL of each nanoclay suspension was added to the cultured osteoclasts, 48 hours after differentiation. 100μL of sterile PBS without particles was used as a control.

Pit formation on the dentine discs and the expression of tartrate resistant acid phosphatase (TRAP) were used as measures of osteoclast activity. To assess pit formation, cells were lysed from the substrate with a 2% trypsin solution. Dentine disks were stained with Mayer's hematoxylin to provide depth dependent contrast changes under phase contrast microscopy. Disks were imaged by phase contrast microscopy (Olympus IX-71, Olympus Inc.) equipped with digital image acquisition. Pit formation was qualitatively compared between nanoclay-treated groups and the control group after seven, 14 and 21 days in culture. TRAP staining of the dentine disc was performed at each timepoint by first washing the dentine in PBS to remove bound culture medium and then fixing the samples in 10% buffered formalin. The discs were

then incubated with a solution of tartrate-containing buffer and a chromogenic substrate at 37°C for 60 minutes. Following a wash in PBS, the discs were imaged with light microscopy.

Results

Structure and Morphology

Scaffold preparation using the supercritical CO_2 method resulted in pure 100PDLA polymer constructs with mean pore diameters of 236 μm (±5 μm). Similar pore diameters were noted for PDLA-clay nanocomposite constructs (both at 1 and 2.5 wt% clay loading), as illustrated in Figure 2, and shown in Table 1. SEM analysis of multiple fractured surfaces showed that the pore sizes were uniform (relatively low standard deviation). No differences in pore interconnectivity were observed as assessed by analysis of fracture surfaces by SEM.

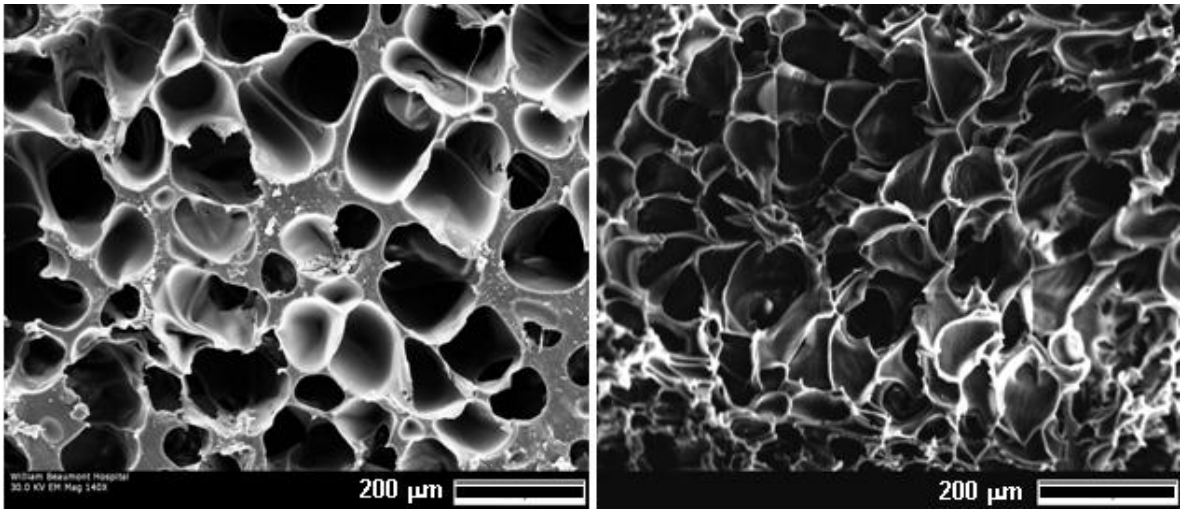

Figure 2. *Scanning electron micrographs of the porous structure of 100PDLA (left) and 100PDLA-2.5wt% (right).*

Scaffolds displayed a dense skin on the outside of the constructs. This layer abruptly transitioned to a porous interior. The morphology of the constructs was thus similar to that of iliac crest bone grafts commonly used in spine surgery, as shown in Figure 3. The addition of nanoclay had no observable effect on the morphology or thickness of the dense shell.

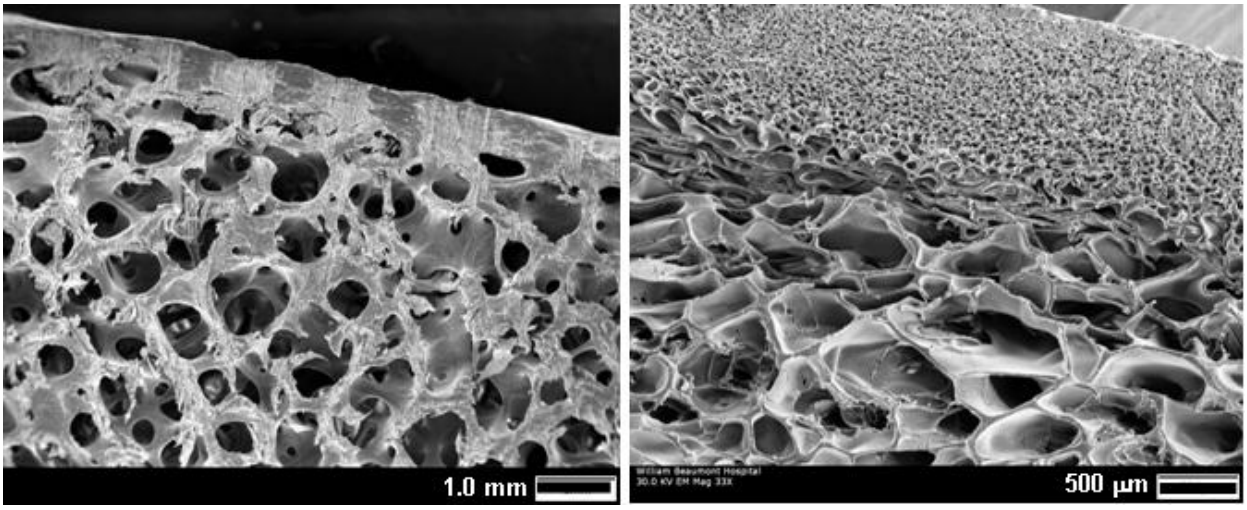

Figure 3. *Scanning electron micrographs of human corticocancellous bone harvested from the iliac crest (left) and a 100PDLA-2.5wt% nanocomposite construct demonstrating a resemblance of both cortical and cancellous bone structure.*

Small Angle X-ray Diffraction

Diffraction spectra of the nanocomposites showed a shift in the d_{001} peak of *pure Cloisite 93A* from 3.36° to 4.41° 2θ, as shown in Figure 4. Using the Bragg equation it was determined that this magnitude of shift in the 2θ position corresponds to an increase in clay platelet spacing of 1.79 nm (from 1.62 nm to 3.41 nm) after $scCO_2$ processing. Increased platelet spacing, as determined by X-ray diffraction has been used to determine the degree of intercalation of organically modified clays in polymer matrices and the extent of polymer – clay interactions present in the system (Horsch et al., 2006; Manitiu et al., 2008; Pavilidou and Papspyrides, 2008; Ray and Okamoto, 2003). The large clay inner- gallery spacing in the nanocomposite indicates that a large degree of dispersion and that strong interactions are present between the polymer and the clay organic modifier. Also, the weak and broad d_{001} spacing in the 100PDLA/2.5wt% 93A

sample compared to the "as received" Cloisite 93A is due to the low clay loading and a wide distribution of clay inner-gallery spacing.

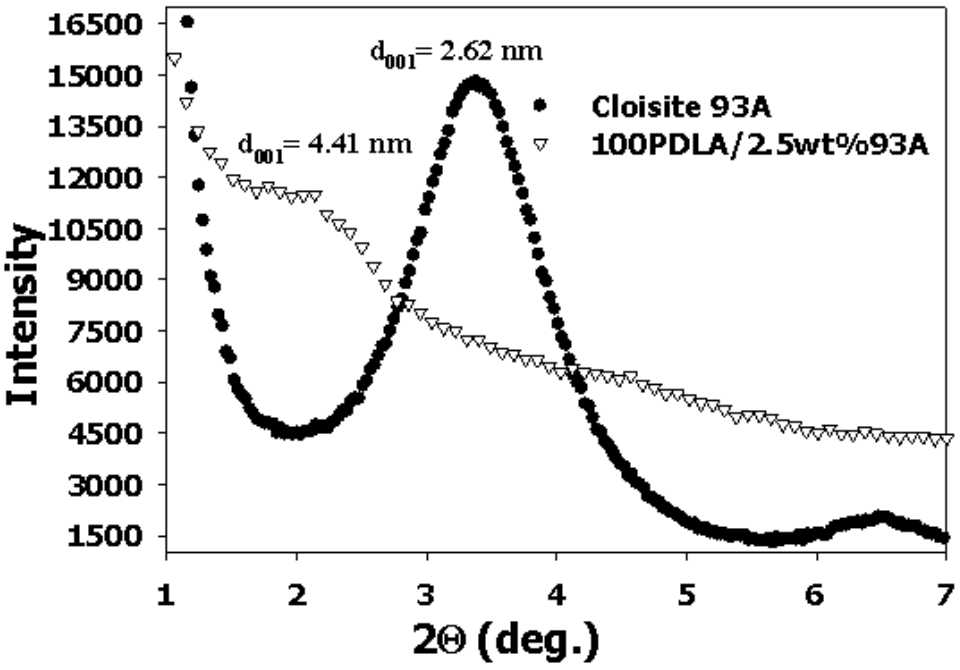

Figure 4. *Small angle X-ray diffraction spectra of pure Cloisite 93A nanoclay and 100PDLA-2.5wt% demonstrating a significant increase in d-spacing of the clay.*

Rheology

Oscillatory shear rheology was performed on reactangular slabs of $scCO_2$-processed constructs after being melt pressed into a mold at 80ºC to remove all bubbles (no pores). This is to assess the degree of clay dispersion and the extent of polymer-clay interactions (Horsch et al., 2006; Manitiu et al., 2008; Pavilidou and Papspyrides, 2008; Ray and Okamoto, 2003). In melt rheological studies the storage (G') and the loss (G'') moduli are plotted as a function of oscillatory shear frequency, as shown in Figure 5. The frequency at which they cross (crossover frequency) is characteristic of the matrix polymer relaxation time. Upon addition of clay, to the

PDLA matrix, a shift in the G'/G" crossover frequency, from 0.23 to 0.10 rad/s was observed. More importantly, an increase in the storage and loss moduli was seen upon addition of 2.5% clay. Such observations can be attributed to a significant decrease in mobility of polymer chains due to extensive interaction with the dispersed nano-clay (Horsch et al., 2006; Manitiu et al., 2008; Pavilidou and Papspyrides, 2008; Ray and Okamoto, 2003), which typically improves the mechanical properties.

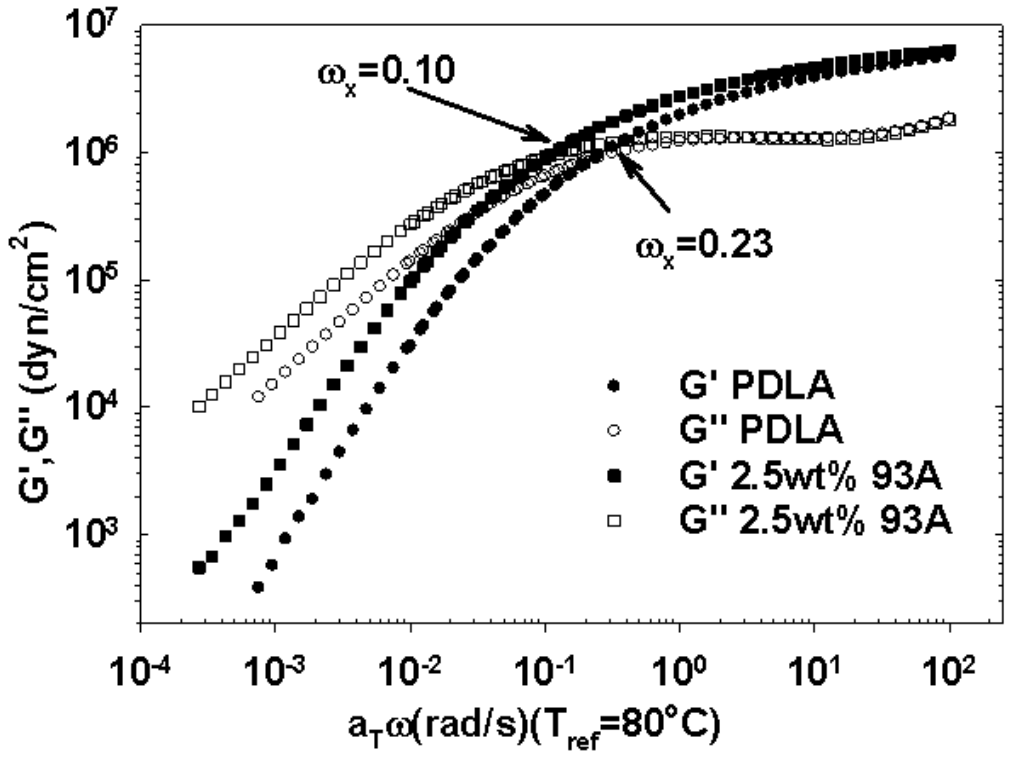

Figure 5. *Time-temperature superposed graphs of storage (G') and loss (G'') moduli of 100PDLA and 100PDLA-2.5wt%.*

Mechanical Testing of Constructs

Pure PDLA constructs exhibited a compressive strength of 3.41 Mpa (±0.54 Mpa) and a compressive modulus of 33.79 Mpa (±9.30 Mpa). The addition of 1wt% Cloisite 93a nano-clay to the 100PDLA increased the compressive strength to 6.10 Mpa (±0.83 Mpa) and compressive

modulus to 45.92 Mpa (±15.33 Mpa), as shown in Figure 6. Nanocomposite constructs containing 2.5wt% nano-clay showed an average compressive strength of 7.15 Mpa (±2.02 Mpa) and average compressive modulus of 68.42 Mpa (±32.41 Mpa). Statistical analysis showed that the increase in compressive strength upon addition of 1wt% of nanoclay was significant ($p = 0.008$) when compared to pure samples, while the change in modulus was not significant ($p=1.000$). The increase in compressive strength upon addition of 2.5wt% nanoclay was significant when compared to pure samples ($p<0.001$), as was the change in modulus ($p=0.040$). The increase in compressive strength from 1wt% to 2.5wt% nanoclay was not significant ($p=0.545$), nor was the increase in compressive modulus ($p=0.265$). A post-hoc power analysis revealed the statistical power to be 98.9% for the comparison of compressive strengths, and 49.6% for the compressive moduli.

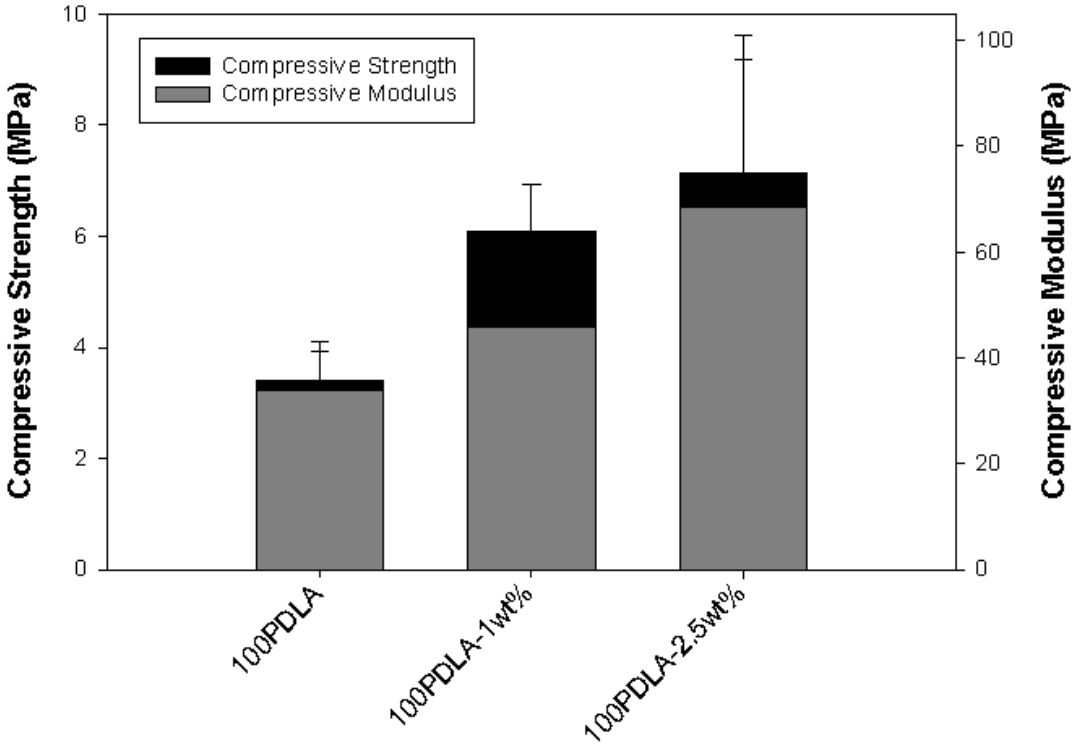

Figure 6.*Compressive strength and compressive modulus of porous cores of 100PDLA, 100PDLA-1wt% and 100PDLA-2.5wt%.*

Biocompatibility of Constructs-

Alkaline phosphatase activity and expression of osteoprotegerin by human osteoblasts cultured on the porous constructs was quantified by ELISA at days 1, 3, 5 and 7. On Day 1, alkaline phosphatase activity was similar between controls (polystyrene culture plates) and constructs ($p=0.093$), as shown in Figure 7. Expression of osteoprotegerin was higher for control wells when compared with 100PDLA-2.5wt% constructs ($p=0.007$). At Day 3, 100PDLA constructs had the highest alkaline phosphatase activity, but the only statistically significant difference was between 100PDLA and 100PDLA-2.5wt% constructs ($p=0.013$). Osteoprotegerin expression was also highest for 100PDLA constructs at Day 3 with significant differences between control wells, 100PDLA-1wt% and 100PDLA-2.5wt% constructs ($p<0.001$, $p<0.001$ and $p<0.001$, respectively). On Day 5, both control wells and 100PDLA-1wt% constructs showed higher alkaline phosphatase activity ($p=0.006$ and $p=0.035$, respectively). 100PDLA constructs again showed the highest expression of osteoprotegerin with significant differences between control wells, 100PDLA-1wt% and 100PDLA-2.5wt% constructs ($p=0.001$, $p=0.004$ and $p<0.001$, respectively). By Day 7, the differences in alkaline phosphatase activity and osteoprotegerin expression were again not significant ($p=0.162$ and $p=0.135$, respectively).

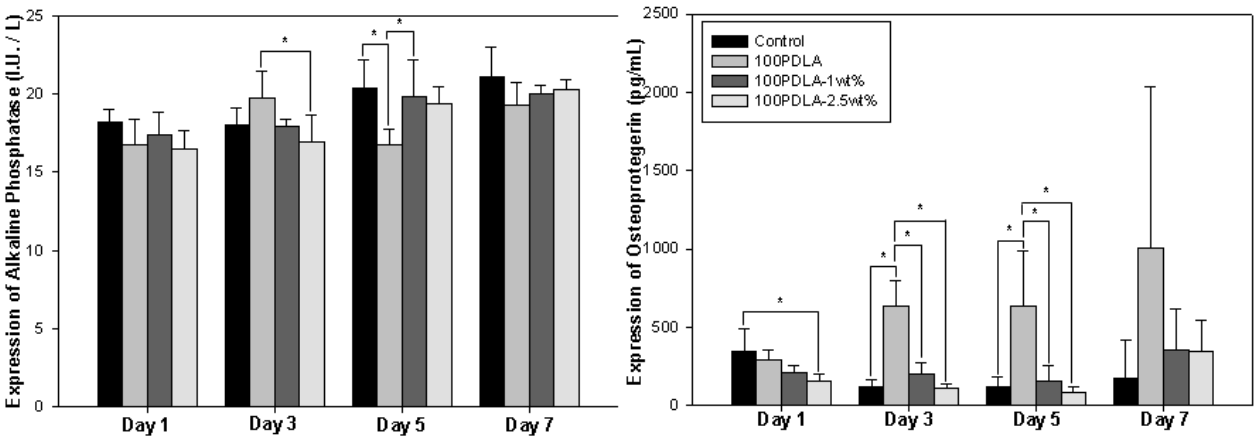

Figure 7.*Alkaline phosphatase activity (left) and osteoprotegerin expression (right) of human osteoblasts cultured on 100PDLA, 100PDLA-1wt% and 100PDLA-2.5wt% compared against polystyrene controls.*

Examination of the nanocomposite scaffolds after culturing cells for 21 days revealed copious amounts of extracellular matrix deposition (Figure 8). The deposits were comprised mainly of calcium and phosphorus as determined by EDX. This composition is indicative of the mineralization process. Cells and calcium phosphate deposits could be seen within pores deep in the porous network of the constructs. The presence of cells and deposits in the center of the constructs indicates that cells are able to infiltrate the open porous structure of the nanocomposite constructs. Some surface degradation was noted on the outermost pore walls on both nanocomposite formulations. This degradation manifested as irregularly shaped pores and erosive scalloping. There were no qualitative differences noted in the degradation behavior of the pure PDLA and PDLA-clay constructs.

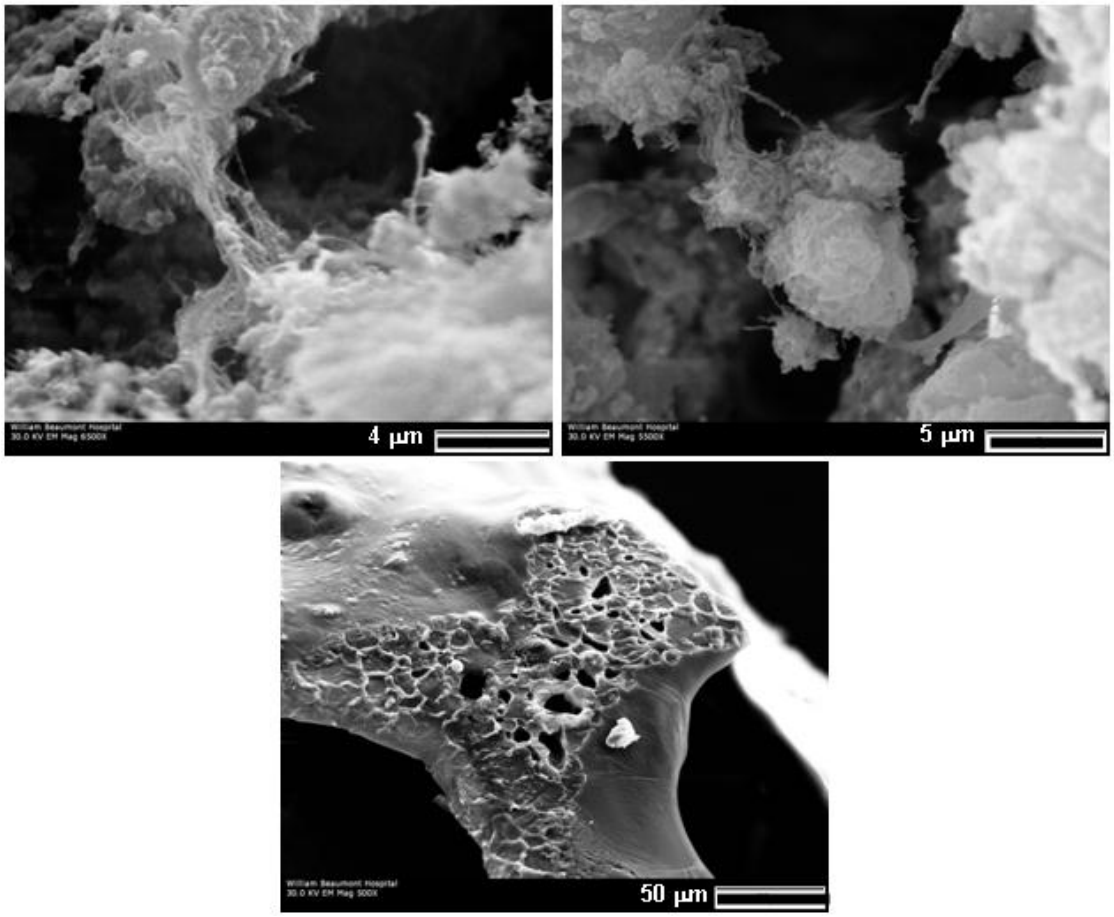

Figure 8. *Scanning electron micrographs of 100PDLA-2.5wt% 93A constructs after 28 days in culture with human osteoblasts. The top two images show a fibrous extracellular matrix deposited by the osteoblasts, which is rich in calcium and phosphorus. The bottom image displays some degradation of the polymer as a function of exposure to the culture media.*

Nanoclay-Treated Osteoclast Pit Formation and TRAP Expression

Pit formation by osteoclasts was qualitatively assessed with phase contrast microscopy, as shown in Figure 9. Discs from osteoclasts exposed to saline should no pit formation at seven days. Very little pit formation was noted at the seven day timepoint on discs from osteoclasts exposed to Cloisite 93A. Pit formation was very evident on discs from osteoclasts treated with Cloisite 30B at day seven. Pits increased in both size and number on discs from osteoclasts

treated with Cloisite 30B. A slight increase in the number of pits was noted for Cloisite 93A treated osteoclasts at the 14 day timepoint. At the 21 day timepoint, pit formation was visible on all substrates.

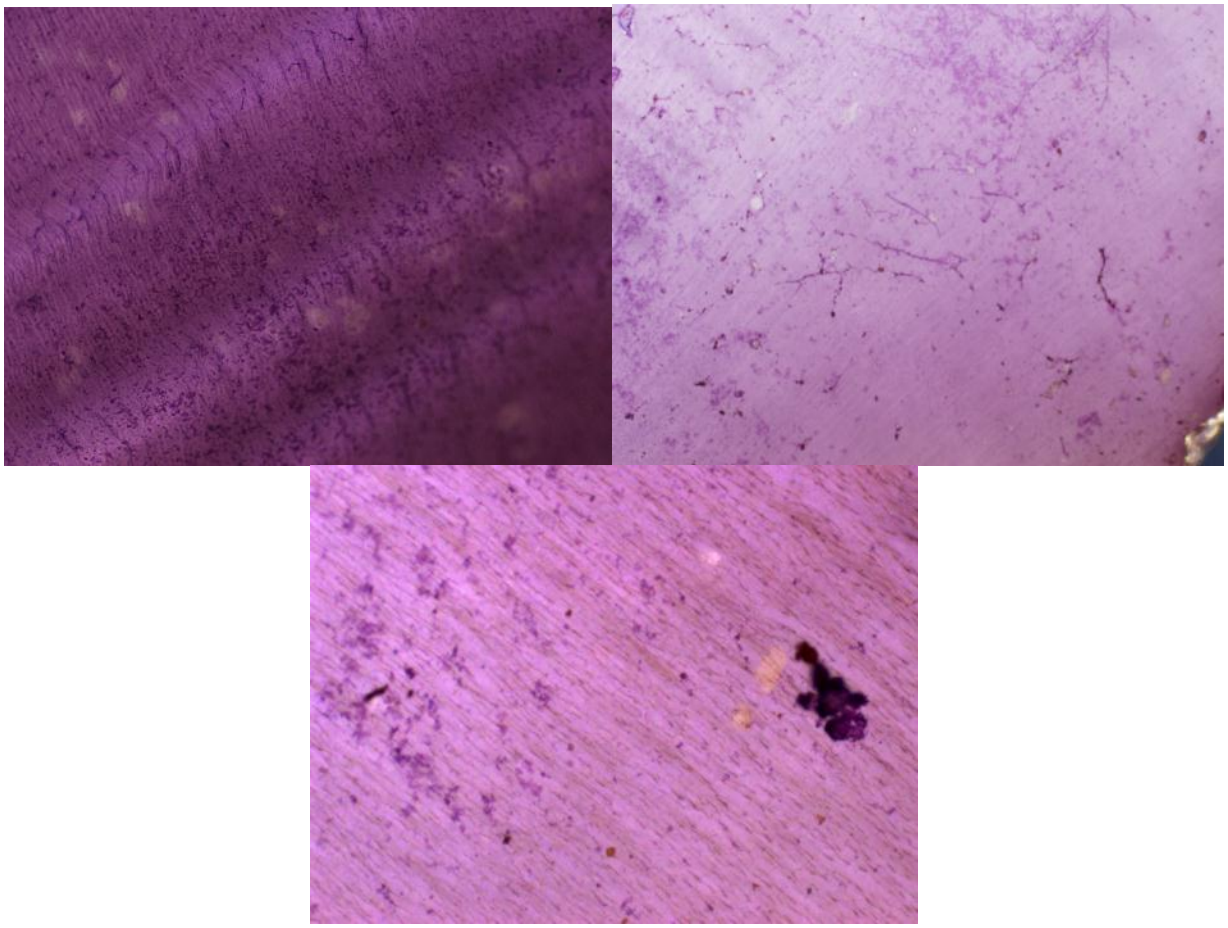

Figure 9. *Dentine discs stained with Mayer's hematoxylin to reveal pit formation by osteoclasts exposed to PBS (top left), Cloisite 93A in PBS (top right) and Cloisite 30B (bottom).*

TRAP staining intensity, which is correlated with resorptive activity within osteoclasts, was assessed by light microscopy. No significant difference in the red-brown TRAP staining was found between osteoclasts treated with saline and those treated with Cloisite 93A at any time point. However, Cloisite 30B-treated osteoclasts elicited the most intense expression of TRAP at each time point, as shown in Figure 10.

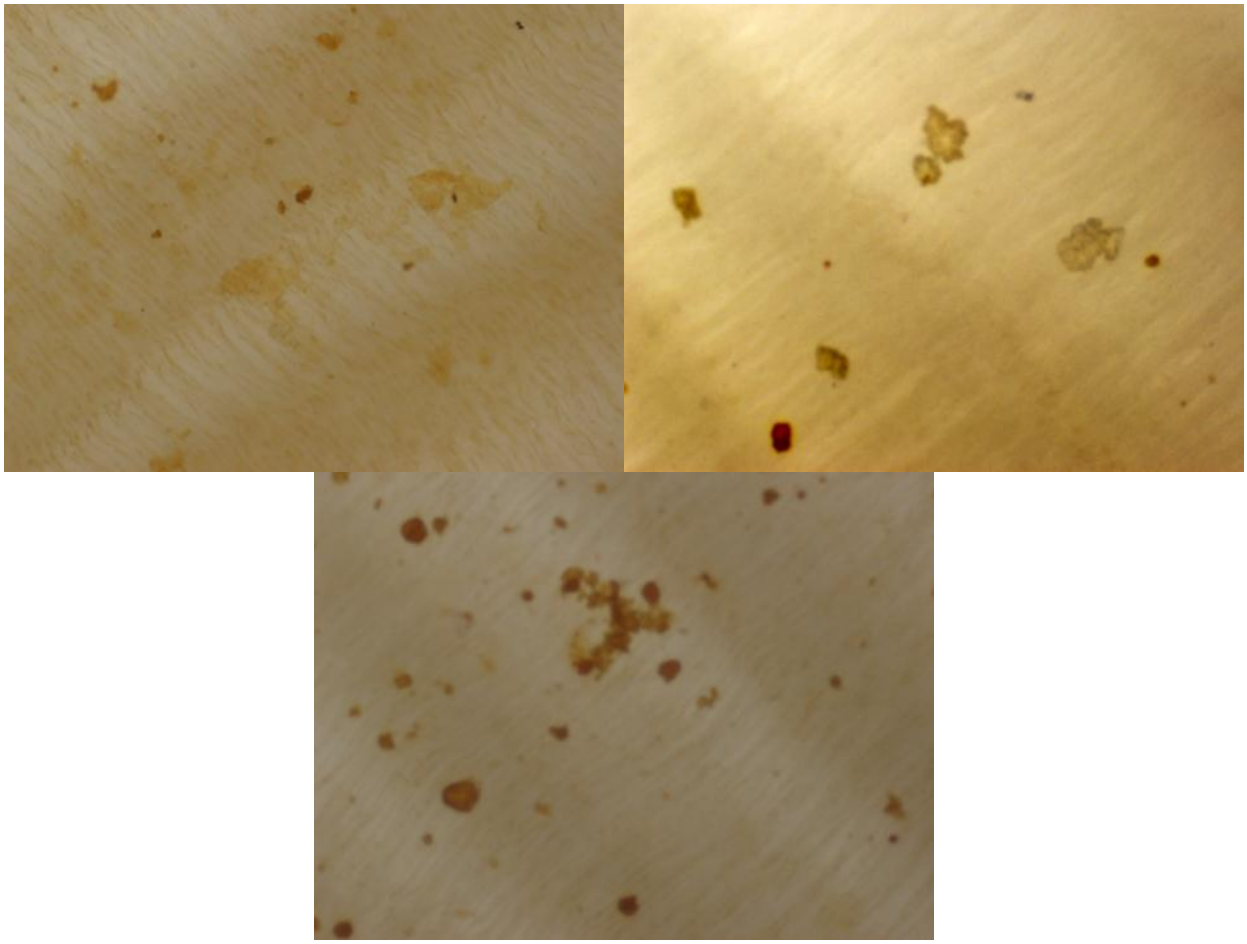

Figure 10. *TRAP staining of osteoclasts on dentine disks exposed to PBS (top left), Cloisite 93A in PBS (top right) and Cloisite 30B in PBS (bottom).*

Discussion

The porous morphology of the resorbable PDLA nanocomposites indicates suitability for use as a scaffold for bone growth. Pore sizes in the range of 100-300 μm have been shown to be sufficient to support neovascularization, and cellular infiltration (Moroni et al., 2009; Khan et al., 2008). Both pure and nanocomposite constructs synthesized for this study exhibited average pore diameters of 236.2 μm, 243.1μm and 239.8 μm for 100PDLA, 100PDLA-1 and 100PDLA-2.5 constructs, respectively. Pore interconnectivity is also essential for the *in vivo* viability of scaffolds, as it ensures the ability to transport nutrients to the center of the constructs. Though

no quantitative techniques were employed in this study, SEM of fracture surfaces showed that both pure and nanocomposite scaffolds had a high degree of interconnectivity. Overall, no significant effect of nano-clay addition was seen on the resulting morphology of the nanocomposite constructs. Both pure and nanocomposite constructs demonstrated a dense shell, which transitioned abruptly to a porous interior. The addition of clay had no observable effect on the thickness or morphology of the shell, or its transition to a porous interior. This morphology is similar to that of the cortico-cancellous bone grafts commonly employed in orthopaedic surgery (Malloyo and Hilibrand, 2002; Samartzis et al., 2003; Wigfield and Nelson, 2001). In these grafts, the dense cortical shell provides rigid support during biomechanical loading. Due to the similarity in structure, it is hypothesized that the dense shell of the nanocomposite scaffolds would play a similar role. This hypothesis was not tested in this study, as all mechanical testing was performed on porous cores taken from the interior of the constructs.

Small angle X-ray diffraction showed a significant increase in the 2θ position of the [001] plane of incorporated nano-clay. The shift of the peak to a lower 2θ position is indicative of an increase in the spacing of clay platelets (Horsch et al., 2006; Manitiu et al., 2008; Pavilidou and Papspyrides, 2008; Ray and Okamoto, 2003). The basal spacing of the pure nano-clay used in this study was found to be 2.62 nm. After $scCO_2$ processing the clay-polymer mixtures, the spacing increased to 4.40 nm. The measured increase in spacing is due to polymer chain infiltration between the clay layers (Horsch et al., 2006; Manitiu et al., 2008). During processing, CO_2 is able to diffuse in between the clay platelets as well as increase the mobility of the polymer, which is solvated by the CO_2. This facilitates polymer chain infiltration between clay platelets and further increases platelet spacing. Upon rapid depressurization, the expansion of CO_2 within the particles forces a fraction of the clay platelets apart, significantly increasing

the surface area available for polymer interaction. This increase in dispersion as well as the intercalation of polymer between clay platelets results in reinforcement of the polymer matrix and reduced mobility of the polymer chains, and can be a key factor in mechanical property improvements (Horsch et al., 2006; Manitiu et al., 2008; Pavilidou and Papspyrides, 2008; Ray and Okamoto, 2003).

Rheology is a commonly used tool in nanocomposite characterization for investigating polymer-particle interaction effects, as well as particle dispersion effects. Characterization of the rheological behavior of the pure PDLA and PDLA-clay nanocomposite constructs showed that the nano-clay reduced the mobility of polymer chains within the construct. A shift in the frequency at which the storage (G') and loss (G") moduli cross indicates a change in the so-called "characteristic relaxation time" of the polymer. In this case, a reduction in the crossover frequency from 0.23 rad/s to 0.10 rad/s is indicative of over a doubling of the relaxation time of the polymer. Additionally, the low frequency "terminal" region of the storage modulus has a reduced slope when compared to the pure polymer which indicates that there is a significant amount of clay dispersion, and improved polymer-clay interactions in the processed construct (Ray and Okamoto, 2003). Such strong polymer clay interactions and dispersion are necessary for the efficient transfer of stress from the matrix to the filler that is necessary to enhance mechanic properties.

Mechanical testing of the porous constructs showed significant improvements in compressive strength with the addition of as little as 1wt% nano-clay. Nanocomposites with 2.5 wt% nano-clay showed the highest compressive strength and compression modulus. Results from mechanical testing show that the nanocomposite constructs compare favorably to cancellous and cortico-cancellous human bone. Compressive strengths of the nanocomposites

reported in this study exceed the ranges of human cancellous bone from the mandible and lumbar vertebral bodies as reported in literature (Giesen et al., 2001; Jensen et al., 1990; Mosekilde and Mosekilde, 1986; Yeni and Fyhrie, 2001). Mosekilde, et al. measured the whole vertebral body ultimate compressive strength to range from 1.5 to 7.8 Mpa (Mosekilde and Mosekilde, 1986). The compressive strengths of thenanocomposites at 50% strain are within the range of the ultimate compressive strength of human lumbar vertebral bodies (approximately 2.0 – 8.0 Mpa) reported by Ebbesen, et al (Ebbesen et al., 1999). Mechanical testing data presented in this study are for porous cores taken from the pure and nanocomposite constructs. It is hypothesized that the dense shell that is present on the outside of the constructs will increase the resistance to mechanical loading, thereby improving its suitability for load-bearing applications.

The mechanical properties of the nanocomposite scaffolds also compare favorably to those reported for other synthetic polymer nanocomposite constructs (Georgiou et al., 2007; Mathieu et al., 2005; Gualandi et al., 2010; Teng et al., 2007; Khan et al., 2008; Rezwan et al., 2006). In a recent review article by Rezwan, et al., the reported compressive strengths for PLGA, PLLA and PDLLA matrices filled with calcium phosphates, Bioglass or phosphate glass fabricated using a variety of techniques range from 0.07 to 0.42 Mpa (Rezwan et al., 2006). Mathieu, et al. have reported that utilizing a similar supercritical CO_2 process a compressive strength of up to 6.0 Mpa was achieved in PLA-βTCP and PLA-HA composites (Mathieu et al., 2005). The improvements in compressive strength and modulus observed in the polymer-clay nanocomposites is likely due to the high reinforcement capacity of the nano-clays. The nano-clay platelets that are dispersed in the polymer matrix during $scCO_2$ processing have a very large aspect ratio, allowing for greater polymer-clay contact and restriction of polymer chain mobility. The degree with which these nano-clays can be dispersed in the polymer matrix also improves

mechanical properties, when compared to polymer constructs reinforced with calcium phosphates. Agglomeration of calcium phosphate particles within polymer matrices has been cited as a potential reason for the relatively modest improvements in strength (Georgiou et al., 2007; Mathieu et al., 2005). The use of organic modifiers improves the ability of nano-clays to be dispersed in polymer matrices (Horsch et al., 2006; Manitiu et al., 2008; Pavilidou and Papspyrides, 2008; Ray and Okamoto, 2003). Rapid depressurization and polymer chain infiltration during $scCO_2$ processing also facilitates improved dispersion of the nano-clays, leading to improvements in mechanical behavior(Horsch et al., 2006; Manitiu et al., 2008).

Preliminary investigations of biocompatibility of the supercritical CO_2-processed resorbable polymer nanocomposite constructs suggest an overall neutral, or bioinert response by human osteoblasts. While alkaline phosphatase activity and osteoprotegerin expression was higher for control and 100PDLA constructs at certain time points, these differences were insignificant after seven days in culture. Aluminosilicate materials, similar in composition and structure to the nano-clays used in this study, have been shown to positively influence osteoblast proliferation, differentiation and mineralization (Haroun et al., 2009; Katti et al., 2008). However, this is the first study to examine human osteoblast response to nano-clay which is highly dispersed in a resorbable polymer matrix by $scCO_2$. The nano-clays used in this study are organically-modified with alkyl-ammonium salts. However, these moieties are not likely to be exposed to the cellular environment, as they are dispersed in the polymer matrix.. The relatively low weight-percent of clay used in this study also minimizes the chance of organic modifier-induced cytotoxicity. No toxic, or apoptotic response was noted within the cultures, as evidenced by the maintenance of cell attachment and osteoblastic cell morphology.

Ostoeblast extracellular matrix deposition on the nanocomposite constructs also indicates favorable biological interaction. Calcium phosphate-rich deposits could clearly be seen on the surface of the constructs, as well as within pores. This deposition was observed to also occur at the very center of the cultured constructs, which indicates that osteoblasts are able to penetrate the porous network of the nanocomposite constructs. Cellular infiltration of these constructs is important for their *in vivo* use as bone graft substitutes. The diameter of the pores also suggests that these constructs would also support neovascularization, which is integral for nutrient transport. Further, the dense to porous morphology imparted by the $scCO_2$ process closely resembles the structure of cortico-cancellous bone grafts currently used in orthopaedic surgery. This morphology has been shown to be important both in terms of new bone growth, as well as in the support of biomechanical loads *in vivo*.

Osteoclast pit formation and TRAP expression showed a dependence on the type of nanoclay modifier used. Exposure of cultured osteoclasts to Cloisite 30B resulted in consistently higher concentrations of resorption pits at all time points, compared to Cloisite 93A and control wells. Cloisite 93A also elicited the greatest expression of TRAP by the cultured osteoclasts. Since the particle sizes of Cloisite 93A and Cloisite 30B are similar, as are their base compositions (both Montmorillonite clays), it can be deduced that the difference in organic modifier led to the differences observed in resorption pit formation and TRAP expression by the osteoclasts. While differences in biologic response relative to differences in nanoclay modifier have not been described, both Rueda and Styan have detailed the effects of Cloisite 30B clays on cell viability and proliferation. Both in vitro studies showed a dose-dependent reduction of cell viability and proliferation upon exposure to Cloisite 30B. While no assays were performed in the current study to quantify viability and proliferation, the confluence of osteoclasts seemed

similar between treatment groups and time points. Styan et al., characterized the release of quaternary ammonium compounds (QACs) *in vitro* during their fibroblast study. Both Cloisite 93A and 30B contain QACs in the employed modifier. It is hypothesized that the modifier for Cloisite 30B is either less strongly bound to the nanoclay resulting in higher in vitro concentrations of QACs, or that the specific QAC used for Cloisite 30B is more inflammatory.

Conclusions

Supercritical CO_2 processing of resorbable polymer/nano-clay mixtures results in the formation of porous nanocomposite constructs, which exhibit biocompatibility and significant improvements in mechanical properties. Porous resorbable polymer/nano-clay nanocomposite constructs prepared using scCO_2 processing exhibit improvements mechanical properties comparable to human cancellous and cortico-cancellous bone (2.5 fold increase in compressive strength compared to pure polymer constructs). Improvements in mechanical properties of the constructs are related to the dispersion of nanoclay within the polymer matrix and subsequent reduction in polymer chain mobility. The biocompatibility of the constructs, as determined by alkaline phosphatase activity and expression of osteoprotegerin by cultured human osteoblasts, was similar to polystyrene culture plate controls and resorbable polymer constructs without clay after seven days in culture. Further in vivo studies are necessary to determine the full extent of cellular response to polymer-clay nanocomposites, as well as construct degradation kinetics. Supercritical CO_2-processed resorbable polymer nanocomposites represent a potential alternative to autograft and allograft in orthopaedic procedures requiring bone graft.

References

Arribas-Garcia I, Alcala-Galiano A, Garcia AF, Moreno JJ. 2009. Fracture of the anterior iliac crest following monocortical bone graft harvest in bisphosphonate-related mandibular pathological fracture: a case report. Oral Surgery Oral Medicine Oral Pathology Oral Radiology and Endodontics 107(6), e12-4.

Baker KC, Bellair RJ, Manitiu M, Herkowitz HN, Kannan RM. 2009. Structure and mechanical properties of supercritical carbon dioxide-processed porous resorbable polymer constructs. Journal of the Mechanical Behavior of Biomedical Materials 2(6), 620-6.

Chau AM, Mobbs RJ. 2009. Bone graft substitutes in anterior cervical discectomy and fusion. European Spine Journal 18(4), 449-64.

Ebbesen EN, Thomsen JS, Beck-Nielsen H, Nepper-Rasmussen HJ, Mosekilde L. 1999. Lumbar vertebral body compressive strength evaluated by dual-energy X-ray absorptiometry, quantitative computed tomography and ashing. Bone 25(6), 713-24.

Georgiou, G., Mathieu, L., Pioletti, D.P., Bourban P.-E., Manson, J.-A.E., Knowles, J.C., et al. 2007. Polylactic acid-phosphate glass composite foams as scaffolds for bone tissue engineering. Journal of Biomedical Materials Research: Part B Applied Biomaterials 80B, 322-31.

Giesen EBW, Ding M, Dalstra M, van Eijden TMGJ. 2001. Mechanical properties of cancellous bone in the human mandibular condyle are anisotropic. Journal of Biomechanics 34, 799-803.

Gualandi C, White LJ, Chen L, Gross RA, Shakesheff, KM, Howdle SM, et al. 2010. Scaffold for tissue engineering fabricated by non-isothermal supercritical carbon dioxide foaming of a highly crystalline polyester. ActaBiomaterialia 6(1), 130-6.

Haroun AA, Gamal-Eldeen A, Harding DR. 2009. Preparation, characterization and in vitro biological study of biomimetic three-dimensional gelatin-montmorillonite/cellulose scaffold for tissue engineering. Journal of Materials Science: Materials in Medicine 20(12), 2527-40.

Horsch S, Gulari E, Kannan, RM. 2006. Supercritical CO_2 dispersion of nanoclays and polymer clay nanocomposites. Polymer 47, 7485-96.

Hu R.W. and Bohlman H.H. 1994. Fracture at the iliac bone graft harvest site after fusion of the spine. Clinical Orthopaedics and Related Research 309, 208-13.

Hu Y, Grainger DW, Winn SR, Hollinger JO. 2002. Fabrication of poly(alpha-hydroxy acid) foam scaffolds using multiple solvent systems. Journal of Biomedical Materials Research 59(3), 563-72.

JensenKS, Mosekilde L, Mosekilde L. 1990. A model of vertebral trabecular bone architectures and its mechanical properties. Bone 11(6), 417-23.

Kanczler JM, Ginty PJ, White L, Clarke NM, Howdle SM, Shakesheff KM, Oreffo RO . 2010. The effect of the delivery of vascular endothelial growth factor and bone morphogenic protein-2 to osteoprogenitor cell populations on bone formation. Biomaterials 31(6), 1242-50.

Katti KS, Katti DR, Dash R. 2008. Synthesis and characterization of a novel chitosan/montmorillonite/hydroxyapatite nanocomposite for bone tissue engineering. Biomedical Materials 3(3): 034122.

Khan Y, Yaszemski MJ, Mikos AG, Laurencin CT.2008. Tissue engineering of bone: material and matrix considerations. Journal of Bone and Joint Surgery (American) 9, 36-42.

Kim SS, Ahn KM, Park MS, Lee JH, Choi CY, Kim BS. 2007. A poly(lactide-co-

glycolide)/hydroxyapatite composite scaffold with enhanced osteoconductivity. Journal of Biomedical Materials Research: Part A 80A(1), 206-15.

Malloy, KM, Hilibrand, AS. 2002. Autograft versus allograft in degenerative cervical disease. Clinical Orthopaedics and Related Research 394, 27-38.

Manitiu M, Bellair RJ, Horsch S, Gulari E, Kannan RM. 2008. Supercritical carbon dioxide-processed dispersed polystyrene-clay nanocomposites. Macromolecules 41(21), 8038-46.

Mathieu, L.M., Montjovent, M.-O., Bourban, P-E., Pioletti, D.P. and Manson, J.-A.E. 2005. Bioresorbable composites prepared by supercritical fluid foaming. Journal of BiomedicalMaterials Research: Part A 75A, 89-97.

Moroni A, Larsson S, Hoang Kim A, Gelsomini L, Giannoudis PV. 2009. Can we improve fixation and outcomes? Use of bone substitutes. Journal of Orthopaedic Trauma 23(6), 422-5.

Mosekilde L, Mosekilde L. 1986. Normal vertebral body size and compressive strength: relations to age and to vertebral and iliac trabecular bone compressive strength. Bone 7(3), 207-12.

Nam YS, Park TG. 1999. Porous biodegradable polymeric scaffolds prepared by thermally induced phase separation. Journal of Biomedical Materials Research 47, 8-17.

Pavlidou S, Papspyrides CD. 2008. A review on polymer-layered silicate nanocomposites. Progress in Polymer Science 33, 1119-98.

Ray SS, Okamoto M. 2003. Polymer/layered silicate nanocomposites: a review from preparation to processing. Progress in Polymer Science 23, 1524-43.

Rezwan K, Chen QZ, Blaker JJ, Boccacini AR. 2006. Biodegradable and bioactive

porous polymer/inorganic composite scaffolds for bone tissue engineering. Biomaterials 27(18), 3413-31.

Rueda L, Garcia I, Palomares T, Alonso-Varona A, Mondragon I, Corcuera M, Eceiza A. 2011. The role of reactive silicates on the structure/property relationships and cell response evaluation in polyurethane nanocomposites. Journal of Biomedical Materials Research: Part A 97(4), 480-489.

Samartzis D, Shen FH, Matthews DK, Yoon St, Goldberg EF, An HS. 2003. Comparison of allograft to autograft in multilevel anterior cervical discectomy and fusion with rigid plate fixation. The Spine Journal 3(6), 451-9.

Styan KE, Martin DJ, Poole-Warren LA. 2008. In vitro fibroblast response to polyurethane organosilicate nanocomposites. Journal of Biomedical Materials Research: Part A 86A(3), 571-582.

Teng X, Ren J, Gu S. 2007. Preparation and characterization of porous PDLLA/HA composite foams by supercritical carbon dioxide technology. Journal of Biomedical Materials Research: Part B Applied Biomaterials 81, 185-93.

Wang Y, Zhang L, Hu M, Liu H, Wen W, Xiao H, et al. 2008. Synthesis and characterization of collagen-chitosan-hydroxyapatite artificial bone matrix. Journal of Biomedical Materials Research: Part A 86A(1), 244-52.

Wigfield CC, Nelson RJ. 2001. Non-autologousinterbody fusion materials in cervical spine surgery: How strong is the evidence to justify their use? Spine 26(6), 687-94.

Yeni YN, Fyhrie DP. 2001. Finite element calculated uniaxial apparent stiffness is a consistent predictor of uniaxial apparent strength in human vertebral cancellous bone tested

with different boundary conditions. Journal of Biomechanics 34, 1649-54.

Zeng C, Han X, Lee LJ, Koelling KW, Tomasko DL. 2003. Polymer-clay nanocomposite foams prepared using carbon dioxide. Advanced Materials 15(20): 1743-47.

CHAPTER 6: INFLUENCE OF POLYMER END FUNCTIONALITY AND NANOCLAY ORGANIC MODIFICATION ON DISPERSION AND RHEOLOGY

Introduction

Nanocomposites composed of organically-modified Montmorillonite clay dispersed in polymer matrices have garnered significant attention relative to significant improvements in physical properties. Depending on the composite system, the addition of organically-modified clay (nanoclay) can reduce gas permeability, increase flame resistance, improve thermal stability and enhance both static and dynamic mechanical properties. As such, the applications for polymer-nanoclay composites are as varied as the methods for synthesizing them. Owing to the significant improvements in mechanical properties even at low concentrations of nanoclay, polymer-clay nanocomposites have been investigated.

Recently, our group has employed supercritical carbon dioxide ($scCO_2$) processing to create porous resorbable polymer nanocomposites. These nanocomposites are composed of organically modified Montmorillonite clay dispersed in a matrix of poly-D-lactide (PDLA). Processing with $scCO_2$ simultaneously disperses nanoclay throughout the matrix and induces an interconnected porous morphology to the construct. Static mechanical properties of the resulting construct constitute a two-fold change in ultimate compressive strength and significant improvements in compressive modulus. Rheological measurements of heat-pressed, dense PDLA-clay nanocomposites illustrate a significant shift in the frequency of storage and loss moduli cross-over, indicative of a large decrease in the characteristic relaxation time of the polymer matrix. An increased slope in the terminal region of the nanocomposite, compared to pure polymer also indicated favorable polymer clay interactions. Both of these characteristics point towards the restriction of polymer chain mobility as the dominant mode of reinforcement by the organically-modified Montrmorillonite clay in the PDLA matrix.

It is recognized that enhancing the level of favorable polymer-clay interaction will result in an overall enhancement of mechanical properties of the nanocomposite. One potential method of enhancing polymer-clay interaction is to alter the end functionality of the polymer. Chen et al, examined the influence of functionalizing Montmorillonite clay that had already been organically modified with epoxy groups on dispersion within a poly-L-lactide matrix. The addition of the epoxy end groups to the organically-modified clay led to an increase in tensile strength, elastic modulus and elongation at failure when compared to PLLA-clay nanocomposites without epoxy-functionalized clay. Epoxy functionality of the nanoclay enhanced the degree of positive interaction with PLLA polymer chains during melt compounding (Chen et al., 2005).

The purpose of this study is to examine the influence of polymer end functionality and nanoclay organic modification regime on dispersion and melt-rheology of PDLA-clay nanocomposites processed by $scCO_2$. Interactions. Poly-D-lactide with either a lauryl ester, or carboxylic acid end functionality were $scCO_2$ processed with Cloisite 93A or Cloisite 30B. Resulting constructs were characterized with small angle X-ray diffraction (SAXD) and melt-rheology to determine the extent of clay dispersion within the polymer matrix, as well as the improvements in dynamic mechanical properties.

Materials and Methods

Materials

Nanoclays used in this study remained in the as-received state from the manufacturer (Southern Clay Products Inc., Houston, TX). Cloisite 93A, which is a Montmorillonite clay organically modified with methyl dihydroginated tallow ammonium slat (modifier concentration = 95 meq/100 g clay) and Cloisite 30B, which is a Montmorillonite clay organically modified

with methyl, tallow, bis-2-hydroxyethyl quaternary ammonium salt (modifier concentration = 90 meq/100 g clay) were used to create nanocomposites. The size distribution of dry particulate of both Cloisite 93A and Cloisite 30B particles is as follows: 10% less than 2 mm; 50% less than 6 mm and 90% less than 13 mm. Cloisite 93A has a basal d_{001} of 23.6 Å, while the d_{001} for Cloisite 30B particles was 18.5 Å, per the manufacturer.

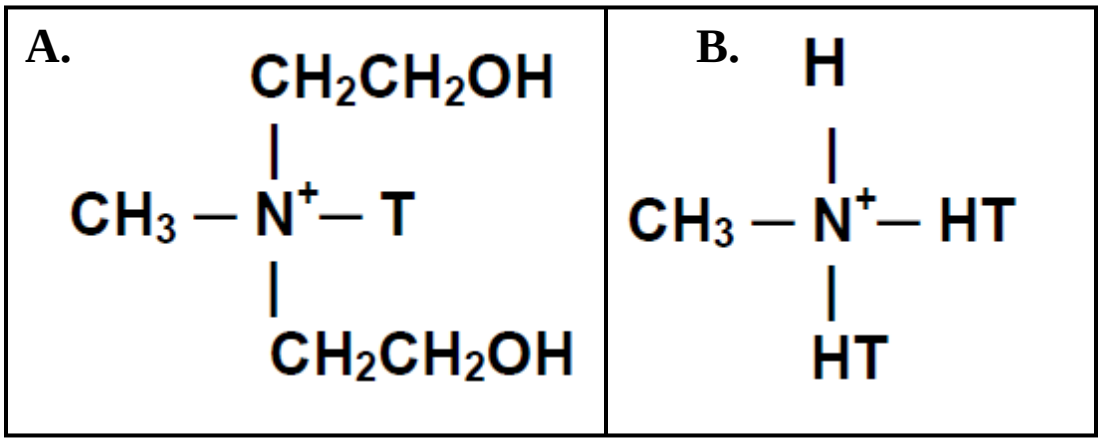

Figure 1. *Chemical structure of the organic modifiers used in Cloisite 30B (A) and Cloisite 93A (B), methyl tallow bis-2-hydroxyethyl quaternary ammonium and methyl dehydrogenated tallow ammonium, respectively*

Two different polymers were used as the matrix component of the nanocomposite. Both polymers were based on pure poly-D-lactide (PDLA, SurModics Biomaterials, Birmingham, AL) and had inherent viscosities in the range of 0.60 – 0.80 dL/g. Terminal group chemistries differed between polymers, as one polymer was terminated by an ester group (PDLA-E) and the other by a carboxylic acid (PDLA-A). All polymers were stored in air-tight containers until processing at a temperature of -20^{o}C.

Nanocomposite Synthesis

To create PDLA-nanoclay composites, polymers were ground to an average particle size of 100-300 μm. Cloisite 30B or Cloisite 93A were mechanically mixed at ambient conditions with either PDLA-E or PDLA-A at 2.5 wt%. This concentration has been previously shown to result in a significant increase in compressive mechanical properties for $scCO_2$-processed nanocomposites composed of ester terminated PDLA and Cloisite 93A. After mechanical mixing, the polymer-nanoclay mixtures were placed in a steel mold within a pressure vessel. The vessel was filled with CO_2 until an internal pressure of 2000 psi was obtained, while maintaining the temperature of the vessel at 90°C. The vessel was maintained at this pressure and temperature for 60 minutes. After 60 minutes, the system was rapidly depressurized at a rate of 2-4 bar/s. Following processing, the nanocomposites were stored at -20°C for 30 minutes before removal from the molds.

Small Angle X-ray Diffraction

The intergallery spacing of nanoclay within the resorbable polymer matrices was assessed by small angle X-ray diffraction (SAXD). Supercritcial CO_2-processed nanocomposites were sectioned into small fragments using a scalpel and palced in a custom zero-background quartz sample holder. Using a RigakuSmartLab Diffractometer with a Cu-Kα X-ray source (λ = 1.54 Å) and an accelerating voltage of 40 kV at a current of 40 mA, scans were collected from 0.1 to 10° 2θ at a rate of 3.0 deg/min with a step size of 0.30 degrees. Several scans were obtained from different locations in the particulate sample and verified to be reproducible by superimposing diffraction patterns. The 2θ angle corresponding to the [001] peak was determined by analyzing the diffraction spectra with software onboard the diffractometer. Bragg's Law of diffraction was then used to calculated the intergallery spacing of the nanoclyas within the polymeric matrix, subtracting 1.0 nm to account for clay platelet thickness. SAXD

scans of pure Cloisite 30B and Cloisite 93A were also obtained in the same manner to verify the supplier-provided d_{001} spacing of the nanoclays.

Rheology

To determine the impact of polymer end functionality and the method of nanoclay organic modification on dynamic mechanical properties, melt-rheological measurements were performed. Supercritical CO_2-processed nanocomposites were heat pressed into rectangular molds between Teflon-coated stainless steel platens at a temperature of 80°C. Samples were than annealed in a vacuum oven at 80°C to remove residual CO_2, which could negatively impact rheology measurements. Following adequate removal of residual CO_2, melt rheological measurements were performed under oscillatory shear using a Rheometric Scientific RSA II rheometer. Rectangular specimens (15.98 mm x 12.7 mm x 0.55 mm) were loaded on the machine in a shear sandwich geometry and allowed to equilibrate for one hour. Rheological measurements were performed at 80ºC and 120ºC for all samples, and time-temperature superposed to create master curves with a reference temperature of 80°C. A frequency range of 0.01-100 rad/s was employed. Storage (G') and loss (G'') moduli were plotted against frequency on the master curves. Melt rheological measurements of nanocomposites were compared to those obtained for pure polymers.

Results

As-received Cloisite 30B and Cloisite 93A exhibited a d_{001}-spacing of 1.98 nm and 2.62 nm, respectively, which corresponds to an intergallery spacing of 0.98 nm and 1.62 nm, respectively. scCO_2-processing of polymer-clay nanocomposites resulted in a shift in the 2θ

peak position, as shown in Figure 2, which corresponded to an increase in intergallery spacing for all polymer-clay combinations, as shown in Table 1.

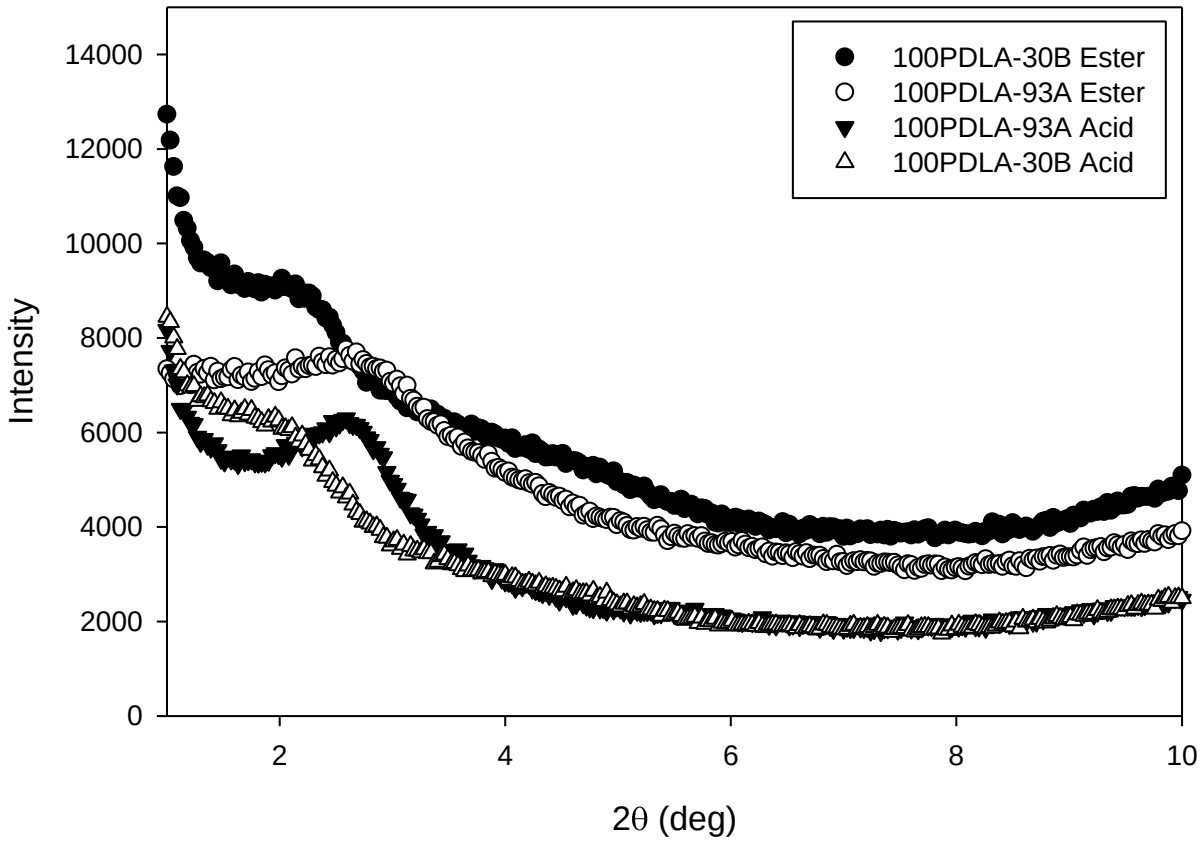

Figure 2. *Small angle X-ray diffraction (SAXD) of Cloisite 93A, Cloisite 30B and nanocomposites of 100PDLA-ester or 100PDLA-acid with each of the nanoclays.*

Cloisite 30B displayed the largest increases in intergallery spacing from the as-received state with an increase of 2.15 nm with PDLA-Ester constructs and 2.55 nm with PDLA-Acid constructs. Cloisite 93A also displayed significant increases in intergallery spacing with a 1.39 nm dilation when processed with PDLA-Ester and 1.69 nm when processed with PDLA-Acid. Acid-terminated polymers yielded the largest increases in clay intergallery spacing in both cases.

Table 1. *Peak positions and corresponding d_{001}-spacing of as-received Cloisite 93A, Cloisite 30B and $scCO_2$-processed nanocomposites of PDLA and nanoclay.*

Clay	Matrix	Peak Position (2θ)	d_{001}-Spacing	Increase in Intergallery Spacing
Cloisite 93A	None	3.36	2.62 nm	--
Closite 30B	None	4.46	1.98 nm	--
Cloisite 93A	PDLA-Ester	2.20	4.01 nm	1.39 nm
Cloisite 93A	PDLA-Acid	2.61	3.38 nm	1.69 nm
Cloisite 30B	PDLA-Ester	2.13	4.13 nm	2.15 nm
Cloisite 30B	PDLA-Acid	1.95	4.53 nm	2.55 nm

Dynamic oscillatory shear measurements demonstrate that acid-terminated PDLA nanocomposites have lower storage (G') and loss (G'') moduli compared to ester-terminated PDLA nanocomposites across a range of frequencies, as shown in Figure 3. Improvements in both G' and G'' were seen for all nanocomposite constructs over pure polymers.

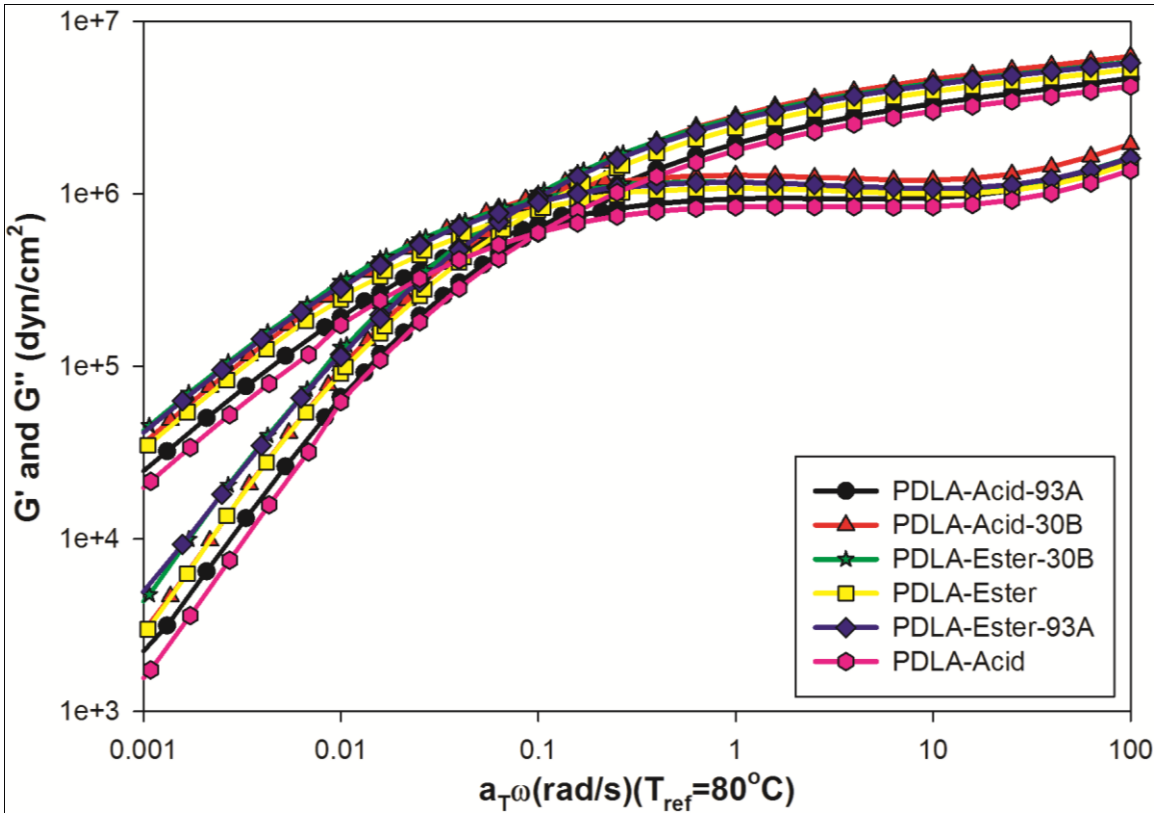

Figure 3. *Rheological measurements performed at 80^{o}C and 120^{o}C time-temperature superposed to create a master curve of G' and G'' at a reference temperature of 80^{o}C.*

Both ester-terminated polymers exhibited a shift in the G'-G'' cross-over frequency, as shown in Figure 4. This effect was most pronounced for PDLA-Ester-93A nanocomposites and is indicative of a reduction in characteristic relaxation time of the polymer. G' and G'' were slightly increased by combining ester-terminated PDLA with Cloisite 30B, but less noticeable after the addition of Cloisite 93A. Almost no shift in the G'-G'' cross-over frequency was observed for acid-terminated polymers was observed. Similarly the magnitude of G' and G'' were unchanged with the addition of Cloisite 93A to acid-terminated PLDA. In contrast, G' and G'' increased significantly when Cloisite 30B was added to the acid-terminated PDLA.

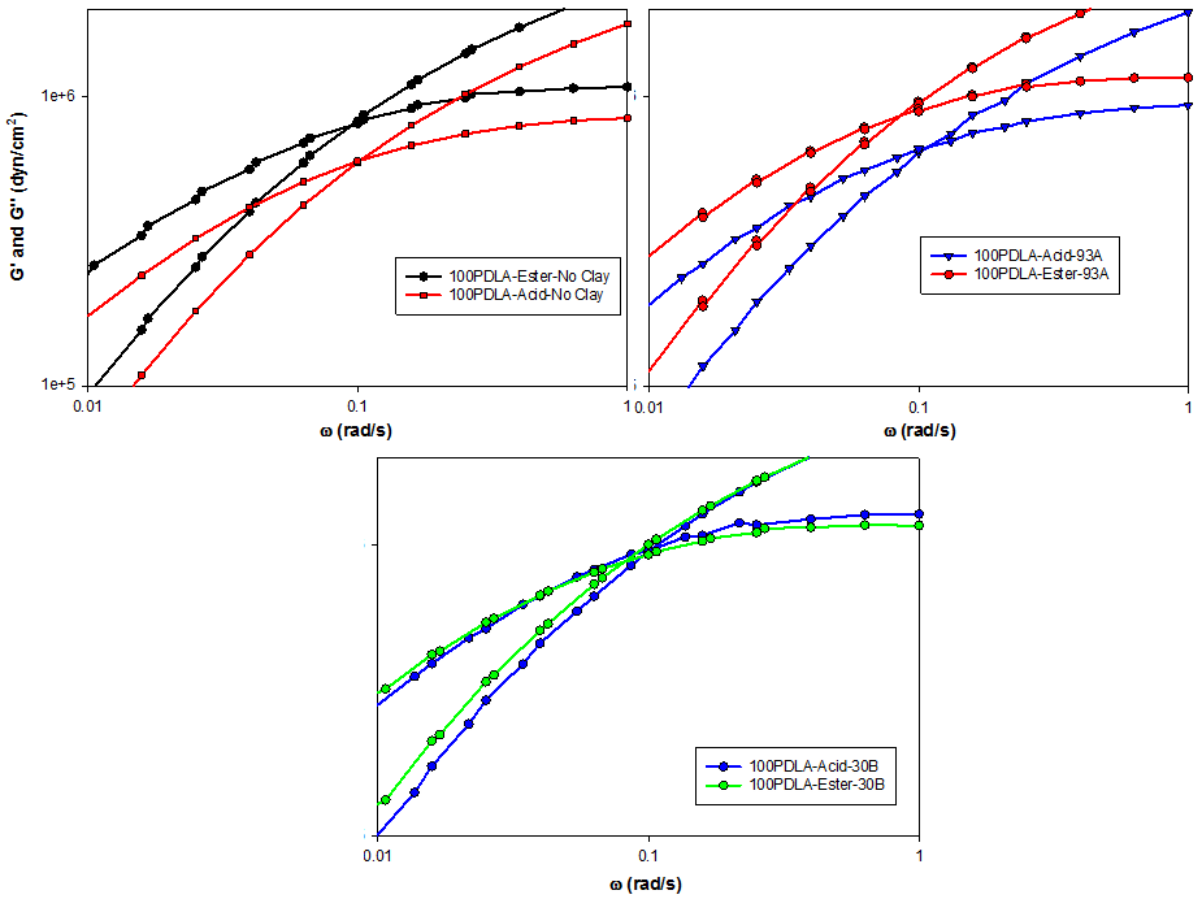

Figure 4. *G' and G'' plotted against frequency for pure polymers (Top Left), PDLA-93A nanocomposites (Top Right) and PDLA-30B nanocomposites (Bottom).*

Tan (δ), which is the ratio of G'' and G', was similar between pure and nanocomposite constructs, as shown in Figure 5. Acid-terminated polymers did show a slightly higher value of this ratio, which is an indicator of the elasticity of the polymer melt. Ester-terminated PDLA with Cloisite 93A and Cloisite 30B resulted in a reduction of Tan(δ) indicating a loss of elasticity upon nanoclay addition.

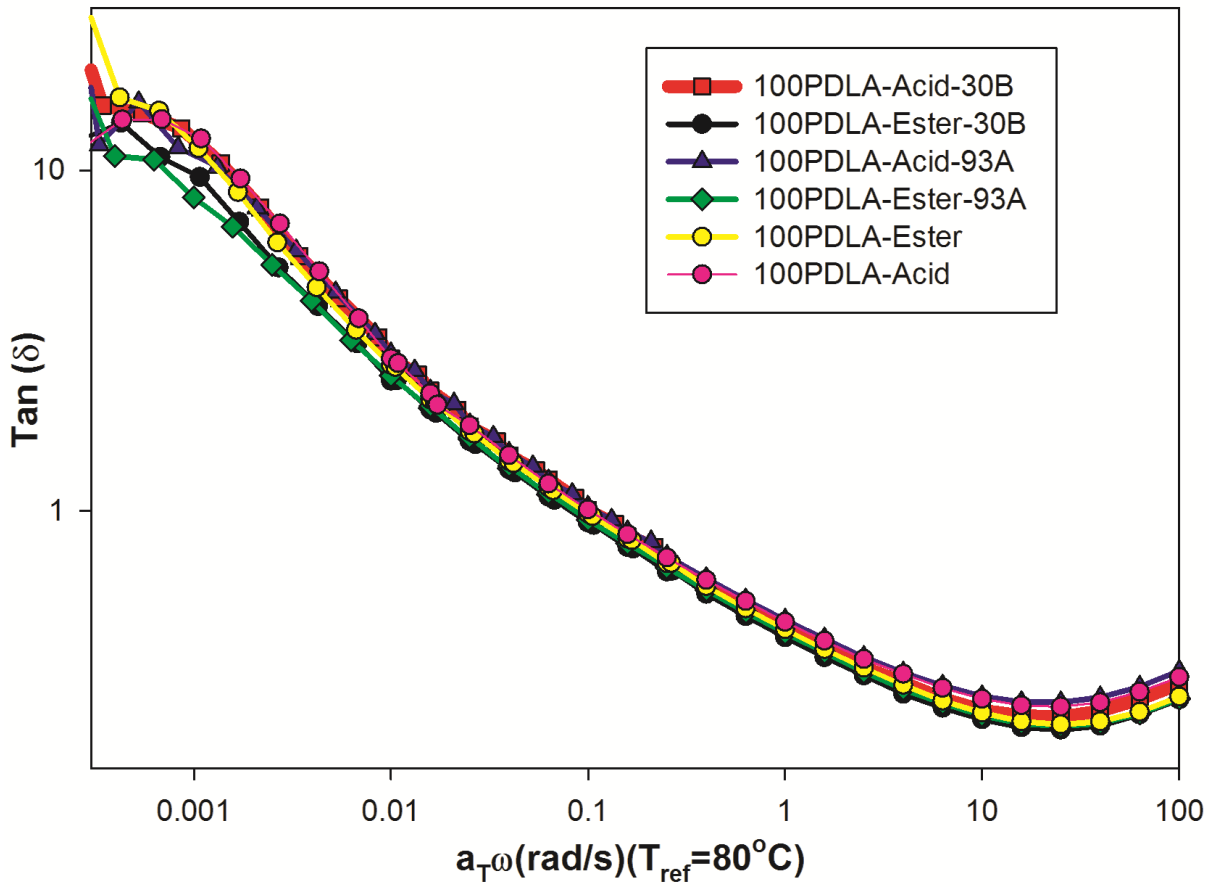

Figure 5. *Tan (δ) of pure and nanocomposite materials.*

Discussion

All nanocomposite constructs exhibited an increase in the intergallery spacing of nanoclay, regardless of end functionality and nanoclay modifier. Acid-terminated PDLA resulted in greater increases in spacing, compared with the ester-terminated polymer. Further, the greatest increase in intergallery spacing was seen with ester-terminated PDLA and Cloisite 30B. These results suggests that there is an effect of both polymer end functionality and nanoclay modifier on the $scCO_2$-mediated dispersion of nanoclay in polymer matrices. It has been previously demonstrated that modification of nanoclay particles to improve interaction with polymer chains leads to an improvement in dispersion. Chen, et al. grafted epoxy groups onto nanoclay particulate and demonstrated significant improvements in dispersion in poly(L-lactide)

(PLLA) matrices (Chen et al., 2005). Tsimpliarki, et al. also investigated the role of nanoclay surface chemistry on dispersion within a PLLA matrix (Tsimpliarki et al., 2011). Both of these studies focused exclusively on the modification of nanoclay, independent of its organic modification, which increases basal plaetelet spacing. To the authors' knowledge this is the first study which examined the role of both polymer end functionality and chemistry of organic modifiers in as-received organically modified Montmorillonite clays on dispersion.

Improvements in rheological behavior of the polymers were seen when Cloisite 93A or Cloisite 30B were added. The most significant improvement observed was a shift in the G', G'' cross-over frequency for PDLA-Ester-93A, which is indicative of a reduction in the characteristic relaxation time of polymer chains. A reduction in this relaxation time suggests more solid-like behavior as a result of the restriction of polymer chain mobility by the dispersed nanoclay (Horsch et al., 2006; Manitiu et al., 2008; Pavlidou and Papaspyrides, 2008; Ray and Okamoto, 2002). Noticeable improvements in G', G'' and Tan(δ) were observed upon the addition of Cloisite 93A or Cloisite 30B to PDLA-Acid. As measurements were not carried out at low frequency ranges, further characterization of rheological behavior of pure and nanocomposite materials was not possible. However, the improvements seen at higher frequencies are indicative of nanoclay-dependent reinforcement of the polymer matrices. The most significant improvements were seen for acid-terminated PDLA. It is unclear if this effect is a function of differential interaction between the carboxylic acid end groups of the polymer and the two different nanoclay modifiers, or if this is simply a function of the difference in initial viscosities between PDLA-Ester and PDLA-Acid.

To further elucidate the influence of polymer end functionality and nanoclay modifier, future rheological measurements should be performed at a lower frequency range (Maiti et al,

2002; Ray et al., 2002; Ray et al., 2002). Considerable sample degradation was observed for frequency ranges below 0.001 rad/s for both pure and nanocomposite samples. For lower frequency ranges, a lower temperature should be used to minimize sample degradation. The principle of time-temperature superposition can then be applied so that data performed at higher frequencies (and higher temperatures) can still be analyzed simultaneously.

Conclusions

Supercritical CO_2-processed PDLA-clay nanocomposites show considerable dispersion during small angle X-ray diffraction measurements. This dispersion seems to be dependent on both the polymer end functionality and the organic modifier of the clay. Further, dynamic oscillatory shear measurements show improvements in rheological behavior of polymer-nanoclay nanocomposites. While it remains unclear if this improvement in construct rheology is a function of polymer end group – nanoclay modifier interaction, differential improvements were observed based on the different clays and polymers tested. We have demonstrated a method of tailoring dispersion and dynamic mechanical properties through modification of polymer and nanoclay surface functionality.

References

Chen G-X, Kim H-S, Shim J-H, Yoon J-S. 2005. Role of expoxy groups on clay surface in the improvement of morphology of poly(L-lactide)/clay composites. Macromolecules 38(9), 3738-3744.

Horsch S, Serhatkulu G, Gulari E, Kannan RM. Supercritical CO_2 dispersion of nano-clays and clay/polymer nanocomposites. Polymer 47, 7485-7496.

Maiti P, Yamada K, Okamoto M, Ueda K, Okamoto K. 2002. New polylactide/layered silicate nanocomposites: Role of organoclays. Chemistry of Materials 14(11), 4654-4661.

Manitiu M, Bellair RJ, Horsch S, Gulari E, Kannan RM. 2008. Supercritical carbon dioxide-processed dispersed polystyrene-clay nanocomposites. Macromolecules 41, 8038-8046.

Pavlidou S, Papaspyrides CD. 2008. A review on polymer-layered silicate nanocomposites. Progress in Polymer Science 33, 1119-1198.

Ray SS, Maiti P, Okamoto M, Yamada K, Ueda K. 2002. New polylactide/layered silicate nanocomposites. 1. Preparation, characterization and properties. Macromolecules 35(8), 3104-3110.

Ray SS, Yamada K, Okamoto M, Ogami A, Ueda K. 2003. New polylactide/layered silicate nanocomposites. 3. High-performance biodegradable materials. Chemistry of Materials 15(7), 1456-1465.

Ray SS, Okamoto M. 2003. Polymer/layered silicate nanocomposites: A review from preparation to processing. Progress in Polymer Science 28, 1539-1641.

Tsimpliaraki A, Tsivintzelis I, Marras SI, Zuburtikudis I, Panayiotou C. 2011. The effect of surface chemistry and nanoclay loading on the microcellular structure of porous poly(D,L lactic acid) nanocomposites. The Journal of Supercritical Fluids 57(3), 278-287.

Zeng C, Han X, Lee LJ, Koelling KW, Tomasko DL. 2003. Polymer-clay nanocomposite foams prepared using carbon dioxide. Advanced Materials 15(20), 1743-1747.

CHAPTER 7: IN VIVO INFLAMMATORY RESPONSE TO AND OSTEOINDUCTIVE CAPACITY OF PDLA-NANOCLAY COMPOSITES PROCESSED BY SUPERCRITICAL CARBON DIOXIDE

Introduction

Owing to the disadvantages associated with autologous and allogenic bone grafts (autograft and allograft, respectively), there is significant interest in developing synthetic substitute materials to enhance in vivo bone growth in clinical applications, such as fracture healing, arthroplasty and spinal arthrodesis (Rezwan et al., 2006; Khan et al., 2008; Moroni et al., 2009). Resorbable polymers, based on polymerized lactic- and glycolic acid are excellent candidate materials due to their nearly four-decade history of clinical use, predictable degradation kinetics and myriad options of processing (Rezwan et al., 2006; Khan et al., 2008). In order to support *in vivo* bone formation capable of withstanding biomechanical loading, these polymers must possess a three dimensional porous morphology. Average pore diameters in the range of 100-300 μm are necessary to support cellular infiltration and neovascularization, which are both integral components to osteogenesis (Khan et al., 2008).

Methods such as thermal- or pressure-induced phase separation, particulate leaching and three dimensional printing have been used to create porous constructs from resorbable polymers (). While these methods are effective in terms of induction of an appropriate porous morphology for bone tissue engineering, the poor static mechanical properties of the constructs preclude their use in load bearing applications. To enhance the mechanical performance of these constructs, researchers have attempted to reinforce the polymeric matrices with a variety of micro- and nano-structured filler materials, including hydroxyapatite, phosphate glass and carbon nanotubes (Rezwan et al., 2006; Khan et al., 2008; Georgiou et al., 2007; Mathieu et al. 2005). Modest gains in compressive mechanical properties have been observed to date, which is often attributed

to poor dispersion of the filler in the matrix, as well as poor interaction between the filler and matrix (Georgiou et al., 2007). Supercritical carbon dioxide ($scCO_2$) processing of organo-modified nanoclays with poly-D-lactide (PDLA) polymers has shown promise in the rapid production of porous resorbable nanocomposites for structural bone graft substitute applications (Baker et al., 2011). With as little as 2.5 wt% of nanoclay, the compressive mechanical properties of the nanocomposite are nearly twice that of pure polymer scaffolds processed by $scCO_2$. The static compressive mechanical properties of $scCO_2$-processed resorbable polymer nanocomposites also compare favorably to native cortico-cancellous bone. Likewise, the porous structure of the nanocomposite constructs mimics the dense shell-porous core morphology of clinically-used autologous and allogenic bone graft materials, such as those harvested from the antero-superior region of the iliac crest (Baker et al., 2009; Baker et al., 2011; Chau and Mobbs, 2009; Moroni et al., 2009).

The use of filler materials with micron and sub-micron dimensions raises a concern regarding the potential immune and inflammatory response to the particulate debris as scaffolds degrade *in vivo*. Materials used in total joint arthroplasty and spine surgery, such as cross-linked polyethylene, poly methyl methacrylate, titanium alloy and CoCrMo alloys have been shown to induce a potent inflammatory response when the material is reduced to a particulate state during *in vivo* mechanical wear (Hallab et al., 2003; Jacobs et al., 2006). This multifactorial response begins with engulfment of particulate debris by local macrophages (Ingham and Fisher, 2005; Purdue et al., 2007; Holt et al., 2007). Responding macrophages express pro-inflammatory cytokines, including tumor necrosis factor-alpha (TNF-α), interleukin-1beta (IL-1β), interleukin-6 (IL-6), interferon-gamma (IFN-γ) and granulocyte/macrophage-colony stimulating factor (GM-CSF) (Ingham and Fisher 2005; Purdue et al., 2007; Smith et al., 2010; Smith et al., 2010). The

expression of these cytokines is dependent on particle characteristics, such as size, concentration, composition and surface area (Wooley et al., 2002; Jacobs et al., 2006; Yang et al., 2002). These cytokines are chemotactic for a number of immune cells, including monocytes. Monocytes recruited to the site by the inflammatory cytokines differentiate into osteoclasts with active bone resorptive capacity (Holt et al., 2007; Purdue et al., 2007). Activated osteoclasts begin to resorb local bone, while the anabolic potential of osteoblasts and osteocytes are suppressed by cytokines in both an autocrine and paracrine fashion (Vermes et al., 2001; Kanaji et al., 2009; Fuji et al., 2011). The net result, if particle concentration is sufficiently high, or increasing is the creation of cavitary defects in bone, which can compromise the stability of implants or lead to fracture (Hallab et al., 2003; Jacobs et al., 2006). A revision procedure is often necessity following particle-induced osteolysis in orthopaedic patients.

Particle-induced osteolysis may be an important factor to consider for resorbable polymer nanocomposites, such as scCO_2-processed PDLA-nanoclay constructs. As the nanocomposites are comprised primarily of a polymer that will undergo hydrolytic degradation *in vivo*, the final disposition of the nanoclay particles is of interest. It is not currently known if the nanocomposites will degrade to a final state of bare nanoclay, or if a particulate form of the nanocomposite will arise as a function of both hydrolysis and cyclic mechanical loading. If the nanoclay persists in "bare" form (not coated with polymer) a significant body of work suggests that silicate-based materials possess a surface functionality conducive to mineralization. Ishikawa, et al. profiled the morphology, alkaline phosphatase activity and markers of mineralization in murine osteoblasts on aluminosilicate nanotubes (Ishikawa et al., 2010). The group found an enhancement of osteoblastic differentiation, proliferation and active mineralization (Ishikawa et al., 2010). If the particulate remains in composite form (i.e.

nanoclay agglomerates coated with PDLA) until complete polymeric degradation, a local inflammatory response may develop in an effort to sequester the particles. The same theory of particle-induced osteolysis holds for several other resorbable polymer nanocomposite systems. Hydroxyapatite is a common filler in synthetic bone graft substitutes, due to the osteoconductivity of bulk hydroxyapatite. However, *in vitro* studies have illustrated the inflammatory and osteolytic potential of calcium phosphate particulate (Bloebaum et al., 1998; Sbokbar et al., 2001; Kalmodia et al., 2011).

In an effort to determine the immune and inflammatory response to resorbable polymer nanocomposite constructs, a study has been performed to characterize the osteolytic potential of bare particulate (filler only) and nanocomposite particulate (small particles of filler with polymer). Hydroxyapatite has been used as a positive control, as it is a material used frequently in bone graft substitute materials in both a clinical and pre-clinical setting. Exposure to bare particulate is meant to represent the worst case scenario, with a completely resorbed polymer matrix exposing the filler material to the biologic environment. A more likely scenario is represented by the nanocomposite particulate. Under cyclic loading, resorbable polymer nanocomposites are hypothesized to reduce to small particles composed of both polymer and clay. Additionally, an ectopic osteogenesis assay was performed to determine if bone formation is influenced by the incorporation of organically-modified Montmorillonite clay in a PDLA matrix.

Materials and Methods

In Vivo Inflammation Study

The murine air pouch model, established by Wooley, et al. is a well-defined system for assaying the inflammatory and osteolytic potential of the particulate form of materials used in orthopaedic surgery (Wooley et al., 2002; Yang et al., 2002; Yang et al., 2002; Ren et al., 2006; Ren et al., 2006). In accordance with an IACUC-approved protocol, 20 female Balb/C mice underwent serial injections of air (1 c.c. each)on the dorsum to create a highly biologically active, fluid-filled pouch. Air injections were performed every other day for a period of 5 days. On day five, after confirming the integrity of the air pouch, the mice were injected with bareparticulate (no polymer) according toTable 1.

Table 1. *Treatment groups for bare particulate inflammation study.*

Filler	Polymer	Sample Size	Concentration (mg/mL)
None (PBS control)	None (PBS control)	5	N/A
Hydroxyapatite	None	5	100
Cloisite 93A	None	5	100
Cloisite 30B	None	5	100

A separate phase of the study was conducted to examine the inflammatory response to nanocomposite particulate, as described in Table 2. Particulate in this format is thought to be a more accurate representation of debris that would be generated *in vivo* during construct degradation. In accordance with the same IACUC-approved protocol, 25 female Balb/C mice underwent serial injections of air (1 c.c. each) on the dorsum for a period of 14 days. Air injections were performed every other day for the first 7 days until the pouch remained stable and inflated. Injections were performed every two days after that. On day 14, after confirming the integrity of the air pouch, the mice were anesthetized with 1-2% inhaled isoflurane and the air pouches were incised. A 1.0 cm incision provided adequate access to the pouch. Following the incision, 100 mg of particles were implanted into the pouch. The incision was closed with 5-

0 Prolene suture and wound adhesive (NexaBand) was applied to create a water tight closure. After closure, the dorsum pouches were injected with 0.5 cc of saline.

Table 2.*Treatment groups for polymer and nanocomposite particulate inflammation study.*

Filler	Polymer	Sample Size	Mass of Particles
None (PBS control)	None	5	N/A
None (polymer only)	100 PDLA	5	100 mg
Hydroxyapatite	100PDLA	5	100 mg
Cloisite 93A	100PDLA	5	100 mg
Cloisite 30B	100 PDLA	5	100 mg

Mice were allowed ad libitum activity and free access to food and drink following the particulate injection. 48 hours after exposure, the animals were euthanized by asphyxiation in a CO_2 chamber and subsequently underwent cervical dislocation as a means of assurance of death. Dorsal pouch tissue was aseptically harvested with care to ensure that membranous tissue remained intact and sectioned into two equal volume specimens. Half of the tissue was immersed in zinc-buffered formalin, while the remainder was snap frozen in liquid nitrogen and subsequently stored at -80^{o}C until analysis.

Preparation of Polymer and Nanocomposite Particles for Inflammation Study

For animals receiving an injection of bare particulate (no polymer), ultrasonication in 70% ethanol was used to remove bound endotoxin from the particles. Following 10 minutes of sonication in 70% ethanol, the particles were transferred to 95% ethanol and left to dry in a sterile laminar flow culture hood overnight. Particulate was then rinsed three times with sterile PBS andresuspended in sterile PBS at a concentration of 100 mg/mL immediately prior to

injection. Each volume was vortexed prior to injection to ensure an equal distribution of particulate.

Polymer-coated particulate was utilized to simulate debris generated *in vivo* during the hydrolytic breakdown of PDLA. Freeze fracturing and subsequent grinding of $scCO_2$-processed polymers and nanocomposites failed to produce a particle size conducive to implantation. As such, a solvent casting method was used in the production of polymer and nanocomposite particulate. The solvent casting method consisted of dissolving 2.0 g of 100PDLA in 50mL of chloroform under constant agitation. Following adequate dissolution, particulate (hydroxyapatite, Cloisite 93A or Cloisite 30B) was stirred in until a homogenous mixture was obtained. Hydroxyapatite was loaded into the polymer at 45wt%, while Cloisite 93A and Cloisite 30B were loaded at 2.5wt%. The disparity in the amount of filler is reflective of the high hydroxyapatite content used by other researchers to achieve adequate increases in mechanical properties (Rezwan et al., 2006; Khan et al., 2008).

The mixtures were then cast in sterile Pyrex petri dishes. Mixtures were allowed to air dry for 24 hours in a sterile laminar flow hood. Following air dyring, the mixtures were lyophilized at a pressure of 0.045mBar for 48 hours. Particulate of a size conducive to injection was generated from the dried mixtures by a combination of chopping with a razor and grinding with mortar and pestle under liquid nitrogen. Particulate was suspended in 70% ethanol and ultrasonicated for 10 minutes to remove any bound endotoxin and subsequently transferred to absolute ethanol to drive off extra water. The particulate was again lyophilized at a pressure of 0.045 mBar for 96 hours in RN-ase and DNA-se free cryotubes in premeasured 100 mg doses. Approximately 200 mg of each particulate mixture was kept for imaging by scanning electron microscopy.

Histology and Cytokine Analysis

Half of the harvested pouch tissue was dehydrated and embedded in paraffin. 5.0μm sections were created using a microtome and subsequently stained with hematoxylin and eosin (H&E). Five H&E slides per pouch were cut for analysis. The H&E-stained sections were analyzed under a light microscope to qualitatively assess the infiltration of the pouch tissue by inflammatory and immune cells. Additionally, measurements of membrane thickness were made using digital image analysis software (Scion Image, Scion Corp.). An average of eight measurements per slide were made.

The remainder of the pouch tissue was homogenized in a buffer solution containing a protease inhibitor cocktail and TritonX100. The concentration of five pro-inflammatory cytokines including interleukin-1beta (IL-1β), interleukin-6 (IL-6), granulocyte/macrophage-colony stimulating factor (GM-CSF), macrophage inflammatory protein-2 (MIP-2) and interferon-gamma (IFN-γ), was quantified using a bead-based multiplex ELISA (Human Pro-inflammatory Cytokine Panel A, R&D Systems Inc., Minneapolis, MN). Cytokine expression was normalized to the total protein content in each sample, as determined by a total protein assay.

Preparation of Polymer and Nanocomposite Implants for Osteoinductivity Study

Ectopic osteogenesis assays are commonly used tools to study the ability of a scaffold to induce or support bone formation (Ishaug-Riley et al., 1997; Jeon et al., 2007; Ji et al., 2010; Barbieri et al., 2010). For the ectopic osteogenesis phase of the experiment, porous constructs were synthesized using $scCO_2$ processing, as previously described (Baker et al., 2009; Baker et al., 2011). Pure PDLA (no clay) constructs were processed at a temperature of 35^{o}C and a

pressure of 2000 psi. After 60 minutes of exposure to $scCO_2$, the reactor vessel was rapidly depressurized to produce a porous construct. Nanocomposite constructs, comprised of PDLA and 2.5wt% Cloisite 93A, were also synthesized with $scCO_2$ processing. A processing temperature of 90^{o}C and a pressure of 2000psi was used to generate constructs with a pore size similar to the pure PDLA constructs. Following $scCO_2$ processing, all materials were handled aseptically and stored in sterile locations.

A biopsy punch was used to take porous cores from the constructs with a diameter of 6.0 mm. The cores were then sectioned into discs with a thickness of 1.0 mm. While the specimens were handled aseptically, discs were nonethelessultrasonicated in 95% ethanol for 15 minutes to remove any bound endotoxin. Following drying, discs were stored in a sterile laminar flow hood until use.

Half of the pure polymer discs and half of the nanocomposite discs were selected at random for growth factor loading. Discs were immersed in 100 μL of a solution of E. Coli-expressed recombinant human bone morphogenetic protein-2 (rhBMP-2, R&D Systems Inc., Minneapolis, MN). The solutions were comprised of rhBMP-2 reconstituted with 4.0 mMHCl at a protein concentration of 100 μg/mL (potential for 20 μg of rhBMP-2 per disc) per manufacturer's instructions. After 10 minutes of immersion, which is consistent with current clinical use of rhBMP-2, the discs were removed from the solutions and air dried.

In Vivo Osteoinductivity Assay

In accordance with an IACUC-approved protocol, 36 female Balb/C mice were anesthetized and dorsum shaved. After preparing the surgical site in a sterile fashion, an incision was made on the dorsum of the mice over the hind limb. The gluteus muscle was identified and

an intramuscular pouch was created using blunt dissection. Upon preparation of the gluteal pouch, polymer or nanocomposite discs, according to Table 3, were inserted. The limb was ranged to ensure a low likelihood of extrusion of the disc during normal gait. Wounds were closed with suture and wound adhesive and the animals were allowed ad libitum activity upon recovery from the anesthetic.

Table 3. *Treatment groups for the in vivo osteoinductivity assay.*

Group	Description	n	Time Points
1	100PDLA	9	2, 4 and 6 weeks
2	100PDLA + 20 μg of rhBMP-2	9	2, 4 and 6 weeks
3	100PDLA-2.5wt% 93A	9	2, 4 and 6 weeks
4	100PDLA-2.5wt% 93A + 20 μg of rhBMP-2	9	2, 4 and 6 weeks

Histology and μ-Computed Tomography Analysis

Mice were sacrificed at two, four and six post-operative weeks by CO_2 asphyxiation and subsequent cervical dislocation. Euthanized mice underwent μCT analysis of ectopic bone formation. A scan power of 80 kVp and a voxel size of 50 μm^2 was used for all animals. Reconstructed DICOM images were analyzed by ImageJ software (National Institutes of Health, Bethesda, MD).

Following μCT imaging, the gluteal pouch and contents were aseptically harvested and immersed in zinc-buffered formalin. Specimens were dehydrated and embedded in paraffin. 5.0μm sections were taken from the specimens and stained with H&E. Approximately five H&E slides per animal were cut and analyzed by light microscopy.

Results

Inflammatory Response to Bare Particulate

All animals tolerated both the air injections, as well as the particle injections. Multiplex ELISA analysis of pro-inflammatory cytokine expression within the pouch tissue showed a substantial increase in IL-1β, IL-6 and MIP-2 for mice receiving injections of Cloisite 30B and Cloisite 93A, compared to PBS control and hydroxyapatite particles, as shown in Figure 2.Cloisite 93A particles elicited the highest level of IL-1b (93.8 +/- 44.8 pg/mL), which was significantly higher than both PBS controls ($p = 0.009$, 14.4 +/- 2.6 pg/mL) and hydroxyapatite ($p = 0.014$, 18.6 +/- 7.4 pg/mL), but not significantly higher than Cloisite 30B ($p=0.67$, 58.9 +/- 47.4 pg/mL). Cloisite 93A particles also induced the highest expression of IL-6 (545.6 +/- 272.2 pg/mL), which was again significantly higher than PBS control ($p<0.001$, 12.1 +/- 3.6 pg/mL) and hydroxyapatite particles ($p=0.001$, 11.3 +/- 4.1 pg/mL), but not significantly different than Cloisite 30B ($p=0.590$, 362.4 +/- 132.6 pg/mL). GM-CSF was highest in the Cloisite 93A group (20.7 +/- 14.7 pg/mL), followed by Cloisite 30B (17.8 +/- 14.5 pg/mL), PBS controls (0.4 +/- 0.5 pg/mL) and hydroxyapatite (0.4 +/0 0/4 pg/mL). No significant difference was found between the groups in terms of GM-CSF expression, which may have been due to a Type II statistical error. MIP-2 expression was again highest for the Cloisite 93A group (312.9 +/- 0.00), which was significantly higher than all other groups ($p<0.001$). In contrast, IFN-g expression was highest for PBS controls (25.8 +/- 3.2 pg/mL), which was significantly higher than Cloisite 93A ($p=0.017$, 12.1 +/- 6.1 pg/mL), but not significantly different from the hydroxyapatite group ($p=1.00$, 24.7 +/- 7.9 pg/mL) or the Cloisite 30B group ($p=0.236$, 17.2 +/- 6.4 pg/mL).

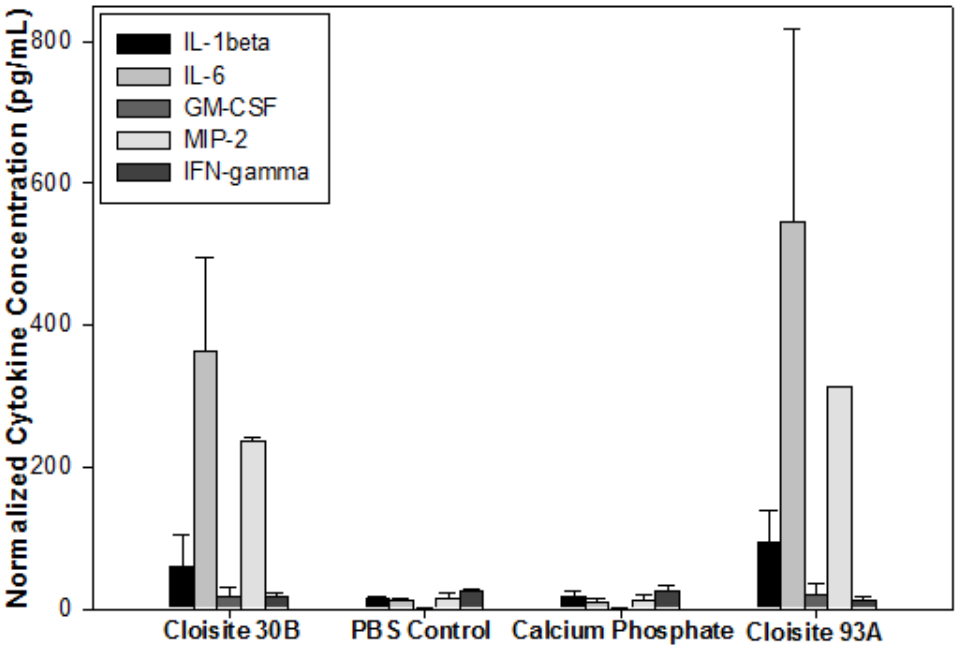

Figure 1. *Multiplex ELISA characterization of pro-inflammatory cytokine expression in air pouch tissue injected with PBS (control), hydroxyapatite particles, Cloisite 30B or Cloisite 93A.*

Analysis of histolgic sections of the mouse pouch tissue revealed a thick membranous tissue structure within the core of specimens, as shown in Figure 2. This was likely the reactive membrane formed both by serial injections of air, as well as injections of particulate. Inflammatory infiltrate was observed to be more intense in animals receiving injections of Cloisite 93A and Cloisite 30B. Cellular contents of the infiltrate tissue was predominantly histiocytes, which is indicative of an early phase of inflammatory response. Foreign body giant cells were identified in the tissue samples from mice receiving Cloisite 30B particulate. Inflammatory infiltrate in tissues from mice receiving hydroxyapatite particles was minimal. Cell contents of these tissue sections were predominantly fibroblastic, similar to the control tissues.

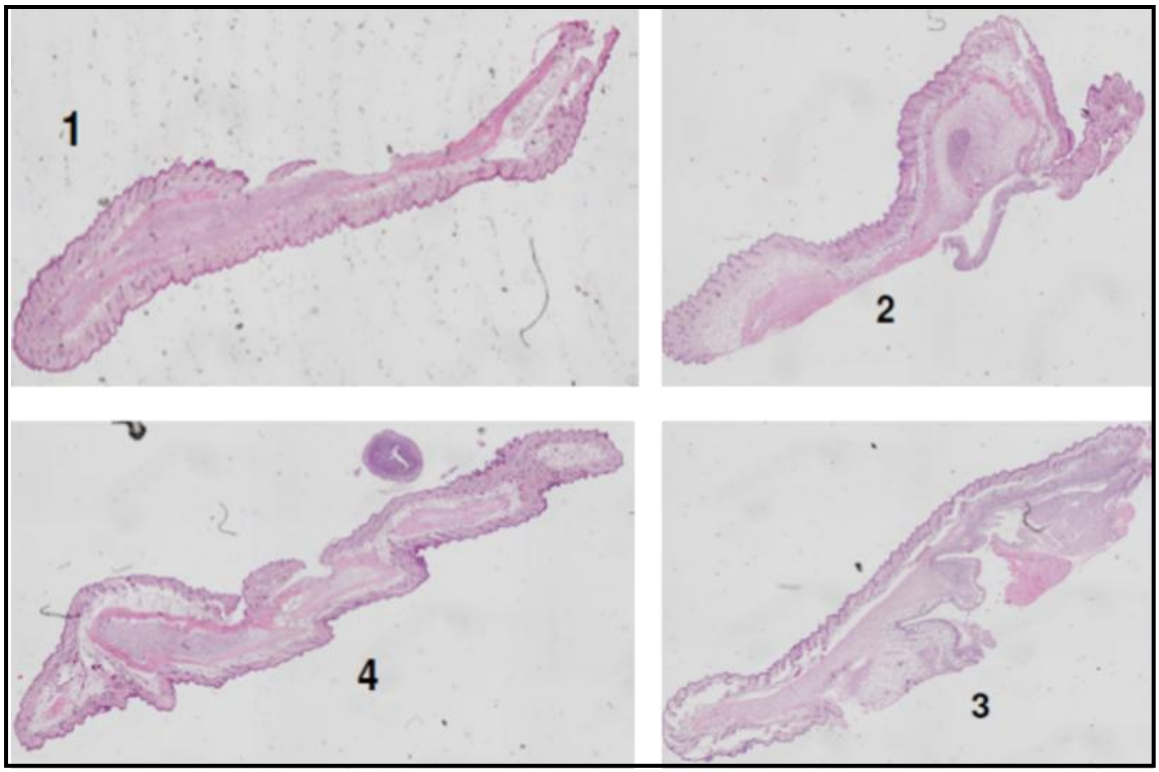

Figure 2. *Histologic sections of mouse air pouches that received saline injection (top left), 100 mg/mL of hydroxyapatite particulate (top right), Cloisite 93A (bottom left) and Cloisite 30B (bottom right) particulate.*

Histologic evaluation of pouch tissues harvested after 48 hours of exposure to Cloisite 93A, Cloisite 30B, hydroxyapatite or PBS revealed significant differences in membrane thickness, as shown in Figure 3. Tissues exposed to Cloisite 30B had the thickest membranes (598.31 +/- 137.22 μm), which was not significantly different from those exposed to hydroxyapatite ($p=1.00$, 572.39 +/- 90.60 μm), but was significantly higher than tissues from PBS controls ($p=0.004$, 507.61 +/- 114.00 μm) and Cloisite 93A ($p<0.001$, 470.77 +/- 115.95 μm). Membrane thickness in tissues exposed to Cloisite 93A particles was significantly lower than tissues exposed to hydroxyapatite ($p<0.001$), but not significantly lower than tissues exposed to PBS ($p=0.937$).

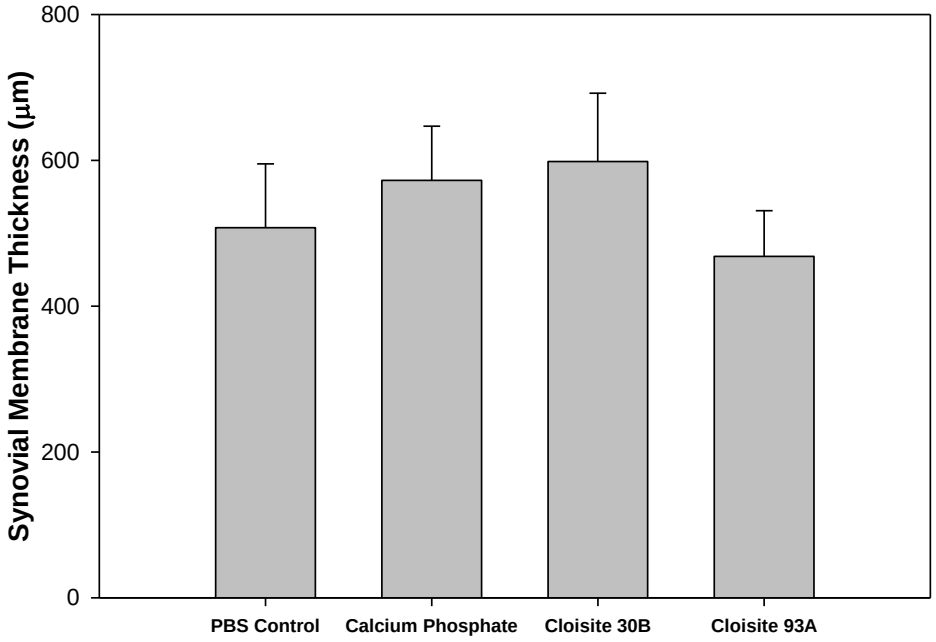

Figure 3. *Histological measurements of air pouch membrane thickness from mice receiving an injection of PBS, hydroxyapatite (calcium phosphate), Cloisite 30B and Cloisite 93A.*

Inflammatory Response to Nanocomposite Particulate

Nanocomposite particulate produced by solvent casting and subsequent grinding under liquid nitrogen results in similar sizes and morphologies between the treatment groups. All particles possessed a prismatic morphology and apparent aspect ratio of 2:1, with a minor axis of approximately 250 μm. PDLA-HA particulate tended to have a greater degree of nanotexture, which may be the result of the relatively high filler content. PDLA-93A and PDLA-30B particulate, though prismatic in nature, displayed fibrillar protrusions from the main body of the particles, as shown in Figure 4.

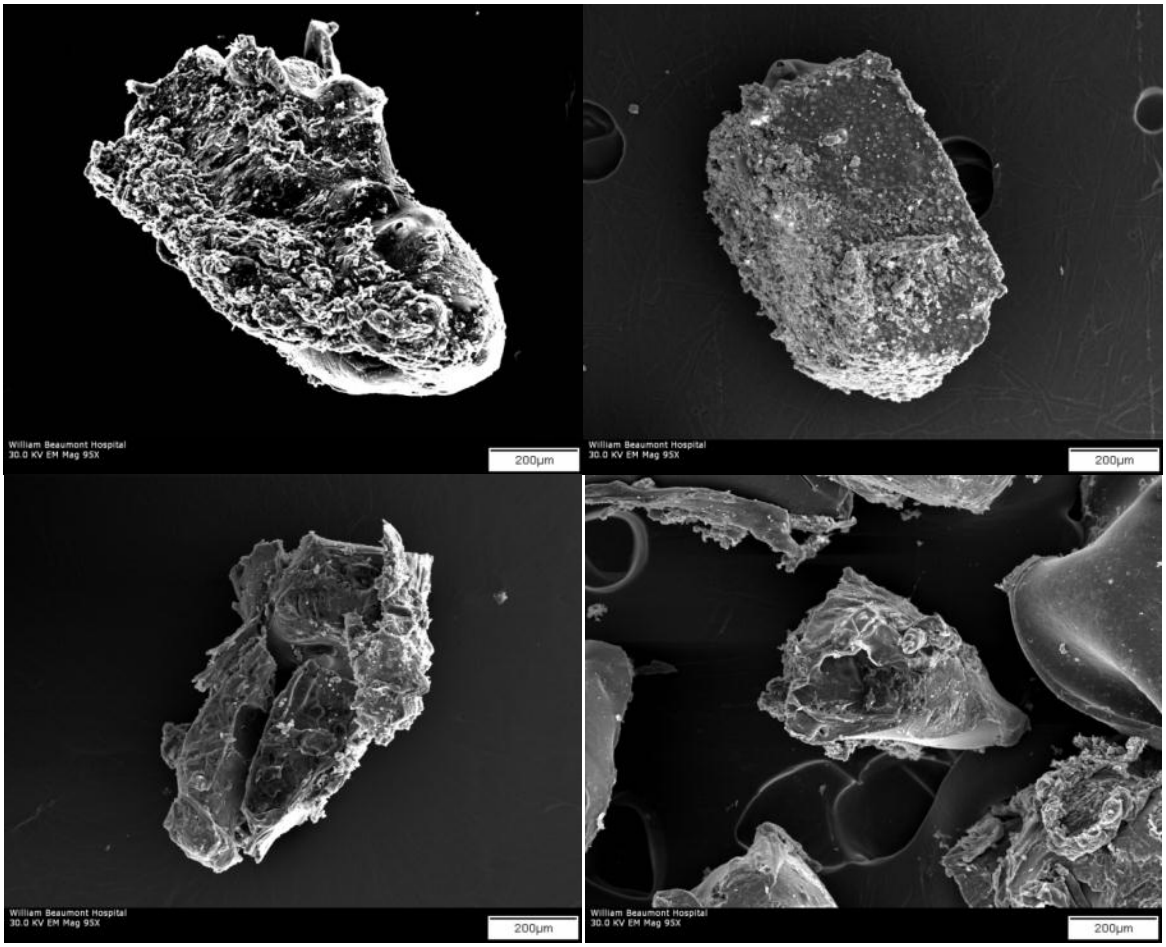

Figure 4. *Scanning electron micrographs of polymer and nanocomposite particulate debris. 100PDLA (top left), 100PDLA-45wt% HA, (top right), 100PDLA-2.5wt%93A (bottom left) and 100PDLA-2.5wt%30B (bottom right).*

One mouse was lost due to a pulmonary embolism immediately following one of the air pouch injections. All other animals tolerated both the air injections and particle implantions well, without incident. All mice that underwent an open procedure to facilitate implantation of particulate showed measurable amounts of pro-inflammatory cytokines upon multiplex ELISA, as shown in Figure 5. IL-6 was outside of the range of the standard curve for all tissue samples and is not reported. MIP-2 expression was largest for PDLA-30B nanocomposite samples (2770.0 pg/mL +/- 1304.3 pg/mL). This value was not statistically significant when compared to

PDLA-93A (p=1.00; 2312.4 +/- 697.0 pg/mL), or PDLA-HA particulate (p=1.00; 2119.1 +/- 542.8 pg/mL). PDLA (no filler) particulate induced the highest expression of IFN-g (175.9 +/- 15.9 pg/mL). No statistically significant differences were found with respect to IFN-g expression between treatment groups and controls. PDLA-HA particulate yielded the greatest expression of IL-1b (250.4 +/- 111.3 pg/mL), though there was no significant difference when compared to PDLA (p=0.139; 111.5 +/- 76.1 pg/mL), PDLA-93A (p=1.00; 195.3 +/- 79.0 pg/mL), or PDLA-30B(p=1.00; 184.8 +/- 61.6 pg/mL). With regards to GM-CSF expression, PDLA-HA particulate again yielded the highest expression (20.0 +/- 9.8 pg/mL) without a significant difference found between any treatment group, or with controls.

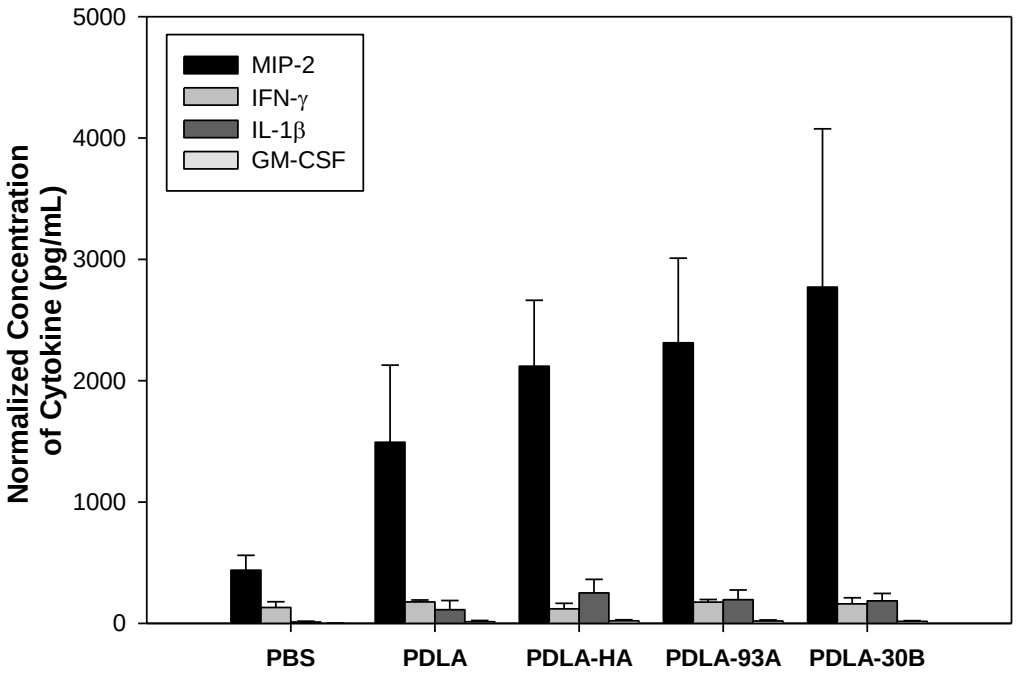

Figure 5. *Multiplex ELISA characterization of pro-inflammatory cytokine expression in air pouch tissue with implanted PDLA particles, PDLA-45wt% hydroxyapatite nanocomposite*

particles, PDLA-2.5wt%93A nanocomposite particles, PDLA-2.5wt% 30B nanocomposite particles and PBS (control).

Osteoinductivity of rhBMP-2-Loaded Nanocomposites

All mice undergoing open implantation of pure PDLA and PDLA-93A discs tolerated the procedure well and none were lost to complications. No animals exhibited constitutional symptoms or physical signs of infection. Upon gross observation of tissues during harvest, no outwardly observable signs of deep infection or foreign body response were noted. Micro-CT of the mice showed some reactive bone formation at the two week and four week time point in all mice receiving PDLA and PDLA-93A constructs without rhBMP-2, as shown in Figure 6. This bone formation was slightly more pronounced in the mice receiving PDLA-93A nanocomposites.

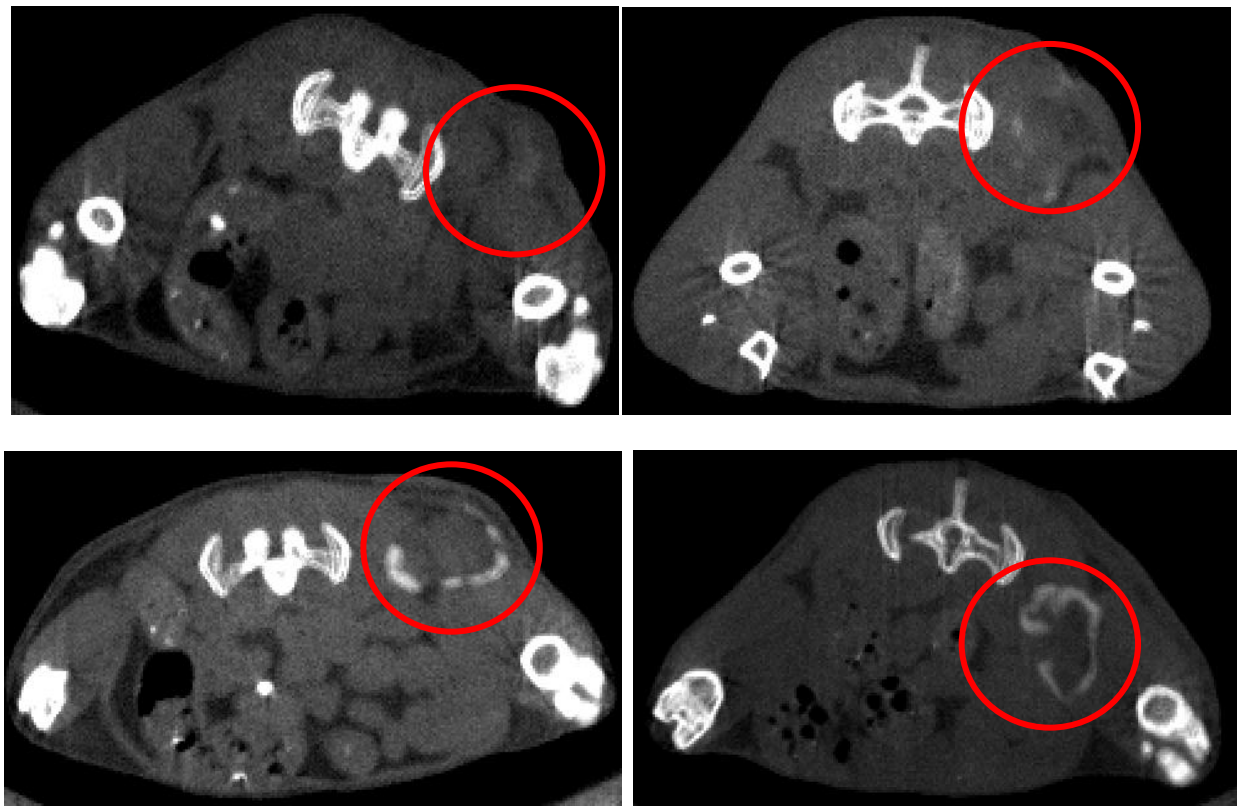

Figure 6. *Axial micro-CT images of in vivo bone growth after two weeks in mice receiving pure PDLA constructs (Top Left) and PDLA constructs with E. Coli-expressed rhBMP-2 (Bottom Left), compared to mice receiving PDLA-93A constructs (Top Right) and PDLA-93A constructs with E. Coli-expressed rhBMP-2 (Bottom Right). The red ring represents the area of construct implantation.*

By six weeks, the reactive bone formation had disappeared in constructs without rhBMP-2, as shown in Figure 7. Both construct types with adsorbed rhBMP-2 displayed a significant amount of bone formation at each of the three time points. Simultaneous orthogonal projections (combined views of axial, sagittal and coronal sections) displayed evidence of appositional, as well as three dimensional bone growth. No differences were observed between animals which received PDLA or PDLA-93A constructs, in terms of CT evidence of bone formation. All animals receiving constructs with rhBMP-2 adsorbed did show more fluid accumulation in the gluteal pouch, which is consistent with growth factor-induced bone formation.

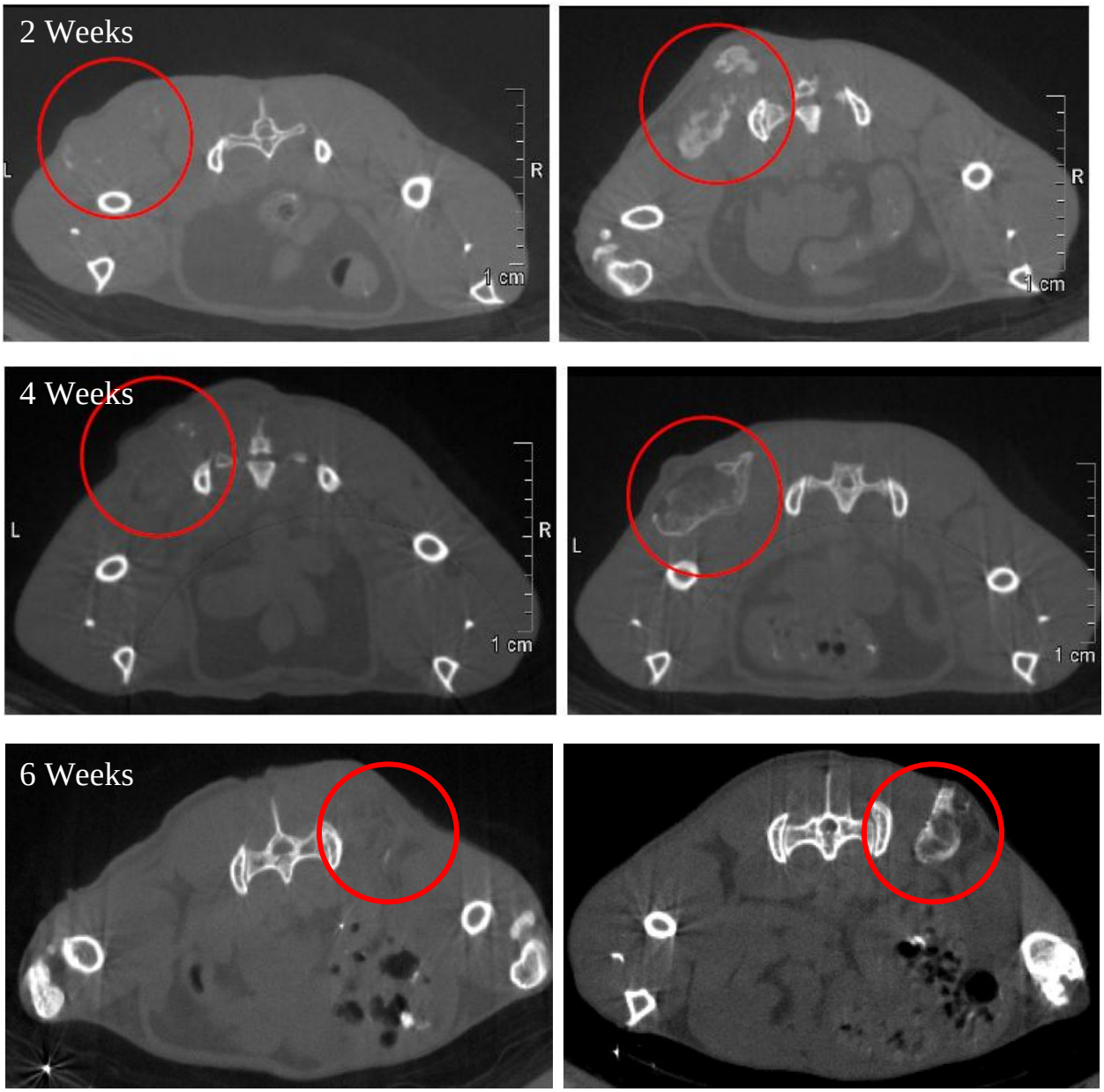

Figure 7. *Axial micro-CT images of in vivo bone growth in PDLA-93A nanocomposites with E. Coli-expressed rhBMP-2 (top right, bottom right) and without rhBMP-2 (top left, bottom left) at two weeks (top row), four weeks (middle row) and six weeks post-op.*

Discussion

In the simulated worst case scenario consisting of the exposure of filler materials directly to the biologic environment, without intervening polymer chains, both Cloisite 93A and Cloisite

30B particulate induced a significantly higher inflammatory response, compared to hydroxyapatite and saline controls. In particular the cytokines IL-1β, IL-6 and MIP-2 were significantly elevated in the clay-treated tissues. While cytokine expression was significantly different, no similar trends were found in measurements of membrane thickness in the pouch tissues. This could be due to the relatively short exposure of the pouch tissue to the particulate. Montmorillonite clay-induced inflammation is not well-described in the musculoskeletal setting. There is a paucity of data in general regarding the immune and inflammatory response to layered silicate structures *in vivo* and *in vitro*. Styan et al., examined the *in vitro* response of fibroblasts to nanocomposites composed of polyurethane reinforced with nanoclays modified with quaternary ammonium compounds (QAC) similar in structure to Cloisite 30B (Styan et al., 2008). This group found a negative effect on fibroblast proliferation and viability and referred to this effect as cytotoxicity, though no studies were performed to confirm cytotoxicity, or rule out apoptosis and necrosis. Liquid chromatography mass spectroscopy demonstrated leeching of QAC from the nanocomposites while in culture, which the authors posited led to the cytotoxicity (Styan et al., 2008). Rueda, et al., also examining polyurethane polymers reinforced with Cloisite 30B, found a similar effect on fibroblast proliferation (Rueda et al., 2011).In contrast, Katti, et al. found that blends of chitosan-Montrmorillonite and hydroxyapatite supported osteoblast function with no observable reduction in viability (Katti et al., 2008). Montmorillonite was observed to act synergistically with hydroxyapatite in supporting cell function by the osteoblasts (Katti et al., 2008). Zhuang, et al. also did not observe a negative effect of Montmorillonite clay in blends of gelatin and chitosan during in vitro analyses (Zhuang et al., 2007). It should be noted that neither Katti, nor Zhuang utilized organically-modified Montmorillonite. While Cloisite 93A is modified with a QAC, no in vitro or in vivo studies have

been performed to date to directly assess the effect of this specific QAC on cell viability or inflammatory response.

When the murine air pouches were challenged with nanocomposite particulate, the differences between nanoclay-loaded and hydroxyapatite-loaded constructs were not as substantial. MIP-2 showed the greatest difference between PDLA-HA, PDLA-93A and PDLA-30B with nanoclay-loaded particulate expressing greater concentrations of the cytokine, but this difference failed to reach statistical significance. PDLA-HA particulate actually induced a higher expression of both IL-1β and GM-CSF, compared to PDLA-93A and PDLA-30B. IL-6 was not reported for the nanocomposites particulate challenge, as technical difficulties with this assay were noted. Future work will include this analyte, as it has been shown to play an important role in inflammatory response and osteoclastogenesis. These results may be attributed both to the reduction of direct contact between nanoclay particulate and the biological environment, as well as the difference in filler content between hydroxyapatite-loaded and nanoclay-loaded particulate. Clinically-used products and pre-clinical tissue engineering constructs tend to use high concentrations of hydroxyapatite, both to enhance mechanical properties and to potentially facilitate osteoconduction. Peng, et al. used 20 wt% hydroxyapatite in a nanospun PLLA nanocomposite scaffold, while Guan, et al. used up to 75 wt% of hydroxyapatite in a PLGAmatrix (Peng et al., 2011; Guan et al., 2004). For the present study, nanocomposite particulate was loaded with 45 wt% hydroxyapatite, as this represented the median concentration of hydroxyapatite used in recent studies. Nanoclay-PDLA particulate was loaded with 2.5wt% Cloisite 93A or Cloisite 30B, as this was the concentration previously shown to result in the greatest gains in compressive strength and modulus (Baker et al., 2011). Though not a focus of this study, $scCO_2$-processed PDLA-93A constructs exhibit compressive

mechanical properties exceeding that of porous constructs with significantly higher concentrations of hydroxyapatite particulate.

Though the final disposition of nanoclay in PDLA nanocomposites remains as conjecture, a significant body of work exists detailing the mineralization of silicate structures. It is likely that in the event of complete matrix degradation, nanoclay would be incorporated within the *de novo* bone. Cunningham, et al. have demonstrated the incorporation of metallic debris within the developing posterolateral spine fusion mass in rabbits inoculated with titanium particulate (Cunningham et al., 2003). Further, Cunningham and colleagues demonstrated no significant reduction in bone formation as a function of exposure to the particulate, despite significantly elevated pro-inflammatory cytokine production and osteoclast activity (Cunningham et al., 2003). Nanocomposites synthesized for this study are not intended to be used in bearing surface applications, such as total joint arthroplasty devices. As such, the final size and morphology of particles will vary significantly with the particle sizes and morphologies used in in vitro and in vivo studies examining the osteolytic potential of mechanical wear debris. No data currently exists, which has examined the physical characteristics of particulate shed from porous resorbable polymer nanocomposites as a function of cyclic loading in an aqueous media. Future research will focus on creating nanocomposites particulate that more closely resembles the physical characteristics of debris found in vivo.

PDLA and PDLA-93A constructs synthesized by $scCO_2$ processing showed the ability to support *in vivo* bone formation, when functionalized with E. Coli-expressed rhBMP-2. Similar to other studies, the constructs displayed both appositional bone growth, as well as three dimensional infiltration of osteogenesis. These results suggest that the interconnected, porous morphology of the constructs are sufficient for bone graft applications where three-dimensional

bone growth is desired and often achieved with the addition of exogenous growth factors. No significant difference was noted between PDLA and PDLA-93A constructs in terms of bone growth at early time points. This results suggests that, despite the increased inflammatory response to nanoclay when compared with hydroxyapatite at identical concentrations, bone growth remains unaffected. Future studies will also seek to characterize neoangiogenesis associated with bone growth on the nanocomposites constructs. Vessel formation is an important requirement for the growth of sustainable osseous tissue. Results from the four week and six week timepoints, are encouraging, as bone resorption is a hallmark of non-viable and non-nutrient supplied neo-osseous tissue.

Conclusions

This is the first study to demonstrate the in vivo inflammatory response to Cloisite 30B, Cloisite 93A and nanocomposite particulate composed of these nanoclays dispersed in a PDLA matrix. The inflammatory response to PDLA-93A and PDLA-30B nanocomposite particulate was substantially equivalent to the more traditional PDLA-HA compositions, suggesting appropriate biocompatibility. Additionally, this study demonstrated the ability of supercritical carbon dioxide-processed PDLA-93A nanocomposites to support exogenous growth factor-induced bone formation. Supercritical CO_2-processed resorbable polymer-clay nanocomposites may be suitable as bone graft substitute in load-bearing orthopaedic applications.

References

Baker KC, Bellair R, Manitiu, Herkowitz HN, Kannan RM. 2009. Structure and mechanical properties of supercritical carbon dioxide processed porous resorbable polymer constructs. Journal of the Mechanical Behavior of Biomedical Materials 2(6), 620-626.

Baker KC, Manitiu M, Bellair R, Gratopp CA, Herkowitz HN, Kannan RM. 2011. Supercritical carbon dioxide processed resorbable polymer nanocomposite bone graft substitutes. Acta Biomaterialia. May 14 [Epub Ahead of Print].

Barbieri D, Renard AJ, de Bruijn JD, Yuan H. 2010. Heterotopic bone formation by nano-apatite containing poly(D, L-lactide) composites. European Cells and Materials 19, 252-261.

Bloebaum RD, Lundeen GA, Bachus KN, Ison I, Hofmann AA. 1998. Dissolution of particulate hydroxyapatite in a macrophage organelle model. Journal of Biomedial Materials Research 40(1), 104-114.

Cunningham BW, Orbegoso CM, Dmitriev AE, Hallab NJ, Sefter JC, Asdouian P, McAfee PC. 2003. The effect of spinal instrumentation particulate wear debris. An in vivo rabbit model and applied clinical study of retrieved instrumentation cases. The Spine Journal 3(1), 19-32.

Fuji J, Yasunaga Y, Yamasaki A, Ochi M. 2011. Wear debris stimulates bone-resorbing factor expression in the fibroblasts and osteoblasts. Hip International April 11 [Epub ahead of print].

Guan L, Davies JE. 2004. Preparation and characterization of a highly macroporous biodegradable composite tissue engineering scaffold. Journal of Biomedical Materials Research: Part A 71A(3), 480-487.

Hallab NJ, Cunningham BW, Jacobs JJ. 2003. Spinal implant debris-induced osteolysis. Spine 28(20), S125-138.

Holt G, Murnaghan C, Reilly J, Meek RM. 2007. The biology of aseptic osteolysis. Clinical Orthopaedics and Related Research 460, 240-252.

Ishaug-Riley SL, Crane GM, Gurlek A, Miller MJ, Yasko AW, Yaszemski MJ, Mikos AG. 1997. Ectopic bone formation by marrow stromal osteoblast transplantation using poly(DL-

lactic-co-glycolic acid) foams implanted into the rat mesentery. Journal of Biomedical Materials Research 36(1), 1-8.

Ishikawa K, Akasaka T, Yawaka Y, Watari F. 2010. High functional expression of osteoblasts on imogolite, aluminosilicate nanotubes. Journal of Biomedical Nanotechnology 6(1), 59-65.

Jeon O, Song SJ, Kang SW, Putnam AJ, Kim BS. 2007. Enhancement of ectopic bone formation by bone morphogenetic protein-2 released from a heparin-conjugated poly(L-lactic-co-glycolic acid) scaffold. Biomaterials 28(17), 2763-2771.

Ji Y, Xu GP, Zhang ZP, Xia JJ, Yan JL, Pan SH. 2010. BMP-2/PLGA delayed-release microspheres composite graft selection of bone particulate diameters and prevention of aseptic inflammation for bone tissue engineering. Annals of Biomedical Engineering 38(3), 632-639.

Kalmodia S, Sharma V, Pandey AK, Dhawan A, Basu B. 2011. Cytotoxicity and genotoxicity property of hydroxyapatite-mullite eluates. Journal of Biomedical Nanotechnology 7(1), 74-75.

Kanaji A, Caicedo MS, Virdi AS, Sumner DR, Hallab NJ, Sena K. 2009. Co-Cr-Mo alloy particles induce tumor necrosis factor alpha production in MLO-Y4 osteocytes: A role for osteocytes in particle-induced inflammation. Bone 45(3), 528-533.

Katti KS, Katti DR, Dash R. 2008. Synthesis and characterization of a novel chitosan/montmorillonite/hydroxyapatite nanocomposite for bone tissue engineering. Biomedic

Jacobs JJ, Hallab NJ, Urban RM, Wimmer RA. 2006. Wear particles. Journal of Bone and Joint Surgery (American) 88-Supplement 2, 99-102.

Ingham E, Fisher J. 2005. The role of macrophages in osteolysis of total joint replacement. Biomaterials 26(11), 1271-1286.

Peng F, Yu X, Wei M. 2011. In vitro cell performance on hydroxyapatite particles/poly(L-lactic acid) nanofibrous scaffolds with an excellent particle along fiber orientation. Acta Biomaterialia 7(6), 2585-2592.

Purdue PE, Koulouvaris P, Potter HG, Nestor BJ, Sculco TP. 2007. The cellular and molecular biology of periprosthetic osteolysis. Clinical Orthopaedics and Related Research 454, 251-261.

Ren WP, Wu B, Peng X, Hua J, Hao HN, Wooley PH. 2006. Implant wear induced inflammation but not osteoclastic bone resorption in RANK (-/-) mice. Journal of Orthopaedic Research 24(8), 1575-1586.

Ren WP, Markel DC, Zhang R, Peng X, Wu B, Monica H, Wooley PH. 2006. Association between UHMWPE particle-induced inflammatory osteoclastogenesis and expression of RANKL, VEGF and Flt-1 in vivo. Biomaterials 27(30), 5161-5169.

Rueda L, Garcia I, Palomares T, Alonso-Varona A, Mondragon I, Corcuera M, Eceiza A. 2011. The role of reactive silicates on the structure/property relationships and cell response evaluation in polyurethane nanocomposites. Journal of Biomedical Materials Research: Part A 97(4), 480-489.

Sabokbar A, Pandey R, Diaz J, Quinn JM, Murray DW, Athanasou NA. 2001. Hydoxyapatite particles are capable of inducing osteoclast formation. Journal of Materials Science – Materials in Medicine 12(8), 659-664.

Smith RA, Hallab NJ. 2010. In vitro macrophage response to polyethylene and polycarbonate-urethane particles. Journal of Biomedical Materials Research: Part A 93(1), 347-355.

Smith RA, Maghsoodpour A, Hallab NJ. 2010. In vivo response to cross-linked polyethylene and polycarbonate-urethane particles. Journal of Biomedical Materials Research: Par A 93(1), 227-234.

Styan KE, Martin DJ, Poole-Warren LA. 2008. In vitro fibroblast response to polyurethane organosilicate nanocomposites. Journal of Biomedical Materials Research: Part A 86A(3), 571-582.

Vermes C, Glant TT, Hallab NJ, Fritz EA, Roebuck KA, Jacobs JJ. 2001. The potential role of the osteoblast in the development of periprosthetic osteolysis: Review of in vitro osteoblast responses to wear debris, corrosion products and cytokines and growth factors. Journal of Arthroplasty 16(8 Supplement 1), 95-100.

Wooley PH, Morren R, Andary J, Sud S, Yang SY, Mayton L, Markel D. Sieving A, Nasser S. 2002. Inflammatory response to orthopaedic biomaterials in the murine air pouch. Biomaterials 23(2), 517-526.

Yang SY, Ren W, Park Y, Sieving A, Hsu H, Nasser S, Wooley PH. 2002. Diverse cellular and apoptotic resonses to variant shapes of UHMWPE particles in a murine model of inflammation. Biomaterials 23(17), 3535-3543.

Yang SY, Mayton L, Wu B, Goater JJ, Schwarz EM, Wooley PH. 2002. Adeno-associated virus-mediated osteoprotegerin gene transfer protects against particulate polyethylene-induced osteolysis in a murine model. Arthritis and Rheumatism 46(9), 251-2523.

Zhuang H, Zheng JP, Gao H, De Yao K. 2007. In vitro biodegradation and biocompatibility of gelatin/montmorillonite-chitosan intercalated nanocomposites. Journal of Materials Science – Materials in Medicine 18(5), 951-957.

ABSTRACT

SUPERCRITICAL CARBON DIOXIDE-PROCESSED RESORBABLE POLYMER NANOCOMPOSITES FOR BONE GRAFT SUBSTITUTE APPLICATIONS

by

KEVIN C. BAKER

August 2011

Advisor: Rangaramanujam M. Kannan, Ph.D.

Major: Biomedical Engineering

Degree: Doctor of Philosophy

Numerous clinical situations necessitate the use of bone graft materials to enhance bone formation. While autologous and allogenic materials are considered the gold standards in the setting of fracture healing and spine fusion, their disadvantages, which include donor site morbidity and finite supply have stimulated research and development of novel bone graft substitute materials. Among the most promising candidate materials are resorbable polymers, composed of lactic and/or glycolic acid. While the characteristics of these materials, such as predictable degradation kinetics and biocompatibility, make them an excellent choice for bone graft substitute applications, they lack mechanical strength when synthesized with the requisite porous morphology. As such, porous resorbable polymers are often reinforced with filler materials. In the presented work, we describe the use of supercritical carbon dioxide ($scCO_2$) processing to create porous resorbable polymeric constructs reinforced by nanostructured, organically modified Montmorillonite clay (nanoclay). $scCO_2$ processing simultaneously disperses the nanoclay throughout the polymeric matrix, while imparting a porous morphology to the construct conducive to facilitating cellular infiltration and neoangiogenesis, which are necessary components of bone growth. With the addition of as little as 2.5wt% of nanoclay, the compressive strength of the constructs nearly doubles putting them on par with human cortico-

cancellous bone. Rheological measurements indicate that the dominant mode of reinforcement of the nanocomposite constructs is the restriction of polymer chain mobility. This restriction is a function of the positive interaction between polymer chains and the nanoclay. In vivo inflammation studies indicate biocompatibility of the constructs. Ectopic osteogenesis assays have determined that the $scCO_2$-processed nanocomposites are capable of supporting growth-factor induced bone formation. $scCO_2$-processed resorbable polymer nanocomposites composed of resorbable polymers and nanocaly exhibit physical, mechanical and biologic properties that make them excellent candidate materials for structural bone graft substitute applications.

AUTOBIOGRAPHICAL STATEMENT

My pursuit led me to Michigan Technological University in Houghton, Michigan. Here, in the bitter cold miles beyond civilization, my progress towards a B.S. degree in Biomedical Engineering started. In my junior year at Michigan Tech, I participated in undergraduate research with an Exercise Physiology group. The following summer, I obtained an internship at Henry Ford Hospital's Bone and Joint Research Center. My senior capstone project at Michigan Tech dealt with the development of a method to deposit calcium phosphate films on orthopaedically-relevant metallic biomaterials. The following summer, I was fortunate enough to obtain another internship, this time with the Orthopaedic Research Laboratories at William Beaumont Hospital where I was exposed to more biomaterials research. After that internship, I finished my B.S. degree at Michigan Tech and immediately began the Master's program in Materials Science and Engineering. My graduate research was focused an offshoot of my senior capstone project, but rather than focusing on metallic materials, I studies methods to enhance deposition and adhesion of calcium phosphate films on polymeric and other organic substrates. After finishing the M.S. degree at Michigan Tech, I took a research position in the Orthopaedic Research Labs at William Beaumont Hospital in January of 2006 and married my wife that I met in graduate school. One year later, I began the Ph.D. program at Wayne State University under Dr. Rangaramanujam M. Kannan and became a father, shortly thereafter. Under his supervision, I performed work related to the development of porous, resorbable polymer nanocomposites synthesized by supercritical carbon dioxide processing. Following completion of the Ph.D. program, I will remain at William Beaumont Hospital as Director of the Orthopaedic Research Laboratories and have much more time to spend with my wife and two sons.